INVESTIGATIONS INTO ALLOSTERIC MECHANISMS OF G PROTEIN

ACTIVATION

By

Tarjani Mahesh Thaker

Dissertation

Submitted to the Faculty of the

Graduate School of Vanderbilt University

in partial fulfillment of the requirements

for the degree of

DOCTOR OF PHILOSOPHY

in

Biochemistry

December, 2013

Nashville, Tennessee

Approved:

Tina Iverson

Heidi Hamm

Charles Sanders

Vsevolod Gurevich

Martin Egli

For my mother and my father.

ACKNOWLEDGEMENTS

First and foremost, I would like to thank my research advisor, Dr. Tina Iverson, for taking me into her lab and giving me a science home over the past five years. Her mentorship has molded me into the scientist that I am today, and I owe her a debt of gratitude for being a fantastic teacher and role model not just for women in science, but budding researchers everywhere. I am especially grateful to her for her patience, invaluable advice, scientific and otherwise, her encouragement of my academic and research endeavors, and above all, for teaching me to "see the trees in the forest".

I would like to thank my committee members: Dr. Charles Sanders, Dr. Martin Egli, Dr. Seva Gurevich, and Dr. Heidi Hamm. I was truly lucky to have assembled an exceptionally supportive group of individuals whom could not have been better equipped to navigate the many terrains of my dissertation project(s). I would like to thank Dr. Sanders for teaching me everything I know about phospholipids. It is an understatement to say that the work presented here would not have been possible without his expertise. He has also been an excellent example of a truly gracious scientist, which I admire immensely and hope to emulate. As the only other x-ray crystallographer on my committee, I would like to thank Dr. Egli for his expert insight, and for generously allowing me to use his laboratory as a resource. I spent many nights in front of the Egli

lab DynaPro in hopes of some data, which I eventually did get and resulted in my first publication. This was a transformative experience and gave me the confidence (and courage) to continue to pursue a project that often felt not just intellectually, but also physically daunting. I truly underestimated the role that Dr. Gurevich would play in my graduate career. I could always count on him to see the silver lining whenever I felt hopeless about whatever trivial experimental result happened to disagree with me. His enthusiasm for both science and my dissertation project was truly infectious, and I am grateful to him for his constant words of encouragement. Lastly, I would like to thank Dr. Heidi Hamm for giving me a second home. Her laboratory was as much an integral part of my scientific training as the Iverson lab, and I am indebted to her for allowing me to use so many of the Hamm lab resources to pursue the study of G proteins.

I was lucky to have worked alongside a team of talented and hilarious people in the Iverson lab without whom graduate school would have been far less enjoyable. An "Iversonite" is a truly special breed and I am grateful to have shared the title with Dr. Mikio Tanabe, Dr. Thomas Tomasiak, Dr. Timothy Panosian, Tasia Pyburn, Michael Funk, Dr. Jessica Vey, Prashant Singh, Dr. Kathryn McCulloch, Kendra Vann, Qiuyan Chen, Beth Thorneycroft, Maruf Sarwar, Dr. Seoungmin Bong, Dr. Nathaniel Gilbert, and Chrystal Starbird.

I would also like to acknowledge members of the Hamm lab who deserve recognition for their technical and intellectual contributions to this work. I would especially like to thank Dr. Anita Preininger for her mentorship and willingness to always help interpret data or take a look at a manuscript draft. Her attention to detail has been indispensable to my success, and I hope to be half the scientific writer she has proven to

be. Scott Meier and Dr. Ali Kaya taught me everything I know about characterizing G proteins. I like to think I have the science hands that I do today because of these two outstanding "coaches". Lastly, I am indebted to James Gilbert, Karen Hyde, and the other members of the Hamm lab for graciously tolerating my presence on their territory.

Next, I would like to acknowledge the support staff at Vanderbilt University. I especially owe my gratitude to the Pharmacology Department. They took me in as one of their own despite having technically been enrolled in the Biochemistry Department. Gordon Borck, Elaine Brown, Chase Jeffords, Yvonne Smith, and Karen Gieg are among the most helpful and kind people that I have met at Vanderbilt. There was never an administrative or technical issue that this selection of fantastic people was not willing to help with. I would also like to thank the members of the Biochemistry Department, Center for Structural Biology, the C.O.R.E.S. facility in the Department of Cell and Developmental Biology, the Mass Spectrometry facility, and the skilled and patient beamline staff at the Advanced Photon Source. This work was entirely possible because of their expertise and assistance.

Lastly and most importantly, I would like to acknowledge my beloved friends and family. To my mother and my father, Mahesh and Gita Thaker, and my sister, Tanvi Thaker, your unconditional love and encouragement helped me reach the finish line. To the dear friends that I have made in Nashville, there is not enough that I can say to express my gratitude for your presence in my life throughout graduate school. You were my family away from home. No amount of formal education could have taught me the things that I have learned about science, the world, and myself through our time together. The experiences and memories we have shared beyond the walls of Vanderbilt University

(and some within) will stay with me for a lifetime. To Thomas Tomasiak and Kelli Kazmier, you two saved me from myself. I am infinitely grateful for the bond that we have forged. Your friendships alone have made this six-year journey entirely worthwhile. Thank you all for your love and support. You gave more than I ever deserved.

TABLE OF CONTENTS

LIST OF TABLES

LIST OF FIGURES

LIST OF ABBREVIATIONS

7.7 MAG	1-(7Z-tetradecenoyl)-rac-glycerol
7.8 MAG	1-(7Z-pentadecenoyl)-rac-glycerol
ACK	Acetate kinase
ADA	N-(2-Acetamido)iminodiacetic acid
α-DM	Methyl α-D-mannopyranoside
AlCl$_3$	Aluminum chloride
AlF$_4^-$	Aluminum fluoride
AMP-PnP	Adenosine 5'-(β,γ-imido)triphosphate lithium salt hydrate
APS	Advanced Photon Source
ATR	all-trans retinal
β$_2$AR	β$_2$-adrenergic receptor
βME	β-mercaptoethanol
cAMP	Cyclic adenosine monophosphate
cGMP	Cyclic guanosine monophosphate
CHAPS	3-[3-Cholamidopropyl)dimethylammonio]-1-propanesulfonate hydrate
CHAPSO	3-([3-Cholamidopropyl]dimethylammonio-2-hydroxy-1propanesulfonate
ConA	Concanavalin A
DHPC	1,2-diheptanoyl-*sn*-glycero-3-phosphocholine
DDM	n-Dodecyl-γ-D-Maltopyranoside
DLS	dynamic light scattering
DM	n-Decyl-β-D-Maltopyranoside

DMPA	1,2-dimyristoyl-*sn*-glycero-3-phosphate
DMPC	1,2-dimyristoyl-*sn*-glycero-3-phosphocholine
DMPG	1,2-dimyristoyl-*sn*-glycero-3-phospho-(1'-rac-glycerol) (sodium salt)
DMPS	1,2-dimyristoyl-*sn*-glycero-3-phospho-L-serine (sodium salt)
DOPA	1,2-dioleoyl-*sn*-glycero-3-phosphate (sodium salt)
DOPS	1,2-dioleoyl-*sn*-glycero-3-phospho-L-serine (sodium salt)
DTT	Dithiothreitol
E. coli	*Escherichia coli*
EC_{50}	Concentration that produces a half-maximal effect
EC_{90}	Concentration that produces a 90%-maximal effect
$G\alpha$	α subunit of heterotrimeric G proteins
$G\alpha_{i1}$	α subunit of the inhibitory heterotrimeric G protein, isoform 1
$G\alpha_s$	α subunit of the stimulatory heterotrimeric G protein
$G\alpha_t$	α subunit of the heterotrimeric G protein, transducin
GDP	Guanosine 5'-diphosphate sodium salt
GMP	Guanosine monophosphate
GPCR	G Protein Coupled Receptor
G_i	inhibitory G protein
GppNHp	guanosine-5'-(β-γ-imino)triphosphate
G_s	stimulatory G protein
G_t	transducin
GTP	Guanosine 5'-triphosphate sodium salt hydrate
GTPγS	Guanosine 5'-O-(3-thiotriphosphate) tetralithium salt

EDTA   Ethylenediaminetetraacetic acid disodium salt dihydrate

FeCl$_3$ Ferric chloride

HCl   Hydrochloric acid

HEPES   N-(2-Hydroxyethyl)piperazine-N'-(2-ethanesulfonic acid)

HTAC   Hexadecyltrimethylammonium chloride

IPTG   Isopropyl-β-D-thiogalactoside

Kan   Kanamycin A

LDAO   n-Dodecyl-N,N-Dimethylamine-N-Oxide

LS-CAT   Life Sciences Collaborative Access Team

MI   metarhodopsin I

MII   metarhodopsin II

MgCl$_2$ Magnesium chloride hexahydrate

MNG-3   2,2-didecylpropane-1,3-bis-β-D-maltopyranoside

MOPS   4-Morpholinepropanesulfonic acid

NaCl   Sodium chloride

NaF   Sodium flouride

OG   n-Octyl-β-D-Glucopyranoside

PEG2000   Poly(ethylene glycol) methyl ether 2,000

PMSF   Phenylmethanesulfonyl fluoride

RhoGt   Rhodopsin-transducin complex

ROS   rod outer segments

Tris-Cl   Tris(hydroxymethyl)aminomethane (pH adjusted with HCl)

CHAPTER I

INTRODUCTION

Introduction

Efficient communication between the cells of the human body is an important determinant of human health. Chemical signals in the extracellular milieu encode specific messages that instruct individual cells to elicit physiological responses to changes in the composition of the extracellular environment. Proteins embedded in the cellular membrane sense these signals and relay their "message" to a repertoire of intracellular proteins that act in concert to regulate a variety of cellular events such as gene expression, cell growth, cell mobility, and even cellular death in response. The integrity of the signal relay is essential to maintaining homeostasis, and disruption of the network of cellular crosstalk at any given point can result in disease ranging from depression and diabetes to heart disease or cancer. One such class of receptor proteins, the G Protein Coupled Receptors (GPCRs), forms a highly diverse and ubiquitous group of membrane proteins that transduce extracellular messages into intracellular responses via their interactions with their signaling partner, the heterotrimeric G protein. The focus of my dissertation research has been to better understand the precise mechanisms by which heterotrimeric G proteins are activated during GPCR signaling.

Historical Perspective

The discovery of heterotrimeric G proteins was preceded by investigations led by Sutherland and colleagues into the biochemical properties of β receptor signaling (17). By the late 70's, it was widely accepted that receptor stimulation by the extracellular hormone, epinephrine, was responsible for adenylyl cyclase activity and the production of cAMP as a second messenger for eliciting a cellular response. Separation by size exclusion chromatography confirmed that the two protein molecules were distinct entities, however the underlying mechanism by which activated receptors were able to regulate adenylyl cyclase still remained to be understood (18). Experiments conducted by Rodbell and colleagues provided a very important clue to this conundrum by showing that, in addition to hormone, GTP was a requirement for the activation of adenylyl cyclase during glucagon signaling (19,20). Indeed, the addition of a nonhydrolyzeable GTP analog (GppNHp) elicited persistent stimulation of adenylyl cyclase (21). Later, it was shown that GTP hydrolysis terminated adenylyl cyclase activity, and guanine nucleotides could regulate the activation state of the protein (22-24). Thus, a model of signal transduction utilizing a GTP-binding protein as the link between hormone-bound receptor and adenylyl cyclase was born (21).

By the turn of the decade, advances in chromatographic techniques allowed Gilman and colleagues to successfully purify what would later be identified as the α, β, and γ subunits of the stimulatory G protein, G_s (28). Importantly, reconstitution of adenylyl cyclase and G_s with membranes from a *cyc-* adenylyl cyclase deficient cell line was sufficient for cAMP production (30), and so the GTPase hypothesis suggested by Rodbell was finally confirmed. Meanwhile, investigations into analogous systems led to

the identification of a class of structurally conserved GTPase proteins. The study of phototransduction in retina revealed the presence of a light-sensitive GTPase that was required for the inactivation of cGMP phosphodiesterase, which hydrolyzes cGMP to GMP (31,32). This phenomenon was attributed to the activity of transducin, G_t, the cognate heterotrimeric G protein of the visual receptor rhodopsin (33,34). Likewise, investigations into the action of the cholera (35-37) and pertussis (38,39) bacterial toxins assisted in the identification of the stimulatory (G_s) and inhibitory (G_i) classes of the G protein, respectively (41).

Since the initial characterizations of GPCRs, and subsequently heterotrimeric G proteins, extraordinary progress has been made towards understanding their architecture, function, and regulation using a variety of structural and biochemical approaches. Rigorous exploration of the relationship between GPCRs and G proteins has implicated a highly sophisticated, allosteric mechanism of G protein activation during GPCR signaling. Yet, ambiguities still remain. In subsequent sections of this introduction, experimental approaches for studying allosteric processes of GPCR and heterotrimeric G protein regulation will be reviewed to establish where progress in the field and our understanding of these processes currently stands.

Overview of Allostery in GPCRs

Biological Importance of GPCRs

GPCRs are transmembrane proteins that mediate a variety of physiological processes. While there is a diverse set of ligands that can activate GPCRs, each receptor has incredible fidelity to a small set of cognate ligands that act as agonists, antagonists, or

inverse agonists to achieve different receptor activation states. Their specificity for regulating a broad number of biological processes has allowed for the development of numerous pharmaceutical therapeutics that modulate GPCR signaling. Indeed, GPCRs are overrepresented as therapeutic targets as they constitute only 3% of all protein-encoding genes in humans, but an estimated 50% of all pharmacological targets (44).

Sequence and Structural Determinants of GPCRs.

Despite the diversity in substrate specificity, GPCRs all share a common architecture comprising seven transmembrane helices (45). They additionally contain six, conserved sequence motifs believed to be critical for regulation of receptor activation states. These are a disulfide bond, an (E/D)RY motif forming the ionic lock, an NPxxY$(x)_{5,6}$F motif, a Y$(x)_7$K(R) motif, three conserved helix kink-inducing prolines, and a CWxP motif comprising the rotamer toggle switch (**Figure 1**) (47,48).

Sequence comparisons of the GPCR superfamily subdivide human GPCRs into three main classes (49). Class A, B, and C GPCRs differ in sequence identity, their substrate preference, and mechanisms of ligand binding. Class A, or the *Rhodopsin* family, is by the far the largest: as of 2008, 802 predicted human GPCRs had been identified, of which 672 belonged to Class A (44,51). Class A GPCRs do not share a high degree of sequence homology and bind diverse ligands, but do contain the conserved transmembrane architecture, sequence motifs required for activation, and are defined by a short, extracellular N-terminus lacking a common domain (49). Human thrombin receptors are an exception and have intrinsic cleavage sites in their N-termini that get cleaved to reveal a tethered ligand able to activate the receptor (56). Peptides, small
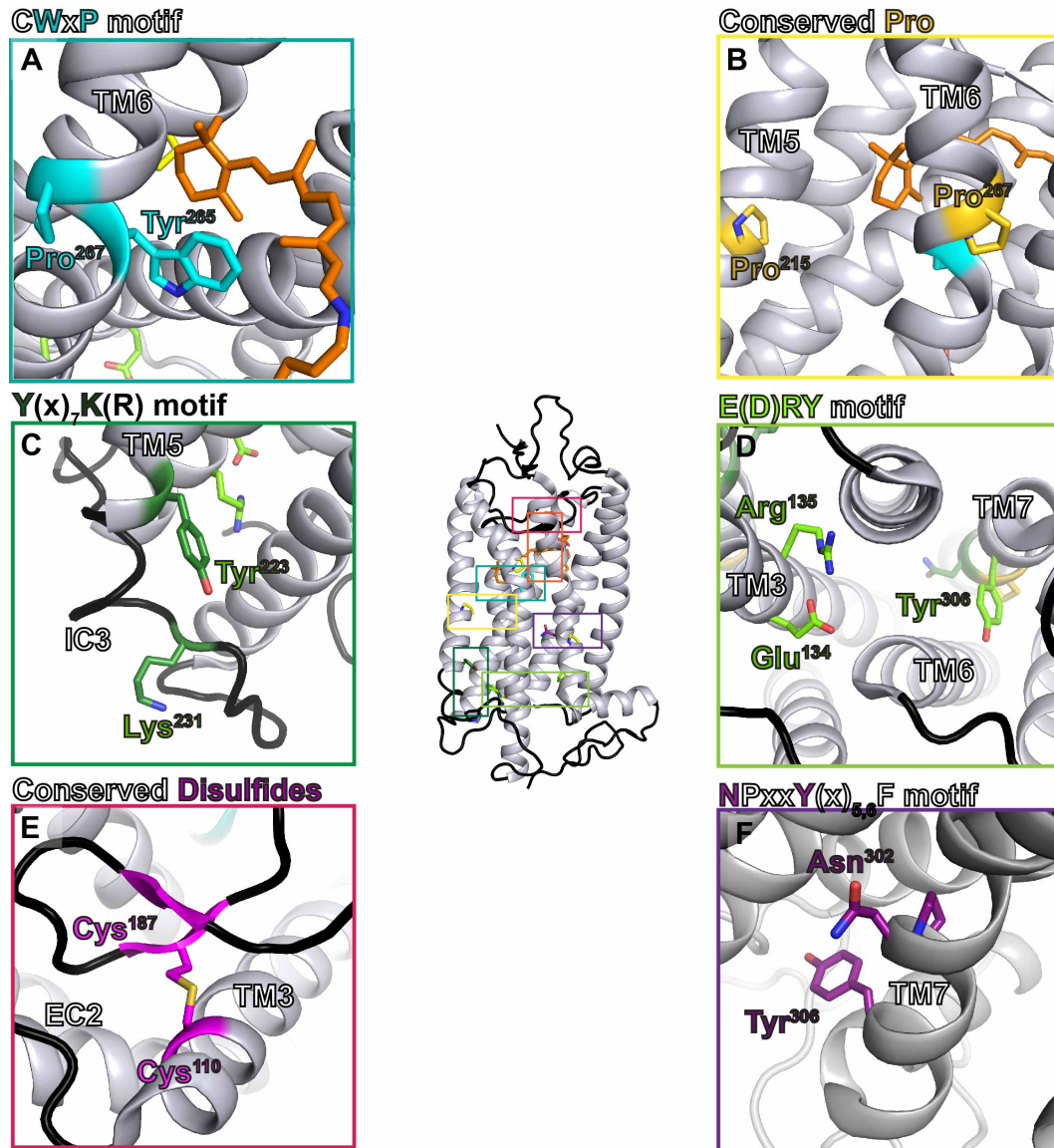
Figure 1: Conserved Structural Motifs of Class A GPCRs. The structure of rhodopsin (PDBID: 1U19 (3)) bound to the inverse agonist, 11-*cis* retinal, represents the prototypical Class A GPCR (*center*). Three intracellular loops (IL) and three extracellular loops (EL) connect seven transmembrane (TM) helices arranged in a tight bundle. Ligand entry occurs on the extracellular side of the receptor and binds within a central cavity. Retinal binding in rhodopsin is highlighted with an *orange* box. Details of the conserved structural motifs are shown in the surrounding panels and are mapped onto the rhodopsin structure in the same color as the panel outline. **A)** The CWxP motif forms the basis of the toggle switch hypothesis and contributes the proline residue that introduces a kink in TM6. **B)** Additional conserved prolines, Pro[215] and Pro[267] in rhodopsin, also introduce kinks in TM helices in GPCRs. **C)** Lys[231] and Tyr[223] of the $Y(x)_7K(R)$ motif form interactions in the activated receptor that contribute to the release of the ionic lock formed by residues of the **D)** E(D)RY motif. **E)** Conserved disulfide helps constrain TM3 and EL2, whereas the **F)** $NPxxY(x)_{5,6}F$ motif forms the basis of a distinct hydrogen bonding network that is comprised of two submotifs: 1) a TM1, TM2, and TM7 linkage and 2) a TM7-cytoplasmic helix 8 linkage mediated by Asn[302] and Tyr[306].

5

organic compounds, and nucleotides are a few examples of the many ligands that can bind to class A GPCRs. Importantly, until recently, receptors of class A were the only GPCRs for which structures had been determined by x-ray crystallography and for which the largest number of pharmaceutical drugs have been developed. By comparison to class A, much less is known about the allosteric regulation of class B and class C receptors.

Class B GPCRs are divided into two families, the *Secretin* and *Adhesion* families (51). *Secretin* receptors are defined by an extracellular hormone-binding domain. They contain conserved cysteine residues in extracellular loops 1 and 2, form a cysteine-bridge network in the N-terminus, and bind peptide hormones (58-60). *Adhesion*s receptors are defined by long N-termini that are highly glycosylated, protrude from the membrane surface, and form a rigid structure containing GPCR proteolytic domains that undergo autocatalytic processing to form two non-covalently attached subunits whose features vary in different receptor subtypes (61-63). The cleavage site is often found between a conserved aliphatic residue such as leucine and small polar residues such as threonine, serine, or cysteine (63-65). Despite the diversity in the functional domains formed in *Adhesion* receptor N-termini, these receptors contain conserved cysteine residues in extracellular loops 1 and 2 like *Secretin* receptors and preferentially bind extracellular matrix molecules (66).

Class C GPCRs contain the *Glutamate* family of receptors and are defined by large extracellular N-terminal domains. Crystal structures of the extracellular portions of the metabotropic glutamate receptor have been determined and provide insight into the topology of Class C ligand binding sites (67). In this receptor, the N-terminus is folded into two conserved domains stabilized by three predicted disulphide bridges formed by

nine conserved cysteine residues (68,69). Amino acids, cations, carbohydrates, and small organic compounds will then bind Class C receptors in structurally similar ligand binding domains within the N-terminus.

Mechanisms of Allosteric Regulation in Rhodopsin

One of the best-characterized GPCRs, rhodopsin, is a member of class A, and the details of rhodopsin activation are generally assumed to apply to the rest of the class. Rhodopsin is responsible for perception of light under low light conditions. Numerous properties of this photoreceptor have made it amenable to characterization by both *in vivo* and *in vitro* methods. Rhodopsin is naturally abundant, easily purified, stable in a variety of detergents, and has spectroscopic properties that provide a convenient method to monitor activation. In addition, ground state rhodopsin covalently ligates an inverse agonist, 11-*cis*-retinal, that locks it into an inactive conformation. This decreases the conformational heterogeneity that often limits x-ray crystallographic studies. Accordingly, rhodopsin was the first GPCR to be characterized by x-ray crystallography in both active and inactive conformations, and eight years elapsed before the structure of any GPCR with a diffusible agonist was determined. Very recently, the structures of 14 unique Class A receptors (**Figure 2**) have been added to the repertoire of GPCR crystal structures (70,71). These structures verify that the relative arrangement of transmembrane helices in the inactive state is largely conserved between rhodopsin and other class A GPCRs. As a result, the mechanisms of activation are likely to be shared.

Rhodopsin is synthesized as an apoprotein called opsin, which lacks the ability to detect light. Covalent linkage of 11-*cis*-retinal to the ε-amino group of Lys[296] forms a
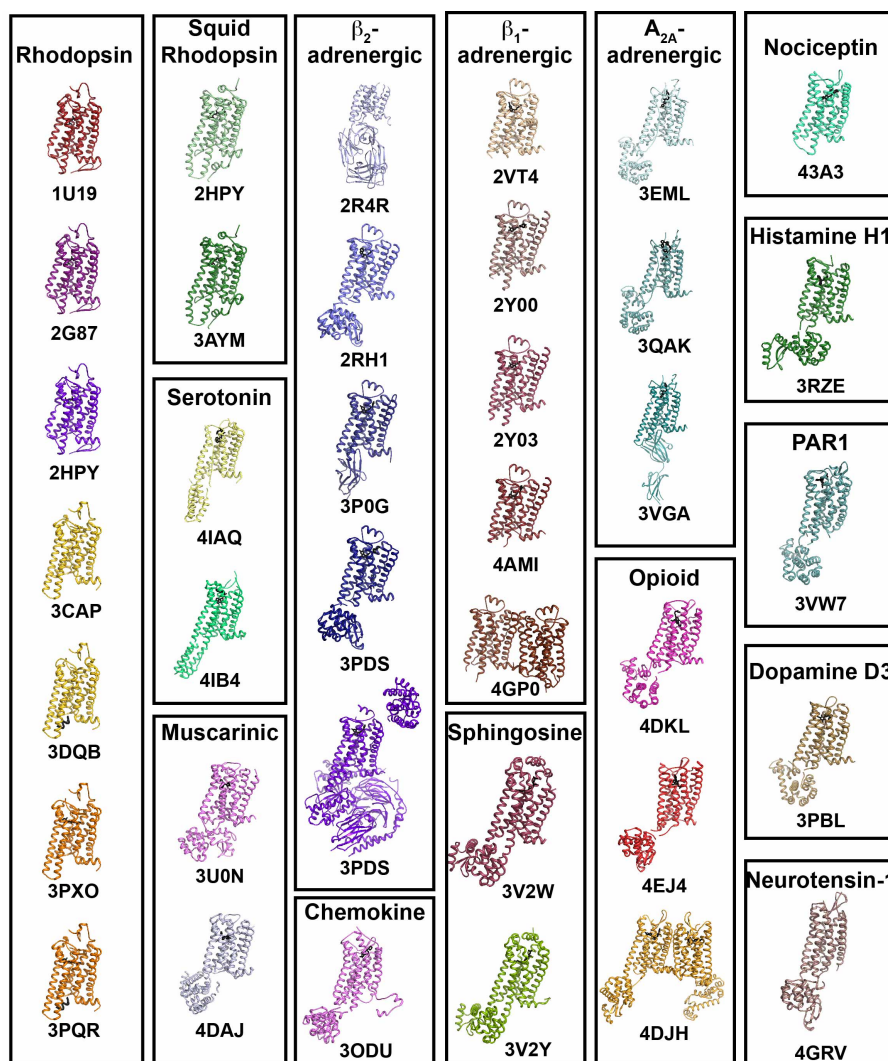
Figure 2: Overview of Class A GPCR Crystal Structures. Structures are shown bound to their ligand (*black* sticks) and are grouped by the subfamily to which the receptor belongs. Engineered extracellular domains and stabilizing binding partners used to aid in the crystallization are displayed for the structures where they were employed.

Schiff base and converts opsin to rhodopsin, conferring light sensitivity. A salt bridge between the Schiff base imine on helix VII and the counterion Glu[113] on helix III stabilizes the covalent linkage by preserving protonation of the Schiff base (72). This results in an optical spectrum characteristic of inactive rhodopsin (73,74). The protonation state of the Schiff base, among other things, contribute to variations in the

absorption spectra of rhodopsin during its reaction cycle (**Figure 3**) (72). Rhodopsin

activation is initiated by the absorption of a single photon of light, which induces

isomerization of 11-*cis*-retinal to all-*trans* retinal, catalyzes transfer of the imine proton

to the Glu[113] counterion, breaks the salt bridge, and releases all-*trans* retinal from a

covalent linkage with rhodopsin (47).
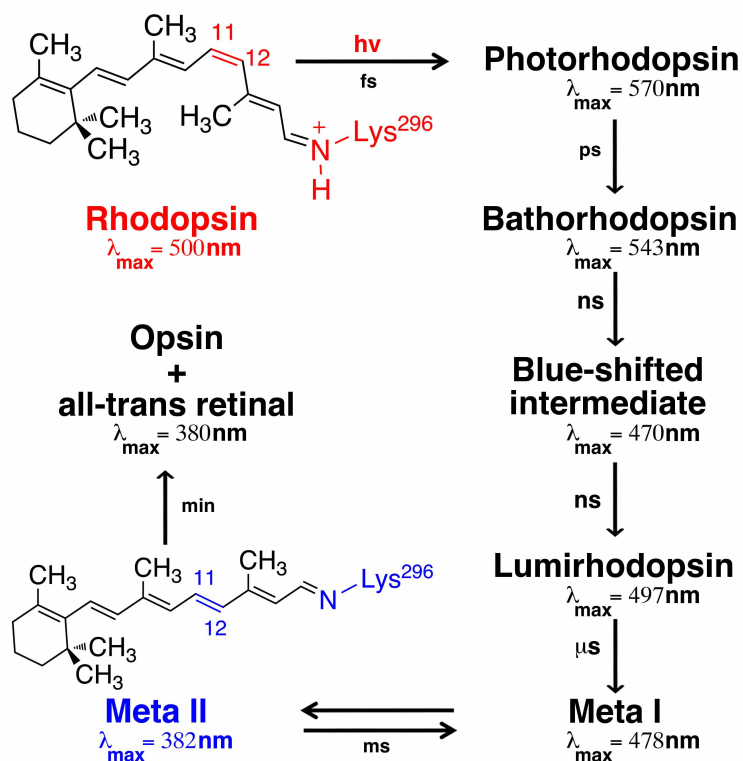
Figure 3: Rhodopsin Cycle of Photointermediate Formation. Opsin covalently bound to 11-*cis* retinal forms the inactive photoreceptor, Rhodopsin (*red*). Upon the absorption of a photon of light (hv), the bound 11-*cis* retinal isomerizes to the all-*trans* form. Rhodopsin then cycles through a series of spectrally unique photointermediates as the chromophore undergoes thermal relaxation. Formation of the Meta II state (*blue*) represents the activated form of the receptor that binds to the cognate G protein, transducin, with high affinity. Hydrolysis of the Schiff base linkage (N-Lys[296]) returns the receptor to the Opsin form and liberates all-*trans* retinal.

EPR, double electron-electron resonance (DEER) spectroscopy, and EM have

showed that large conformational changes accompany rhodopsin activation (75-78). The

most dramatic conformational change is the rigid body movement of helix VI away from helix III (**Figure 4**) (77,78). This conformational change has long been hypothesized to be required for the formation of a cytoplasmic G protein-binding site. For rhodopsin, the cognate G protein is transducin, G_t. Recent crystal structures of opsin and opsin in complex with a high affinity peptide mimicking the C-terminus of the $G\alpha_t$ subunit are consistent with the activated conformations of GPCRs indeed exposing a cytoplasmic pocket accommodating the C-terminus of $G\alpha_t$ (79,80).

Rhodopsin   **Metarhodopsin II**
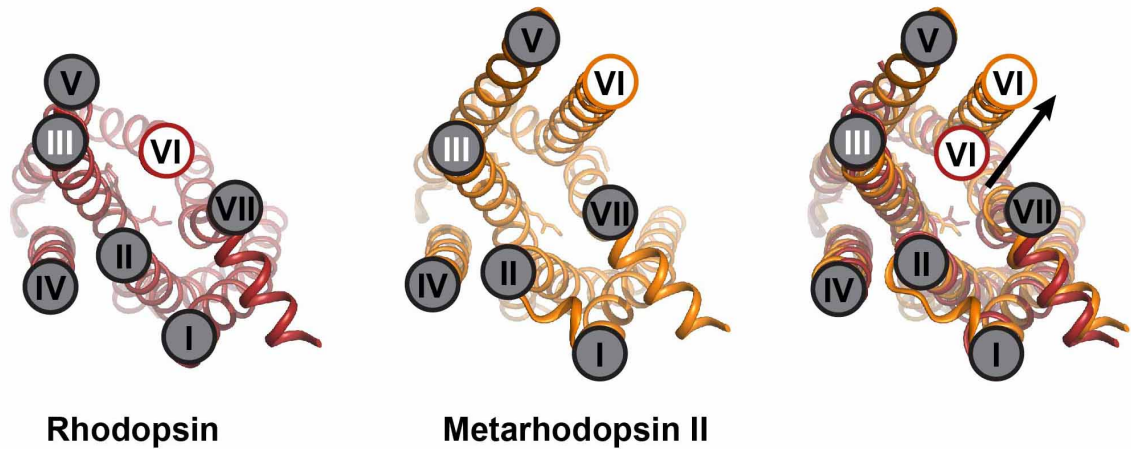
Figure 4: Conformational Changes of the Rhodopsin Intracellular Side. Left panel: Rhodopsin (PDBID 1U19; (3)) is shown in *gray*. Middle panel: Meta II (PDBID 3PQR; (81)) is shown in *blue*. Right panel: An overlay of the structures of rhodopsin and opsin highlights the differences in these structures. These two structures have a 7Å shift in the position of helix VI (*arrow*) that allows meta II to bind the C-terminus of $G\alpha_t$ in an intracellular binding pocket (82). The conformation of opsin is similar to the conformation proposed for rhodopsin upon light activation.

Associated with these transmembrane helical rearrangements is exposure of the (E/D)RY motif to solvent. In the absence of activation, this motif forms the ionic lock believed to stabilize receptors in the ground state (83,84). Salt bridges between Glu[134] and Arg[135] of the (E/D)RY motif and Glu[247] on helix VII constrain rhodopsin in the

inactive conformation in the absence of chromophore isomerization and helical reorganization (85,86). Fourier transform infrared (FTIR) spectroscopy showed that rhodopsin activation is pH dependent (87,88). Proton uptake by Glu[134] in response to the reorientation of helices III and VI is associated with metarhodopsin II formation, which is characterized by an absorption maximum at 380 nm (89-91). Residues Arg[135] and Glu[247], formerly participating in the ionic lock, can then form hydrogen bonding interactions with residues of the $Y(x)_7K(R)$ motif on helix V to stabilize the active receptor conformation. A broken ionic lock and loss of the agonist were observed in the crystal structure of opsin bound to a high affinity peptide (80).

Taken together, all of these studies point to an active conformation of the receptor that allows binding of G proteins to the cytoplasmic surface located over a 25 Å distance from the agonist binding site. This interaction between activated receptor and cognate heterotrimeric G proteins initiates G protein signaling.

Overview of Allostery in Heterotrimeric G Proteins

Biological Importance of Heterotrimeric G proteins

Heterotrimeric G proteins (Gαβγ) (**Figure 5**) are activated by GPCRs (**Figure 6**). In the activated state, the heterotrimer dissociates into Gα and Gβγ. These dissociated subunits interact with effectors to regulate downstream signaling pathways. For example, in rhodopsin signaling, activated $Gα_t$ stimulates rod cGMP phosphodiesterase for the hydrolysis of cGMP to 5'-GMP. The decrease in cGMP causes cGMP-gated Ca^{2+} and Na^+ channels to close and the membrane of the cell to become hyperpolarized. The loss of an inward current results in an electrical signal whose outcome is low-light vision (92).
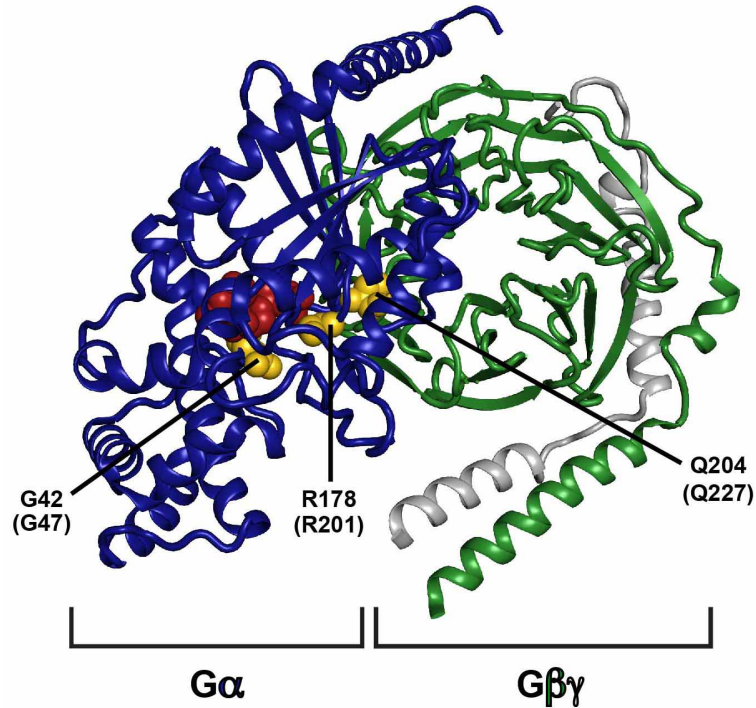
Figure 5: Overview of the Heterotrimeric G protein Structure. Heterotrimeric G proteins are composed of 3 subunits: the nucleotide-binding Gα (*blue*) subunit and the dimeric Gβ (*green*) and Gγ (*gray*) subunits. GDP is shown as *red* spheres in the structure of $G\alpha_{i1}\beta_1\gamma_2$ (PDB ID: 1GP2 (46)). Residues associated with G protein-related diseases are shown as *yellow* spheres and are labeled according to $G\alpha_i$ numbering. The corresponding residue numbering in $G\alpha_s$ is given in parentheses.

Alterations in G protein signaling arising from genetic variation can give rise to severe medical conditions. Missense mutations in heterotrimeric G proteins have been shown to result in progression of human pituitary and thyroid tumors, congenital night blindness, and ocular melanoma (93-96). In one specific example, it was discovered that mutation of a highly conserved glycine residue in the GTPase domain found in both heterotrimeric G proteins and distantly related Ras proteins resulted in congenital night blindness (95). This conserved glycine, residue 38 in $G\alpha_t$ (residue 42 in $G\alpha_{i1}$), is situated in a small loop that forms essential hydrogen bonds with α and β phosphates on both GDP and GTP in the nucleotide-binding pocket of the Gα subunit. A G38D mutation associated with
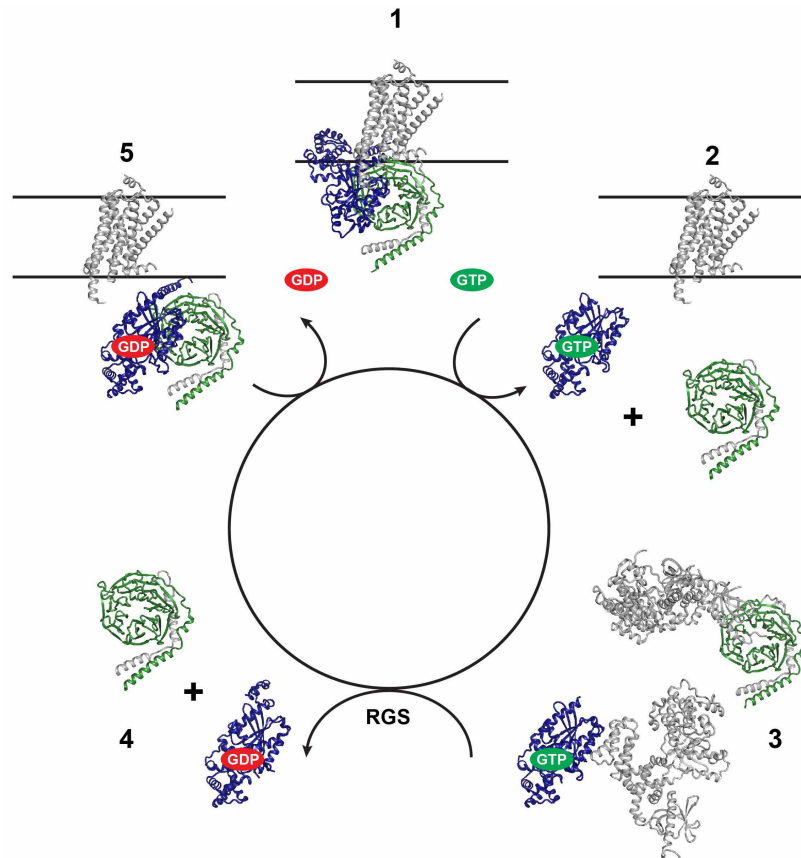
Figure 6: Heterotrimeric G protein Signaling Cycle. GPCRs signal through soluble G proteins. In **State 1**, activated receptor binds to the GDP-bound heterotrimeric G protein and promotes release of GDP from the Gα subunit to form a nucleotide-free receptor-G protein complex. Binding of GTP to the Gα subunit results in dissociation of this high-affinity complex into GTP-bound Gα, and Gβγ (**State 2**), each of which are now able to bind to downstream effectors (**State 3**) and elicit downstream responses. The Gα subunit has intrinsic GTPase activity which is enhanced by Regulators of G protein Signaling. Following hydrolysis of GTP, GDP-bound Gα subunits reassociate with Gβγ subunits (**State 4**) and traffic to the membrane, where they can interact with receptors in the next signaling cycle (**State 5**).

congenital night blindness is thought to disrupt $Gα_t$ GTPase activity. Similarly, a more

severe example of heterotrimeric G protein dysfunction is observed in the transformation

of growth-hormone secreting human pituitary tumors where a mutation in the $Gα_s$ subunit

of the stimulatory heterotrimeric G protein results in elevated basal adenylate cyclase

activity and cAMP production in tumorigenic cells (93). G proteins expressed in

malignant cells contained R201C or R201H and Q227R mutations in the G protein $Gα_s$

subunit. Like G38 in $G\alpha_t$, Q227 of $G\alpha_s$ is also found in the guanine nucleotide-binding pocket (**Figure 5**). Both R201 and Q227 were shown to be required for maintaining $G\alpha_s$ GTPase activity (93). As is the case with these conditions described, G-protein related diseases often arise as a consequence of constitutive activation of the catalytic Gα subunit.

Pathogens can additionally alter G protein signaling and also lead to severe physiological consequences. One of the earliest characterized alterations of G protein signaling by a pathogen showed that infection by *Vibrio cholerae* causes cholera toxin to ADP-ribosylate R201 in the $G\alpha_s$ subunit of heterotrimeric G proteins (97). This inhibits GTP hydrolysis and regulation of adenylate cyclase (24). The resultant increase in cAMP levels in intestinal cells causes severe diarrhea and dehydration in the host (98).

These examples highlight the importance of the G protein-effector interactions in maintaining cellular homeostasis. Effector specificity is determined by the GPCR-activating signal, which then selects the cognate heterotrimeric G protein from a conserved family for tissue- or cell-specific regulation of diverse biological responses.

Sequence and Structural Determinants of Heterotrimeric G proteins

The G protein subtype available for interaction ultimately determines effector specificity. Heterotrimeric G proteins are composed of three subunits: Gα, Gβ, and Gγ. In humans, there are currently 16 known Gα subtypes belonging to 4 subfamilies, 5 Gβ isoforms, and 12 Gγ isoforms, each with differing binding specificities for both effectors and GPCRs (99).

The Gα subunit is the catalytic subunit of the heterotrimeric G protein and is composed of two domains. The Ras-like domain adopts a conserved GTPase fold and

contains a guanine nucleotide-binding site formed by five flanking loops of the GTPase

fold (**Figure 7**). The phosphate (P) loop and the TCAT motif are conserved features of
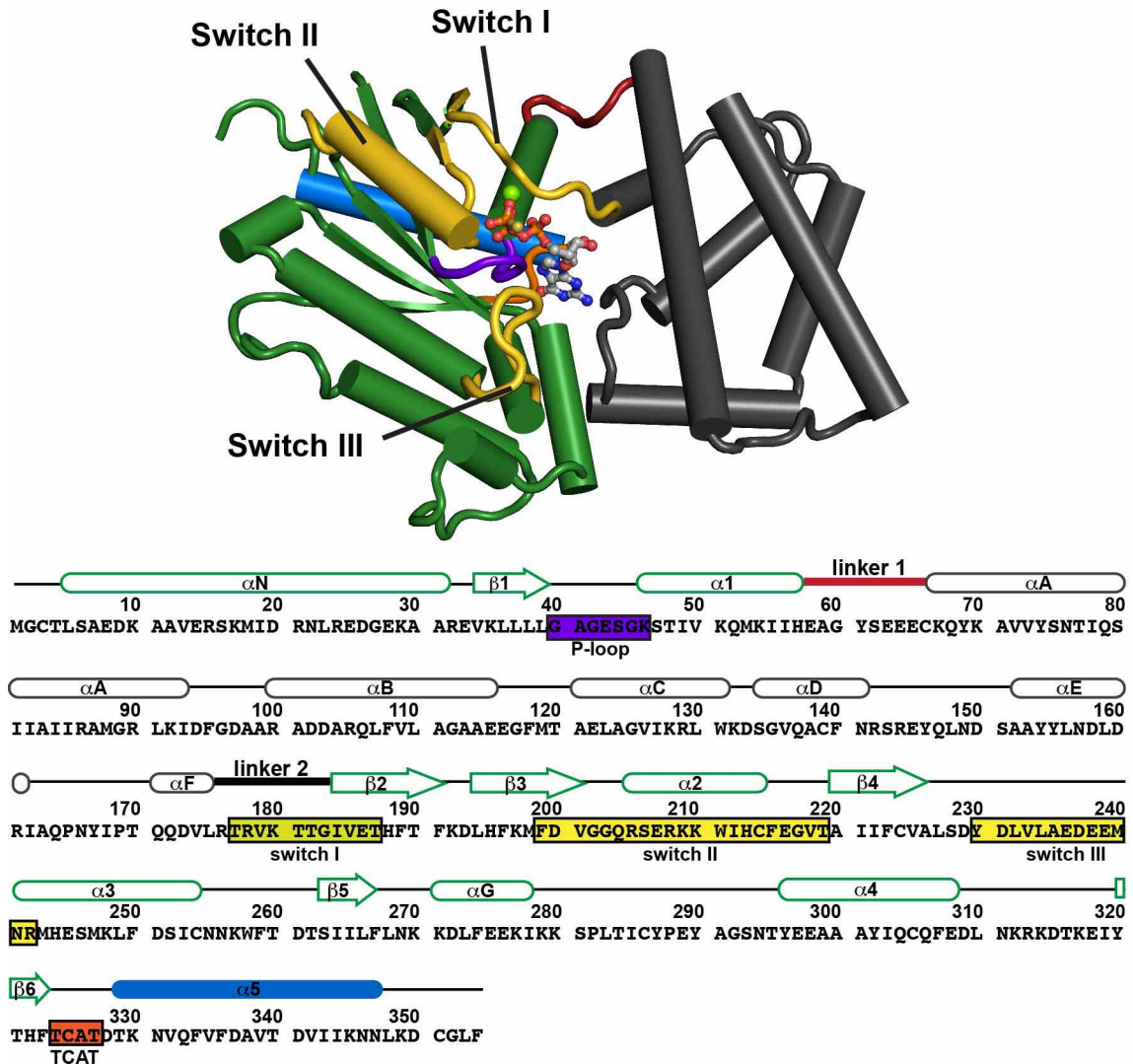
Figure 7: Conserved Motifs of the G protein α Subunit. The Gα subunit is comprised of two domains: the helical domain (gray) and the Ras-like GTPase domain (green) containing elements important to the function and regulation of Gα. Conformationally variable Switch regions (*yellow*) converge on the nucleotide-binding site located at the interface of the two domains. The α5 helix (*blue*), the P-loop (*purple*), and the TCAT motif (*orange*) flank the Switch regions and nucleotide-binding site and facilitate Gα activation.

the Gα subunit observed through the family. An independently folded, unique helical

domain caps the nucleotide-binding pocket, which likely prevents spontaneous nucleotide

15

exchange with solvent and possibly increases the affinity for GTP binding within Gα (43,100). Important lipid modifications on the Gα N-terminus are implicated in heterotrimeric G protein function. Reversible S-palmitoylation of all Gα subtypes except Gα$_t$ and permanent N-myristoylation of Gα$_i$ in the N-terminus assist in plasma membrane tethering, G protein activation, and effector regulation (101,102).

Following heterotrimer dissociation, the Gβγ subunits act as a physiological heterodimer and can be separated only under harsh, denaturing conditions (103). Gβγ dimerization occurs through the N-terminal helices of both subunits forming a coiled-coiled domain (104). Following the short N-terminal dimerization domain, the Gβ subunit has a C-terminal domain of approximately 300 residues adopting a β-propeller fold formed by seven Trp/Asp (WD) repeats. Each repeat contains four antiparallel β-strands arranged in a circular fashion to form a pseudo-torroid. The Gγ subunit is the smallest subunit of the heterotrimeric G protein and is characterized by 2 helices joined by a loop. The N-terminal helix participates in the coiled-coiled domain with the Gβ subunit, while the C-terminal helix extends over the β-propeller domain. 12 Gγ isoforms are C-terminally prenylated by the farnesyl or geranylgeranyl moieties (105-107). Post-translational modification of Gγ has been shown to be essential for effector regulation and in membrane tethering of inactive G proteins (108).

Mechanisms of Allosteric Regulation in Heterotrimeric G proteins

Although heterotrimeric G proteins can act on a diverse variety of effectors, their mechanisms of activation and deactivation are conserved throughout the family (17). Numerous x-ray crystal structures of heterologously expressed Gα in various states of

activation, Gβγ, and the Gαβγ heterotrimer have revealed how the activation state of the protein is encoded into distinct conformations of the Gα subunit (**Table 2**). Comparisons of structures in the GDP, GDP-AlF$_4^-$, and GTPγS bound states revealed that three distinct sites designated as switches I-III adopt different conformations in the presence of different nucleotides (**Figure 8**). These switch regions undergo conformational changes, as much as 8Å for switch II, in response to receptor-mediated G protein activation (109). Switches I and II are located at the Gα-Gβ interface, while switch III is near the Gβγ coiled-coiled. Disparities observed in switch regions of GDP-bound versus GTPγS-bound Gα subunits form the basis for an allosteric mechanism of heterotrimeric G protein activation that links receptor interactions at the plasma membrane to GTP binding within the Gα nucleotide binding site (42).

The duration of heterotrimeric G protein activation and interaction with effectors is determined by the rate of GTP to GDP hydrolysis. While activated Gα subunits have intrinsic GTPase activity, the rate of GTP hydrolysis is dramatically increased, almost 2000-fold, by interactions with regulators of G protein signaling (RGS) proteins (110). This interaction with Gα is necessary for terminating signals in order to avoid overstimulation of signaling pathways. In the case of rhodopsin signaling, retinal RGS binding to Gα$_t$ is necessary for accelerating the termination of photoresponse (111). RGS proteins enhance the rate-limiting step in G protein deactivation by driving the formation of a Gα-GTP conformation that supports GTP hydrolysis. An x-ray crystal structure determined for a RGS4-Gα$_{i1}$ complex helped establish this mechanism of RGS-mediated deactivation of G proteins by defining the interaction surface between the core RGS domain and the Gα$_{i1}$ subunit (112). Absent from the structure was a direction interaction

Table 1: Crystal Structures of Gα Proteins

Family	Gα Subtype	PDB ID	Variant	Ligands	Space Group	Resolution (Å)	Ref
Gi	**Gα$_{i1}$**	1GDD	Wild-type	GDP	I 4	2.20	(4)
	Gα$_{i1}$	1AS3	G42V	GDP	I 4	2.40	(5)
	Gα$_{i1}$	3FFB	T329	GDP	I 4	2.57	(6)
	Gα$_{i1}$	3UMS	G202A	GDP	I 4	2.34	(7)
	Gα$_{i1}$	1Y3A	Wild-type-KB752	GDP	P 1 21 1	2.50	(8)
	Gα$_{i1}$	2ZJZ	K349P	GDP	P 21 21 2	2.60	(10)
	Gα$_{i1}$	1GIT	G203A	GDP-P$_i$	P 43 21 2	2.60	(11)
	Gα$_{i1}$	1AS0	G42V	GDP-P$_i$	P 32 2 1	2.00	(5)
	Gα$_{i1}$	1BOF	Wild-type	GDP/Mg^{2+}	I 4	2.20	(12)
	Gα$_{i1}$	1GFI	Wild-type	GDP-AlF$_4^-$/Mg^{2+}	P 32 2 1	2.20	(13)
	Gα$_{i1}$	1SVK	K180P	GDP-AlF$_4^-$/Mg^{2+}	P 32 2 1	2.00	(14)
	Gα$_{i1}$	3D7M	I56C/Q333C	GDP-AlF$_4^-$/Mg^{2+}	P 43 2 1	2.90	(15)
	Gα$_{i1}$	2G83	Wild-type-KB1753	GDP-AlF$_4^-$/Mg^{2+}	P 32 2 1	2.80	(16)
	Gα$_{i1}$	2ZJY	K349P	GDP-AlF$_4^-$/Mg^{2+}	P 32 2 1	2.80	(10)
	Gα$_{i1}$	1CIP	Wild-type	GppNHp	P 32 2 1	1.50	(9)
	Gα$_{i1}$	1SVS	K180P	GppNHp	P 32 2 1	1.50	(14)
	Gα$_{i1}$	1GIA	Wild-type	GTPγS/Mg^{2+}	P 32 2 1	2.00	(9)
	Gα$_{i1}$	1GIL	Q204L	GTPγS/Mg^{2+}	P 32 2 1	2.30	(13)
	Gα$_{i1}$	1AS2	G42V	GTPγS/Mg^{2+}	P 43 21 2	2.80	(5)
	Gα$_{i1}$	1BH2	A326S	GTPγS/Mg^{2+}	P 32 2 1	2.10	(25)
	Gα$_{i1}$	3FFA	T329	GTPγS/Mg^{2+}	P 32 2 1	2.30	(6)
	Gα$_i$	2XTZ	Wild-type (*A. thal*)	GTPγS/Mg^{2+}	P 21 21 21	2.34	(26)
	Gα$_i$	3QE0	G42R (*E. his*)	GDP/Mg^{2+}	P 61 2 2	3.00	(27)
	Gα$_t$	3V00	G56P	GDP	P 43 21 2	2.90	(29)
	Gα$_t$	1TAD	Wild-type	GDP-AlF$_4^-$/Ca^{2+}	P 1 21 1	1.70	(40)
	Gα$_t$	1TAG	Wild-type	GDP/Mg^{2+}	I 2 2 2	1.80	(42)
	Gα$_t$	1TND	Wild-type	GTPγS/Mg^{2+}	P 1 21 1	2.20	(43)
	Gα$_{i1}$βγ	1GG2	(G203A Gα$_{i1}$)(β$_1$)(C68S γ$_2$)	GDP	P 43	2.40	(46)
	Gα$_{i1}$βγ	1GP2	(Wild-type Gα$_{i1}$)(β$_1$)(C68S γ$_2$)	GDP	P 43	2.30	(46)
	Gα$_i$βγ	4FID	(Wild-type Gα$_i$)βγ	GDP	P 21 21 21	2.62	(50)
	Gα$_t$βγ	1GOT	(Wild-type Gα$_{t/i1}$)β$_1$γ$_1$	GDP	C 1 2 1	2.00	(2)
Gq	**Gα$_q$βγ**	3AH8	(Wild-type Gα$_{q/i1}$)β$_1$γ$_1$-YM254890	GDP	I 41	2.90	(52)
	Gα$_q$βγ	2BCJ	(Wild-type Gα$_q$)(β$_1$)(C68S γ$_2$)(S670A GRK2)	GDP-AlF$_4^-$/Mg^{2+}	P 1 21 1	3.06	(53)
G12	**Gα$_{12}$**	1ZCA	Wild-type	GDP-AlF$_4^-$/Mg^{2+}	P 1 21 1	2.90	(54)
	Gα$_{13}$	1ZCB	Wild-type	GDP	P 43 21 2	2.00	(54)
Gs	**Gα$_s$**	1AZT	Wild-type	GTPγS/Mg^{2+}	P 21 21 21	2.30	(55)
	Gα$_o$	3C7K	Gα$_0$-RGS16	GDP-AlF$_4^-$/Mg^{2+}	P 32 2 1	2.90	(57)
	Gα$_s$βγ	3SN6	(G72S Gα$_s$)(M1Q β$_1$)(C54T/C97A/M96T/M98T/N187E-γ$_2$)-(β2AR)	none	P 1 21 1	3.20	(1)
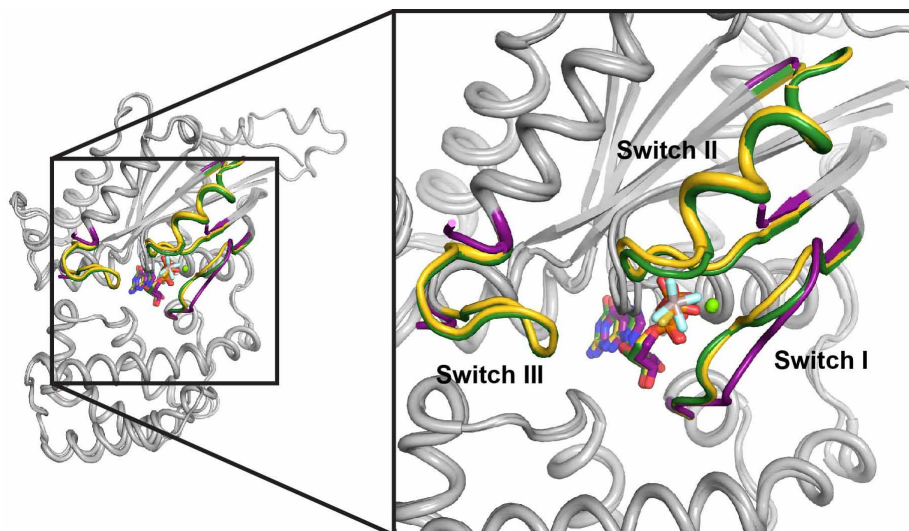
Figure 8: Conformational Diversity in Gα Switch Regions. Conformations of $G\alpha_{i1}$ Switch regions in the presence of GDP (*purple*; PDBID: 1GDD (4)), GTPγS (*green*; PDBID: 1GIA (9)), and GDP-AlF$_4^-$ (*yellow*; PDBID: 1GFI (9)). In GDP-bound $G\alpha_{i1}$, Switch II and III are inherently flexible and electron density corresponding to these regions in the crystal structure is disordered.

between residues of RGS4 and the nucleotide bound to $G\alpha_{i1}$. Notably, it was observed that RGS4 formed contacts with all three-switch regions in the $G\alpha_{i1}$ subunit. Mutagenesis confirmed that the residues comprising the RGS-Gα interface did not directly participate in GTP hydrolysis, but affected the efficiency of GTPase-promoting activity of RGS. Such mutations were found to decrease the binding affinity between RGS and Gα and Gα responsiveness, especially when mutations were introduced into the N-terminal helix of Gα (113). Mutagenesis of residues in switch II, however, highlighted the importance of a conserved glycine, such that its mutation nearly abolished RGS-enhanced hydrolytic activity (114). The conformation of switch II in the RGS4-$G\alpha_{i1}$ complex structure suggests that RGS-binding likely decreases switch II mobility, which contributes to a Gα conformation favoring GTP hydrolysis (112).

Thus, GPCRs act as agonists for G proteins by mediating GTP for GDP exchange and G protein activation, while RGS proteins acts as antagonists against G protein-

effector interactions by mediating GTP hydrolysis and G protein deactivation. Once GTP bound in the nucleotide-binding pocket is returned to GDP to form deactivated Gα, Gβγ can then recombine to form the inactive heterotrimer, thus completing the G protein signaling cycle.

Overview of Receptor-catalyzed Nucleotide Exchange

Biological Importance of Receptor-catalyzed Nucleotide Exchange in Gα

The rate-limiting step in G protein activation is GDP release from the Gα subunit of the heterotrimer and is catalyzed by interactions with an activated GPCR. Disruption of efficient GPCR-G protein coupling and activation of downstream signaling pathways can result in diseases such as diabetes insipidus, Hirschsprung's disease, and retinitis pigmentosa (115,116). In one example of congenital nephrogenic diabetes insipidus (CNDI), diagnosed patients cannot concentrate urine and thus present symptoms of severe dehydration (116). There are numerous mutations in the vasopressin receptor that affect kidney tissue permeability. This example of CNDI is caused by a mutation in a highly conserved arginine residue at position 137 in the vasopressin-activated vasopressin type 2 receptor (V2R). It has been demonstrated that the mutation has no effect on vasopressin binding affinity, but results in loss of adenylate cyclase stimulation mediated by the stimulatory heterotrimeric G protein, G_s (116). R137 is a well-characterized residue and an indispensible member of the ionic lock motif found near the cytoplasmic G protein binding site of GPCRs. An R137H mutation specifically affects the ability of V2R to couple to G_s (116). While the role of this particular mutation provides insight into the requirements of GPCR-catalyzed G protein activation, further characterization of

structural determinants in GPCR-G protein coupling is needed to understand the basis of pathophysiology observed in GPCR-related diseases caused by additional genetic variants (117).

Structural Determinants of Receptor-catalyzed Nucleotide Exchange in Gα

Prior to structural information gleaned from x-ray crystallography, techniques such as site-directed mutagenesis, peptide-mapping, and chemical crosslinking were used to demonstrate that the α4-β6 loop, α3-β5 loop, αN helix, N-terminus, and C-terminus of the Gα subunit as well as the C-terminus of the Gβ subunit all bind to the cytoplasmic surface of GPCRs (2,118-126). Once the crystal structure of transducin ($G\alpha_t\beta_1\gamma_1$) had been determined it became clear that that these structural motifs distantly arranged in the primary sequence formed a contiguous surface. While each individual sequence motif contributes to the stabilization of activated GPCRs, it is their three-dimensional arrangement that forms a stable surface on which the receptor can then bind and promote heterotrimeric G protein activation through catalysis of nucleotide exchange in the Gα subunit (**Figure 9**) (117,127).

Peptide mapping was used to identify the αN helix of the $G\alpha_t$ subunit, the N- and C-termini of the $G\alpha_t$ subunit, and the C-terminus of the $G\beta_1$ subunit of the heterotrimeric G_t (124,126,128). Peptides corresponding to the C-terminal region of $G\alpha_t$ were synthesized and examined for their ability to bind and compete with transducin for rhodopsin binding and stabilize activated rhodopsin in the meta II state using an extra meta II (128). This peptide corresponding to residues 340-350 of $G\alpha_t$ was shown by a spectrophotometric assay measuring metarhodopsin II formation and by a comptetition
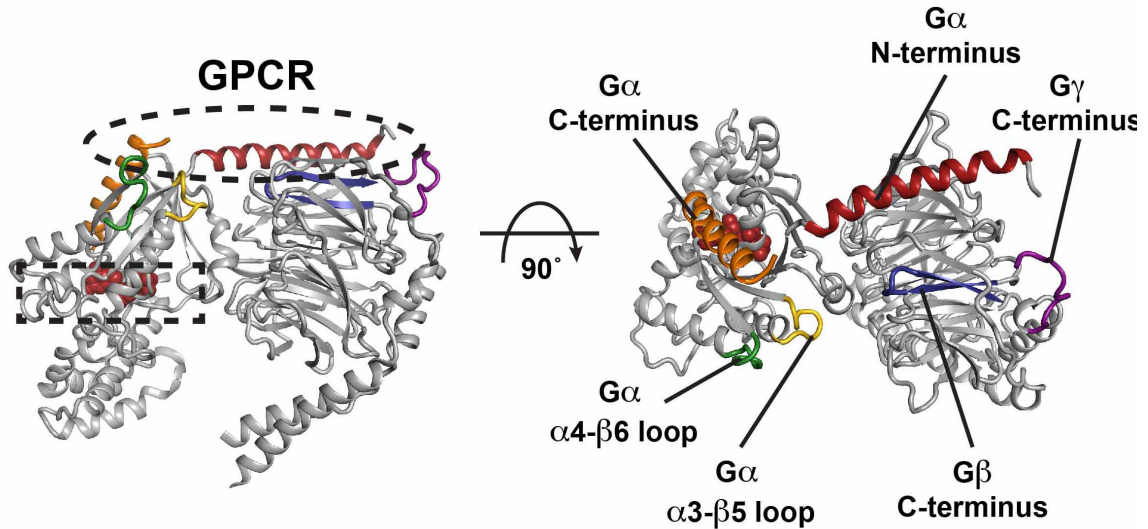
Figure 9: Receptor-binding Elements of the Heterotrimeric G protein. In the heterotrimer (PDBID 1GOT; (2)), the receptor-binding surface (*oval*) is composed of the N-terminus, C-terminus, α4-β6 loop, α3-β5 loop of the Gα subunit and the C-terminus of the Gβ and Gγ subunits and form a contiguous surface distal to the nucleotide-binding site (*box*) in the Gα subunit.

ELISA assay to compete with transducin for rhodopsin binding (117,122). In the same study, a peptide corresponding to residues 8-23 of the N-terminus of Gα$_t$ subunit was also found to bind rhodopsin (128).

Chemical crosslinking of a photoactivatable derivative of a peptide (DAP-Q) corresponding to intracellular loop III of the α$_2$ adrenergic receptor was used to map receptor binding to the N-terminus of the Gα subunit of G$_o$ and C-terminus of the Gβ subunit of G$_o$ (124,126). Chemical crosslinking was also used to confirm the role of the αN helix in the Gα$_t$ N-terminus and the α4-β6 loop of the Gα$_t$ C-terminus specifically in rhodopsin interactions (119,125). In these experiments, rhodopsin containing cysteine mutations in cytoplasmic loops was first treated with either chemically preactivated reagents or photoactivatable reagents and complexed with transducin. Then, trypsin-digested peptide fragments carrying the crosslinked chemical moieties were analyzed by matrix-assisted laser desorption ionization-time of flight (MALDI-TOF) mass

spectrometry (119,125). The αN helix, α3-β5 loop, and the α4-β6 loop of Gα subunits were additionally confirmed as sites of GPCR-interaction by mutagenesis and alanine-scanning (118,121,123).

While Gγ has not been shown to directly interact with the rhodopsin intracellular face, farnesylation of a peptide corresponding to 12 residues of the Gγ C-terminus has been found to contribute to meta II stabilization, which in turn drives ordering of the unstructured peptide upon binding (129,130).

Allosteric Mechanisms of Receptor-catalyzed GDP Release from Heterotrimeric G Proteins

All three subunits of the heterotrimeric G protein have been shown to form contacts with the cytoplasmic surface of activated GPCRs. While the Gα C-terminus has been recognized as a major interaction site, the absence of any one subunit adversely affects receptor-catalyzed nucleotide exchange in the heterotrimeric G protein. Therefore, when formulating the mechanism of receptor-catalyzed G protein activation, contributions from each subunit of the heterotrimer must be considered.

The α5 helix, found at the C-terminus of the Gα subunit, was previously shown in the x-ray crystal structure of the heterotrimeric G protein to form a direct connection from the major site of receptor interaction to the nucleotide-binding pocket in Gα (**Figure 7, 9**) (2). Mutagenesis to introduce a glycine linker between the α5 helix of Gα$_{i1}$ and its receptor binding C-terminus resulted in uncoupling of receptor binding and nucleotide exchange (131). This result led to a proposed mechanism of allosteric activation where receptor-induced perturbations of the α5 helix C-terminus destabilize nucleotide binding

using a rotation and translation of the α5 helix. Site-directed spin labeling (SDSL) and EPR of a recombinant Gα$_{i1}$ subunit labeled at sites along the α5 helix identified that GDP release requires a receptor induced rotation and translation of the α5 helix (131). A recombinant Gα$_{i1}$ double cysteine mutant I56C/Q333C that locks the α5 helix into the proposed receptor-bound conformation dramatically elevated nucleotide exchange in the absence of receptor and suggested that the α5 helix dipole is responsible for weakening stabilizing interactions between the bound nucleotide and the Gα (132).

While extensive research has allowed description of how activated receptors manipulate protein conformations in the Gα subunit to exert allosteric control of their preferred nucleotide binding state, much less is understood about how receptor interactions with the Gβγ subunit contributes to nucleotide exchange in Gα. Historically, two major hypotheses have been proposed: the gear-shift model and the lever-arm model. In the gear-shift model, it has been proposed that the Gβ subunit rotates into the GTP-binding domain of the Gα subunit, closing in on the Gα subunit, and providing the force necessary to push the helical domain away from the bound nucleotide, thus allowing GDP release. Mutagenesis experiments support this model of receptor-catalyzed activation of heterotrimeric G proteins (133,134). In the lever-arm model, nucleotide exchange is catalyzed by an activated receptor binding induced tilt of the βγ subunits relative to the α subunit (133,135). Specifically, the Gβγ dimer must interact with switch II connecting the helical domain of the α subunit to its GTPase domain, forming a lip that acts as an exit route for GDP when the tilt motion is induced. This allows the β subunit to act as a lever and opens the binding pocket for GDP release (133). This model was confirmed by engineering G proteins to mimic the tilted Gβγ conformation and

measuring the ability of mutant G proteins to regulate 2nd messenger production. EPR data showing flexibility in switch II at the Gα-Gβγ interface provides further support of this model (109,133).

New insights into the mechanism of G protein activation were revealed by two recent crystal structures of activated β2-adrenergic receptor (β2AR). The first structure was that of the activated form of the receptor stabilized by llama antibodies termed nanobodies (52). The second structure was that of the activated receptor stabilized by its physiological signaling partner, the Gα$_s$βγ heterotrimer (G$_s$) (53). Both structures exhibited conformational changes in transmembrane helices 5 and 6. The β2AR-G$_s$ structure additionally confirmed the stabilizing effects of Gαβγ association on the agonist-bound state of the receptor and the presence of a translation of the α5 helix of Gα. Unanticipated observations revealed by the β2AR-G$_s$ structure include ordering of intracellular loop 2 on β2AR, a lack of extensive contacts between the receptor and the Gβγ subunits of Gα$_s$βγ, and a large displacement of the helical domain relative to the Ras-like GTPase domain of Gα$_s$ (**Figure 10**). These data, taken together, offer a possible mechanism for receptor-catalyzed GDP release from Gαβγ that is largely consistent with the models suggested by biochemical and structural data obtained thus far (136,137).

Summary

The combined efforts of complementary biochemical, biophysical, and crystallographic studies have provided insight into the fundamentals of G protein activation. However, many of these findings inform on the endpoints, and much is yet to be understood about the transient features of the process. These include the underlying
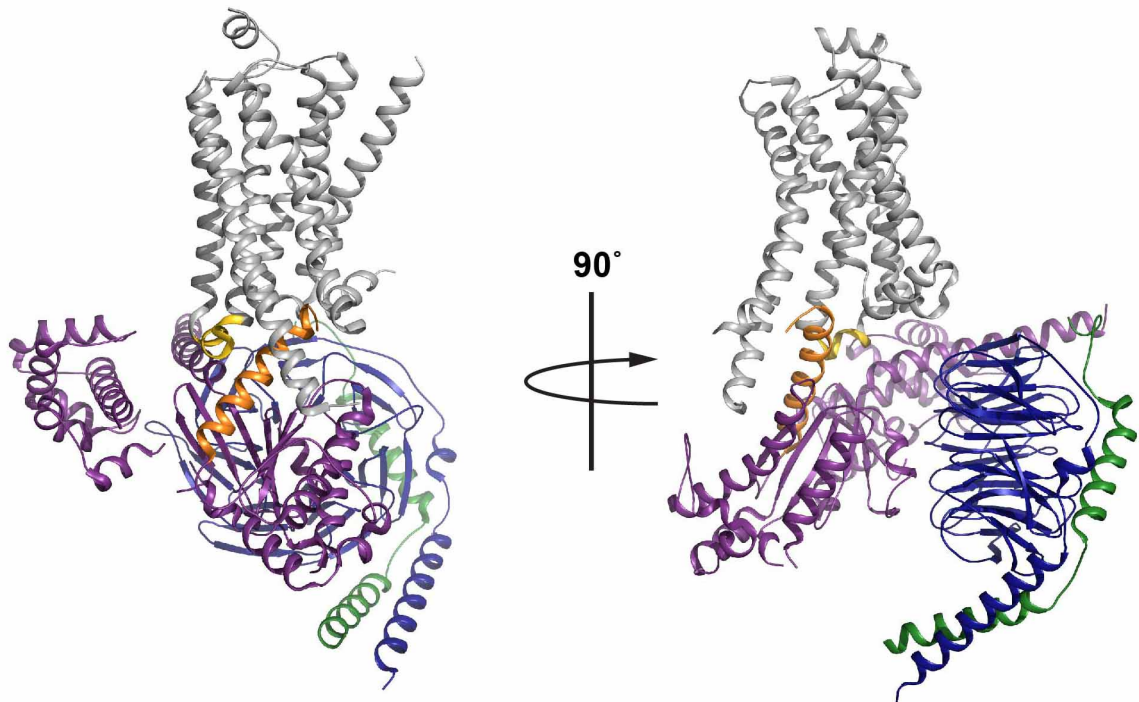
Figure 10. Overview of the β2-adrenergic-Gα$_s$βγ Complex Structure. The structure of the β2-adrenergic-Gα$_s$βγ complex (PDBID: 3SN6 (1)) is shown with Gα$_s$-stabilizing nanobody and the T4 lysozyme fusion protein removed for clarity. The α5 helix (*orange*) of the Gα$_s$ subunit (*purple*) is shown bound to the receptor (*gray*) and in close proximity to the receptor intracellular loop 2 (*yellow*). The Gβ (*blue*) and Gγ (*green*) subunits of the heterotrimeric G protein form expected contacts to Gα$_s$, but lack extensive interaction with the receptor.

mechanism of allostery employed in G protein activation, and how the many dynamic events that have been described coordinate together to facilitate the process of nucleotide exchange. In addition, much is yet to be learned about the determinants of GPCR-G protein specificity, the extent of receptor dimerization and its influence on G protein activation, the role of post-translational modifications in the regulation of G protein signaling, and until very recently, very little was also known about the nucleotide-free state of the G protein. The inherently transient nature of GPCR-G protein complexes and limitations in *in vitro* techniques available for studying such systems are the primary barriers to studying such aspects of G protein function. However, recent advances in

membrane protein biochemistry and structural biology have led to not only the successful determination of GPCR structures from 14 unique families over the last four years, but also the first ever structure of the receptor-bound G protein complex between the β2AR receptor and the G_s heterotrimer. While these events represent one of the biggest accomplishments in the study of receptor-mediated G protein regulation, it is important to continue working towards improving membrane protein technology and applying techniques that are presently available to the study of additional members of the GPCR and G protein superfamilies. In light of these recent advances, it is also important to revisit the results from previous studies and consider them in the context of such new structural and biophysical information. With this goal in mind, structural and biochemical studies such as those presented here attempt to contribute to the overall understanding of allostery in G protein function.

CHAPTER II

MATERIALS

Buffers and Salts

ADA (Fluka 00307), Ammonium sulfite monohydrate (Sigma-Aldrich 358983), Aluminum chloride (Aldrich 563919), Bis-tris (Sigma B9754), EDTA (Sigma-Aldrich E5134), Ferric chloride (Aldrich 451649), HEPES sodium salt (Sigma-Aldrich H7006), Magnesium chloride hexahydrate (Sigma-Aldrich M2670), Magnesium sulfate (Sigma-Aldrich M7506), MOPS (Sigma 69948), Potassium-sodium tartrate tetrahydrate (Sigma-Aldrich 217255), Sodium chloride (Sigma Aldrich S7653), Sodium fluoride (Sigma Aldrich S7920), Sodium succinate dibasic (Sigma-Aldrich 14160), Sodium phosphate monobasic (Sigma-Aldrich S0751), Sodium tartrate dihydrate (Sigma-Aldrich 228729), Sucrose (Sigma S0389), Tris base (Sigma-Aldrich T4661), Urea (Sigma U5378).

Detergents and Lipids

The following detergents were purchased from Anatrace: DM (D322) DDM (D310), LDAO (D360), MNG-3 (NG310), OG (0311). The follow detergents and phospholipids were purchased from Avanti Polar Lipids: DHPC (850345P), DMPA (830845P), DMPC (850305P), DMPG (840445P), DMPS (840033P), DOPA (840875P), DOPS, 7.7 MAG (850530), 7.8 MAG (850531). Additional detergents and phospholipids: CHAPS (Sigma C3023), CHAPSO (Sigma C3649), Monoolein (NuChek Prep M-239).

AMP-PnP (Sigma A2647), GDP (Sigma G7127), GTPγS (MP Biosciences 215903210), GTP (Sigma G8877), methyl-α-D-mannopyranoside (Sigma M6882).

Resins and Columns

Concanavalin A column (GE HealthScience 28-9520-85), HiTrap Blue HP sepharose (GE Life Sciences), Poros HQ50 column (Applied Biosystems 16817), Superdex 200 GL10/300 GL column (GE Life Sciences), TALON Cobalt Resin (Clontech 635502).

Miscellaneous

Dithiothreitol (DTT) (Sigma 43815), Ethylene glycol (Sigma-Aldrich 32558), Glycerol (Sigma 65516), Hexadecyltrimethylammonium chloride (HTAC) (Fluka 52366), Isopropyl-β-D-thiogalactoside (IPTG) (Sigma I6758), Kanamycin A (Kan) (Research Products Inc K22000), β-mercaptoethanol (β-ME) (Aldrich M6250), Pefabloc (Centerchem Inc), PEG2000 (Fluka 81321), Phenylmethanesulfonyl fluoride (PMSF) (Sigma 78830).

CHAPTER III

COUPLING EFFICIENCY OF RHODOPSIN AND TRANSDUCIN IN BICELLES

Introduction

Transient complexes between integral membrane receptors and their signaling partners mediate cellular responses to disparate signals and are of high biological importance. However, these complexes are challenging to study with *in vitro* biochemical methods, since purified receptors in detergent often have both reduced functional competence and lower affinity for their binding partners, as compared to receptors in native membranes. To help develop tools for the stabilization of membrane proteins with soluble signaling partners, we selected the GPCR rhodopsin and cognate G protein G_t as a model system. These proteins provide an ideal system for monitoring complex stability, since complex formation can be monitored spectrophotometrically.

Rhodopsin is highly enriched in the rod outer segment (ROS) membranes of the retina and is responsible for low-light vision. Rhodopsin itself consists of the apoprotein (opsin) and the chromophore, 11-cis-retinal, which binds to Lys296 and acts as an inverse agonist (47). Absorption of a single photon photoisomerizes 11-cis-retinal to all trans-retinal (ATR), which is an agonist for rhodopsin. Subsequent conformational changes within rhodopsin are associated with conversion to the metarhodopsin II (MII) state, which is evidenced by a shift in the wavelength of maximum absorbance by rhodopsin from 500 nm to 380 nm (138,139). MII binds to the GDP-bound form of cognate heterotrimeric G protein, transducin (G_t-GDP), and catalyzes the release of GDP from the

$G\alpha_t$ subunit, which is the rate-determining step of the G protein signaling cycle. In this high-affinity, rhodopsin-G_t(empty) complex, the activated receptor is thought to stabilize the nucleotide-free form of the Gα subunit, which, in turn, stabilizes the agonist-activated, MII form of rhodopsin. As a result, spectrophotometric monitoring of the MII signal can be used to measure formation of the catalytically competent rhodopsin-G_t(empty) complex.

Previous studies indicated that pH, temperature (140,141), and the presence of phospholipids (142-144) all influence the formation of the rhodopsin-G_t complex. Despite known dependence upon phospholipids, many biochemical assays investigating complex formation and G protein activation are conducted in detergent micelles that are relatively poor membrane substitutes for studying receptor signaling. Furthermore, the rhodopsin and G_t interaction is significantly disturbed when detergent solubilized rhodopsin is used in functional assays (143-145). Detergent micelles and native membranes differ in many of their physical properties including packing, curvature and charge distribution. Any of these factors may result in the observed decrease in G_t affinity for detergent-solubilized rhodopsin as compared to rhodopsin in rod outer segment membranes. Interestingly, the addition of phospholipids or fatty acids (phosphatidylcholine, phosphatidylserine, phosphatidylethanolamine or docosahexaenoic acid) to detergent solubilized rhodopsin has been shown to increase the stability and protein-protein interaction capability of rhodopsin (143,146-148). While mixing exogenous phospholipids with detergent solubilized rhodopsin has improved protein-protein interactions, the physical and structural properties of phospholipid-containing

31

micelles are heterogeneous, making the contributions from the above factors difficult to interpret.

A number of artificial membrane models (149-154) might be used to investigate the underlying mechanism by which native membranes stabilize the rhodopsin-G_t(empty) complex. Bicelles offer distinct advantages over other artificial membrane models since they can be easily manipulated in solution and compared to other phospholipid bilayer systems such as nanodiscs, bicelles are easily prepared with a high yield. Additionally, bicelles do not interfere with the majority of biophysical measurements, and have been shown to increase the stability of purified GPCRs as compared to receptors solubilized in detergent (149). Furthermore, in the last decade, bicelles have been successfully used in crystallization, resulting in structures for bacteriorhodopsin (150), the β_2-adrenergic receptor (151), xanthorhodopsin (152) and the mouse voltage dependent anion channel (153).

Bicelle morphology (**Figure 11**) is hallmarked by a disc-like bilayer composed of long chain phospholipids that are capped by either short chain phospholipids or detergents (155). While bicelle structure is highly dependent on lipid composition, temperature, pH and hydration, their biochemical properties can be influenced by phospholipid-specific differences in chain lengths, saturation, and head groups (155-158). Previous studies have shown that negatively charged phospholipids such as DMPS, DMPG or DMPA can be mixed with neutral phospholipids to prepare negatively charged bicelles (158-161), which are useful for studying the effect of negatively charged phospholipids on the activity of membrane proteins. In this study, we used bicelles to investigate the effects of membrane morphology, temperature, pH, and surface charge

density on the rhodopsin-G_t(empty) complex. Our results demonstrate that charge density

of the bilayer is important for the formation and stability of the high affinity complex.
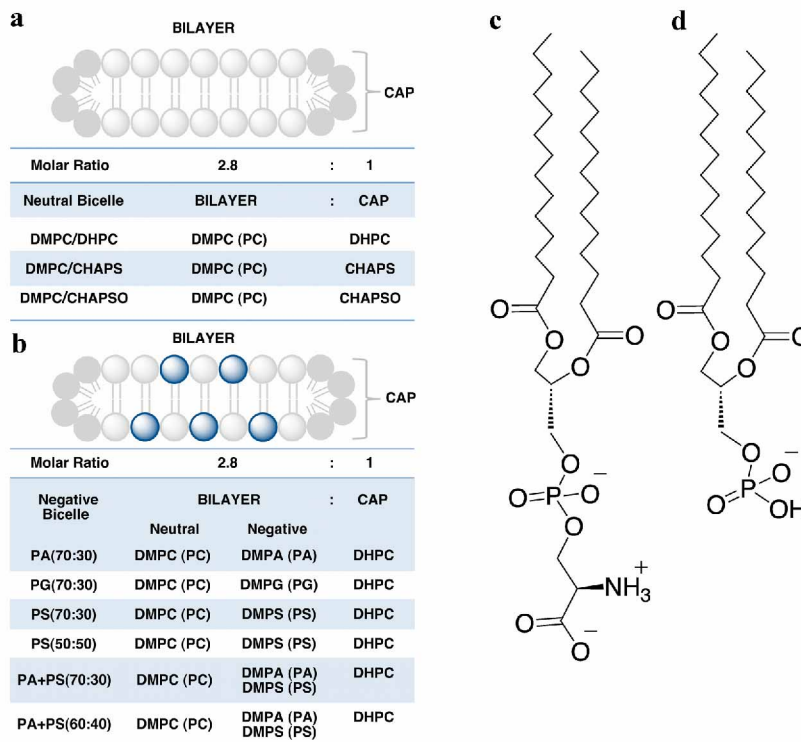
Figure 11: Bicelle Morphology and Composition. Bicelles are disc-like membrane structures composed of long-chain phospholipids and capped by either detergents or short-chained phospholipids. The radius of the disc is dependent on the long-chain phospholipid to detergent or short-chain phospholipid molar ratio (q ratio). The width of the bilayer is dependent on the acyl-chain length of the long-chain phospholipid. In this study, all bicelles compositions were prepared in a 2.8:1 phospholipid:detergent molar ratio with 14:0 phospholipids comprising the bilayer. **A)** Neutral bicelles were composed of DMPC bilayers capped with 6:0 DHPC, CHAPS, or CHAPSO. **B)** Negatively charged bicelles were composed of 14:0 phospholipids mixed with DHPC (6:0) in a 2.8:1 ratio. The ratio of neutral to negatively charged phospholipids is indicated within the parentheses in the graph. Schematic representation of **C)** DMPS and **D)** DMPA phospholipids.

33

Preparation of Urea Washed ROS Membranes

Under dim red light conditions, ROS membranes were stripped with 7 M urea as described (162). Briefly, ROS membranes were washed twice with EDTA buffer (10 mM Tris-HCl, 1 mM EDTA, 1 mM DTT, pH 7.5) and once with urea buffer (10 mM Tris, 1 mM EDTA, 1 mM DTT, 7 M Urea, pH 7.5). After the final wash, the membranes were resuspended in buffer A (10 mM MOPS, 200 mM NaCl, 2 mM $MgCl_2$, 1 mM DTT, 100 μM PMSF, pH 7.5) and aliquot stored at -80 °C.

Purification of Rhodopsin

Urea washed ROS membranes were solubilized in 50 mM Tris-HCl (pH 7.5) containing 100 mM NaCl and 20 mM DDM or 1% LDAO at 4 °C for 45 min. Insoluble material was removed by centrifugation at 20.000 x g for 1 hour at 4 °C. Detergent solubilized rhodopsin was purified by using Concanavalin-A chromatography as described (163). Briefly, the Concanavalin-A column was equilibrated with binding buffer (20 mM Tris-HCl, pH 7.4, 1 mM $MgCl_2$, 1 mM $CaCl_2$, 1 mM $MnCl_2$, 250 mM NaCl, 1 mM DTT, 0.5 mM DDM) for 48 hours at a flow rate 0.3 ml/min. Detergent solubilized rhodopsin was loaded onto the column in a continuous loop for 4 hours. The column was then washed with binding buffer (10 column volumes) and bound protein was eluted with 20 mM Tris-HCl, pH 7.4, 100 mM NaCl, 500 mM methyl α-D-mannoside and 0.5 mM DDM. Rhodopsin was concentrated using a 10 kDa cutoff concentrator and concentration of rhodopsin was determined by measuring the absorbance of rhodopsin at 500 nm before and after photo-bleaching. Molar extinction

coefficients of detergent solubilized rhodopsin and rhodopsin in ROS membrane were taken as 40.600 M^{-1} cm^{-1} and 42.000 M^{-1} cm^{-1}, respectively.

Transducin Purification

G_t, was prepared as previously described (164). Briefly, ROS membranes were washed four times with isotonic buffer (5 mM Tris-HCl, 130 mM KCl, 0.6 mM $MgCl_2$, 1mM EDTA, 1 mM DTT, pH 8.0) and two times with hypotonic buffer (5 mM Tris-HCl, 0.6 mM $MgCl_2$, 1mM EDTA, 1 mM DTT, pH 8.0). Membrane pellets were then washed twice with hypotonic buffer containing 0.1 mM GTP to release G_t from the membrane. Membranes were pelleted by centrifugation and the supernatant concentrated with a 10 kDa cutoff concentrator. Protein samples were dialyzed against a 20 mM Tris-HCl, pH 7.5, buffer containing 0.2 M NaCl, 10 µM GDP, 5 mM β-mercaptoethanol, 10% glycerol. Protein purity was assayed by SDS-PAGE, and protein concentration determined by Bradford assay (165).

Nucleotide Exchange Assay

Basal nucleotide exchange was determined by monitoring the intrinsic fluorescence (λ_{ex}: 300nm, λ_{em}: 340 nm) of 500 nM G_t in 10 mM MOPS buffer containing 130 mM NaCl, 1 mM $MgCl_2$ pH 7.2 for 40 min at 15 °C after addition of 10 µM GTPγS (166). Receptor mediated nucleotide exchange was determined in the presence of 500 nM light activated rhodopsin with and without addition of the indicated bicelle mixture. For bicelle experiments, dark rhodopsin was incubated with bicelles in a lipid:protein ratio of 64000:1 on ice for 45 min. before addition of G_t.

Extra Metarhodopsin II Stabilization and Decay Assay

Stabilization of extra MII was assessed as described (164). Briefly, 10 µM urea washed ROS membranes (or detergent solubilized rhodopsin) were incubated on ice for 15 minutes with 10 µM G_t. For bicelle experiments, detergent solubilized rhodopsin was incubated with the indicated bicelles in lipid:protein ratios ranging from 1600:1 to 12800:1 (1-8% final phospholipid concentrations) on ice for 45 min, followed by addition of varying amounts of G_t. Absorbance by rhodopsin-G protein complexes was scanned from 350 to 650 nm both before and after light activation in 50 mM HEPES (at the indicated pH) containing 0.1 M NaCl, 1mM $MgCl_2$, and 1mM DTT. In this assay, an initial dark-adapted spectrum was measured. Rhodopsin was then activated with a flash of light (activating only 10-15% of the rhodopsin). One minute after light activation a second, light adapted spectrum was collected. Rhodopsin absorption at 390 nm normalized to absorption data collected at 440 nm (the isosbestic point) was used to quantify MII formation. The extra MII signal was calculated as the difference between ΔA_{390} (light - dark) and ΔA_{440} (light - dark) (164,167-171). For determination of extra MII decay, dark adapted 10 µM rhodopsin was incubated on ice for 15 minutes with 10 µM G_t (at this concentration over 90% of rhosdopsin was coupled with G_t according to our assay system). Then, the protein sample was completely photobleached for 10 minutes under ambient light. Spectra for the bleached samples were measured every 20 minutes over a course of 6 hours, and then again after 24 and 48 hours. After 48 hours, HCl was added to a final concentration of 260 mM to protonate the retinal Schiff base in rhodopsin and liberate free retinal (164). The half lives of the samples were calculated by

fitting data to an exponential decay equation using GraphPad Prism v. 4.03 (GraphPad Software, San Diego, California).

Bicelle Preparation

Bicelles composed of saturated, long-chain (14:0) DMPC, DMPA, DMPG or DMPS and the detergents (6:0) DHPC, CHAPS, or CHAPSO were prepared as a 35% stock solution with a 2.8:1 lipid to detergent ratio (q ratio) using a procedure modified from (172). Neutral bicelles were composed of DMPC and DHPC, CHAPS, or CHAPSO to form DMPC:DHPC, DMPC:CHAPS, or DMPC:CHAPSO bicelles. Negatively charged bicelles were prepared by substituting a percentage of the total molar lipid content of the neutral bicelles with negatively charged DMPA, DMPG, or DMPS, while maintaining an overall 2.8:1 phospholipid to detergent ratio. The ratio of neutral to negatively charged phospholipids is indicated within the parentheses in Figure 1. A custom extrusion apparatus was used for mixing bicelles. The apparatus was constructed by connecting two 1 mL glass syringes with tubing capped with luer locks. To prepare a 1mL, 35% stock of DMPC:DHPC bicelles, 282.50 mg DMPC was added to one syringe. 337.5 μL of a 20% DHPC solution was mixed with 312.5 μL of water. 200 μL of the DHPC solution was then added to the syringe containing DMPC. The remaining DHPC solution was added to the other syringe. The bicelle mixtures were cycled through their phase transitions 4 times by incubating the entire apparatus at 4 °C and 55 °C. Bicelles were homogenized by extrusion after each incubation. Homogeneous bicelles were transferred into a microcentrifuge tube and centrifuged at 10.000 x g for 1 minute to

remove excess air bubbles. Correctly formed bicelles appeared clear at 4 °C and were stored at -20 °C. See Figure 11 for detailed information on the compositions prepared.

Dynamic Light Scattering

Dynamic light scattering measurements were collected at ambient temperatures (18-22 °C) using a DynaPro instrument (Protein Solutions, Inc). DDM detergent micelles, neutral bicelles, and negatively charged bicelles were prepared in a buffer containing 50 mM HEPES pH 8.0, 100 mM NaCl, and 1 mM $MgCl_2$. A 2 mg/mL Conalbumin protein standard was prepared in 50 mM HEPES pH 7.4. Scattering data reported are the averages of at least 25 scans with 3 independent experiments on 60 μL samples. Data were analyzed by Dynamics V5 software (Protein Solutions, Inc) and molecular translational diffusion coefficients, D_T, were calculated by fitting the data to an exponential autocorrelation function generated by Dynamics V5. The hydrodynamic radius, R_h, was then calculated as a function of the experimental D_T using the equation $D_T = kT/6\pi\eta R_h$, where k is the Boltzmann constant, T is the experimental temperature, and η is the solvent viscosity. R_h was calculated under the assumption that scattering particles conform to diffusion properties observed for globular proteins undergoing Brownian motion in an aqueous saline solution.

Data Analysis

Graphs and statistical analysis were performed using GraphPad Prism version 4.03 (GraphPad Software, San Diego, California).

Results

Formation of the Rhodopsin-G_t(empty) Complex in Detergent

While the formation of the rhodopsin-G_t(empty) complex in ROS membranes is relatively efficient, multiple groups have demonstrated a dramatically decreased yield of the complex when G_t is mixed with purified, detergent-solubilized rhodopsin (145,149,173). This result was recapitulated here with DDM. In our experimental setup, we took advantage of the ability of bound G_t to stabilize the activated MII state of rhodopsin, and monitored formation of the high affinity rhodopsin-G_t(empty) complex spectrophotometrically using the extra MII assay. As anticipated, we observed that the extra MII signal for DDM-solubilized rhodopsin was only 20.7 ± 1.2 % of the maximum signal observed for complex formation in ROS membranes (**Figure 12**), confirming the literature reports of inefficient complex formation in detergent (145,149,173).

Formation of the Rhodopsin-G_t(empty) Complex in Bicelles

Recent evidence supports a chemical role for phospholipids in formation of the rhodopsin-G_t(empty) complex (143,145); however, the influence of geometric constraints of the membrane bilayer has not previously been addressed. Unlike spherical micelles, bicelles mimic the morphology of phospholipid membranes [(**Figure 11**); (174,175)], and thus represent a suitable model system for testing the dependence of rhodopsin-G_t(empty) complex formation on membrane structure.

Our first experiments used well-defined neutral bicelles composed of DMPC:DHPC, DMPC:CHAPS, and DMPC:CHAPSO at a final concentration of 8% (w/v) (157,160,174,176). In the presence of all three bicelle compositions, the observed

extra MII signal from the rhodopsin-G_t(empty) complex was greater than it was in DDM

(**Figure 12**) and reached at least 43.4 ± 7.3 % of the maximum signal observed for

complex formation in ROS membranes.
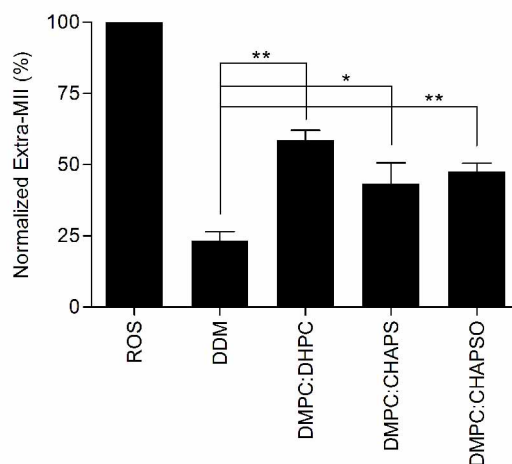
Figure 12: Neutral Bicelles Support Extra MII Sabilization. Normalized quantitation of extra metarhodopsin II in the absence or presence of neutral bicelles. The final concentration of bicelles was 8 %. Data were obtained at 4 °C and normalized to the extra-metarhodopsin signal measured in ROS membranes under the same conditions. Results are mean ± S.E.M. of three independent experiments (* $p < 0.05$; ** $p < 0.01$).

ROS membranes contain both phosphatidylcholine (PC) and phosphatidylserine

(PS) in a concentration of ~45% and ~15%, respectively (177-179). To assess the

contribution of phosphatidylserine phospholipids to rhodopsin-G_t(empty) complex

formation, we prepared bicelles doped with DMPS and capped by DHPC. In the initial

trials, the molar ratio of DMPC to DMPS was fixed at 97:3 (PS (97:3) bicelles). In the

presence of 8% PS (97:3) bicelles, the extra MII signal was 73.4% ± 15.6% of the extra

MII signal observed in ROS membranes, essentially the same as that observed in the

presence of DMPC:DHPC bicelles.

To test the effect of phosphatidylserine percentage in the bicelles on rhodopsin-G_t(empty) complex formation, the ratio of DMPS to DMPC was increased such that the DMPC:DMPS ratios were 70:**30** (PS (70:30) bicelles) and 50:**50** [(PS (50:50) bicelles, **Figure 11**)]. This further increased the yield of extra MII signal (**Figure 13A**) as compared to DDM-solubilized rhodopsin, resulting in 79.5% ± 5.2% of the ROS membrane signal in the PS (70:30) bicelles, and 87.4% ± 10.5% of the ROS membrane signal in the PS (50:50) bicelles. These data suggest that the concentration of PS indeed contributes to formation of functional rhodopsin-G_t(empty) complexes (**Figure 13A**).

Phosphatidylserine contains specific fatty acids and a negative charge associated with the head group. In GPCR signaling, non-specific electrostatic interactions between peripherally bound G proteins and the cell membrane influence the ability of the G protein to target to the membrane and guide its orientation on the membrane surface such that it is poised to interact with receptor (180-182). To deconvolute the contribution of chemical structure and negative charge that PS confers to the stabilization of the rhodopsin-G_t(empty) complex, we used bicelles containing negative charges from phosphatidic acid (PA). Although PA isn't an abundant component of ROS membranes, it is important for regulation and regeneration of 11-cis retinal (183) and in the photo-transduction pathway as a precursor in the regulation of diacylglycerol and phosphatidylinositol (184,185). The formation of the rhodopsin-G_t(empty) complex in 8% PA (97:3) bicelles was similar to that found in the presence of 8% PS (97:3) bicelles, and it wasn't significantly different from that measured in the presence of neutral bicelles. Similar to PS (70:30) bicelles, complex formation in the presence of 8% PA (70:30) was also improved, increasing complex formation to 85.9% ± 4% of that measured for ROS

(**Figure 13B**). This suggests that the negative charge of the surface of the membrane bilayer is of greater importance to the stabilization of rhodopsin-G_t(empty) complex than any specific chemical component. The phase transition properties of PA (50:50) and all
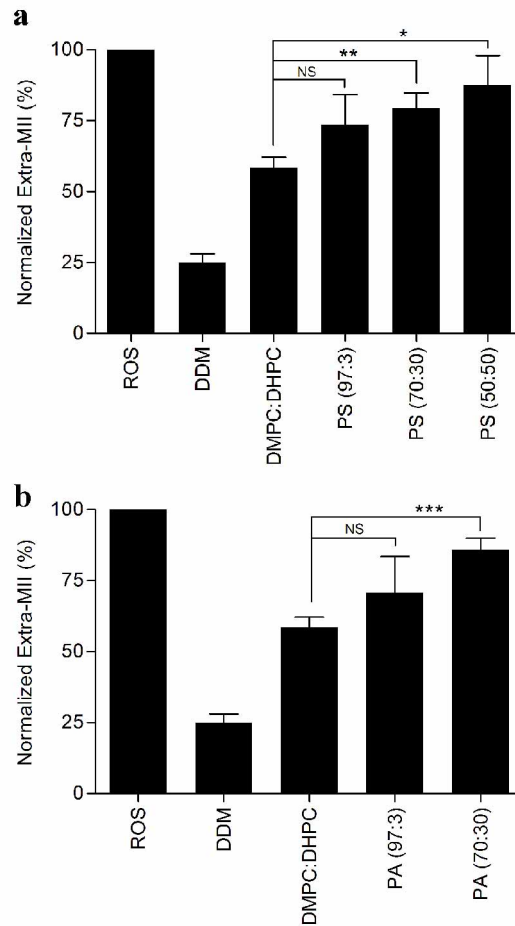
Figure 13: Anionic Lipid Enhances Extra MII Stabilization. Quantitation of extra-metarhodopsin II in the presence of different negatively charged bicelles. Extra-metarhodopsin II was assessed in the presence of **A)** DMPS or **B)** DMPA containing bicelles. The ratio of neutral to negatively charged phospholipids, DMPC:DMPS (or DMPA), was 97:3, 70:30 or 50:50 in these bicelles. The final concentration of bicelles was 8%. The average lipid:rhodopsin ratio was 12800:1. Data were collected at 4 °C and normalized to the extra-metarhodopsin signal measured in ROS membranes under the same conditions. Results are mean ± S.E.M. values of three independent experiments (* $p < 0.05$; ** $p < 0.01$; *** $p < 0.001$; NS, Not Significant).

bicelles containing negatively-charged phosphatidylglycerol precluded detection of extra MII formation because of difficulties in sample handling.

Rhodopsin activation is also dependent on the receptor:lipid ratio (186-188). We evaluated the limiting concentration of total lipid, as well as the ratio of neutral to negatively charged lipids, required to stabilize extra MII formation. We decreased the concentrations of PS (70:30), PA (70:30), and PS (50:50) bicelles from 8% to 4%, and phospholipids were reduced from 2% to 1%, and we then assessed their ability to stabilize extra MII formation. The change in extra MII signal in the presence of decreasing total concentrations of PS (70:30), PS (50:50), and PA (70:30) phospholipids was not statistically significant between 8% and 1% (**Figure 14A**). This suggests that total phospholipid concentration is not a determinant of rhodopsin-Gt(empty) complex formation in the context of our assay.

To test the effect of different head groups in the negatively charged bicelle preparations on rhodopsin-Gt(empty) complex formation, PA and PS bicelles were mixed together to form a composition containing both PA and PS in the bicelle bilayer. The final concentration of negatively charged bicelles was 8% (4% PA + 4% PS bicelles). The yield of extra MII signal was further increased. We observed 94.3% ± 3.76 % of the ROS membrane signal in the presence of PA + PS (70:30) bicelles and 96.4% ± 3.50 % of the ROS membrane signal in the presence PA + PS (60:40). While not statistically significant, there was nevertheless a trend towards greater extra MII formation using a combination of PA and PS in bicelles, compared to bicelle preparations containing either PA or PS (**Figure 14B**).
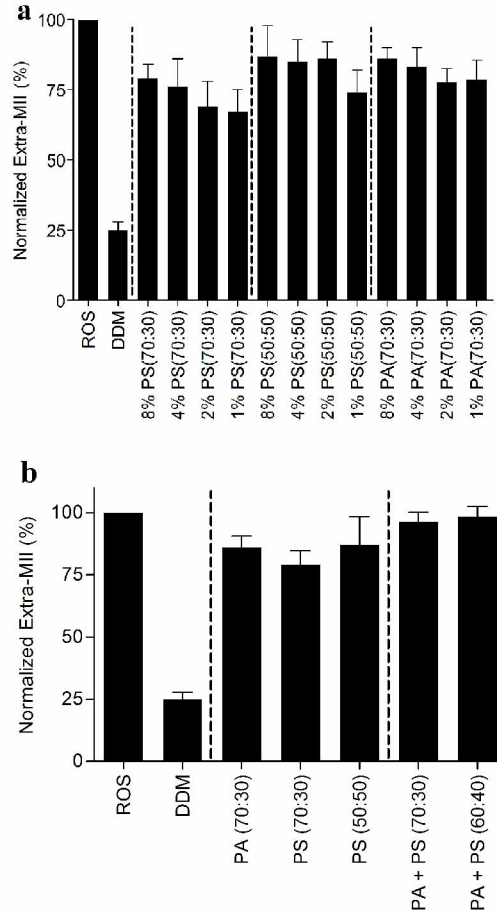
Figure 14: Complex Mixtures of Anionic Lipids in Bicelle Preparations. The effect of bicelle concentration on rhodopsin-G_t(empty) formation. **A)** The effect of varying concentrations of PS (70:30), PS (50:50) and PA (70:30) bicelles on rhodopsin-G_t(empty) complex formation. Final concentration of bicelles was decreased from 8% to 4% and phospholipids concentration decreased from 2% to 1% (with lipid:rhodopsin ratios of 12800:1 to 1600:1) as indicated in the graph. **B)** The effect of mixing PA and PS bicelles on rhodopsin-G_t(empty) formation. The final concentration of negatively charged bicelles was 8% (4% PA + 4% PS bicelles). The average lipid:rhodopsin ratio was 12800:1. The ratio of neutral to negatively charged phospholipids is indicated within parentheses in the graph. Data were collected at 4 °C and normalized to the extra-metarhodopsin signal measured in ROS membranes under the same conditions. Results are mean ± S.E.M. values of three independent experiments.

Characterization of Negatively-charged Bicelles by Dynamic Light Scattering

Since not much is known regarding the morphology of bicelles containing

negatively charged lipids, we verified that the addition of the negatively charged lipids

did not disrupt bicelle formation using dynamic light scattering techniques. In neutral

44

bicelles, dynamic light scattering experiments (156,189,190), NMR (155,156,174,189) and atomic force microscopy (156) have been used to characterize bilayer properties. Hydrodynamic radii have been determined for DMPC:DHPC bicelles, and NMR studies have confirmed that their morphology exhibits a disc-like planar bilayer at concentrations of 3% and higher (174,189,191), while concentrations of DMPC:DHPC below 3% may be more indicative of a vesicular morphology (174). The presence of charged phospholipids has been shown to directly affect the physical properties of phospholipid membranes, but their effects on bicelle morphology and size are largely unknown (192,193). Dynamic light scattering (DLS) was performed to determine the homogeneity and molecular size of negatively charged bicelles compared to neutral bicelles (**Figure 15**). All DLS measurements were performed between 18-22 °C. Although data collection at temperatures used in the functional experiments performed in this study (4 °C and 15 °C) would have been ideal, technical limitations restricted these measurements to ambient temperatures. The calculated hydrodynamic radii derived from translational diffusion coefficients for scattering detergent micelles (190) and DMPC:DHPC bicelles were comparable to those previously reported (**Figure 15**) (189,191). Compared to neutral bicelles, negatively charged bicelles exhibited larger hydrodynamic radii in solution (**Table 2**). The hydrodynamic radii of 8% PA (70:30), PS (70:30), and PS (50:50) bicelles were determined to be 5.7 ± 0.1 nm, 5.4 ± 0.1 nm, and 5.4 ± 0.3 nm, respectively (**Figure 15**). Introducing heterogeneity into the negatively charged lipid content did not affect the bicelle size; 8% PA+PS (70:30), PA+PS (60:40) bicelles were determined to have hydrodynamic radii of 5.4 ± 0.1nm and 5.4 ± 0.1 nm, respectively (**Figure 15**). Consistent with previous studies on DMPC:DHPC bicelles (174), decreasing the bicelle
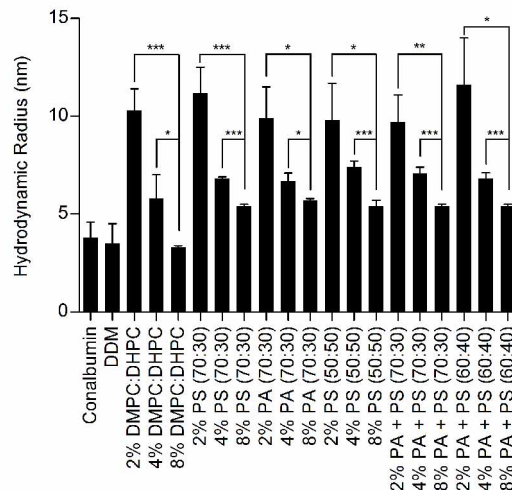
Figure 15: Dynamic Light Scattering Measurements on Negatively-charged Bicelles. Data was collected on samples at final phospholipid concentrations of 2%, 4%, and 8% in solution. All samples were prepared in extra MII assay buffer (50 mM HEPES pH 8.0, 100 mM NaCl, 1 mM MgCl$_2$). 2 mg/mL Conalbumin (75 kDa) and 0.5 mM DDM (70 kDa) were prepared as positive controls. Hydrodynamic radii were determined by Dynamics V5 software, with light scattering data collected at 18-22°C on a DynaPro detector. The ratio of neutral to negatively charged phospholipids is indicated within the parentheses in the graph. Results are are means ± S.E.M. of at least 25 scans with two independent experiments (* $p < 0.05$; ** $p < 0.01$; *** $p < 0.001$; NS, Not Significant).

concentration below 3% dramatically affected their size. The hydrodynamic radii in the presence of a total lipid concentration of 2% for neutral or negatively charged compositions were over 12 nm, a size more typically observed in large vesicles, suggesting that the lipids no longer aggregate into disc-like bicelle membranes (**Table 2**) at ambient temperatures required for DLS measurements. While this may not be the case at lower temperatures used in our functional studies, we nevertheless chose to focus the remainder of our studies on complex formation in the 8% bicelle system, which maintain a disk like bicelle structure according to our DLS measurements.

Having identified bicelle compositions that allow the efficiency of rhodopsin-G$_t$(empty) complex formation to approach that observed in ROS membranes, we next

Table 2: Dynamic Light Scattering Measurements of Negatively-charged Bicelles[a]

Bicelle Composition	D$_T$ (10^{-9}cm^2/s)	R$_h$ (nm)	MW (kDa)	PolyD (nm)	% PolyD	PolyD Index
Conalbumin	659.9	3.8	74.4	0.8	21.4	0.1
DDM	737.2	3.5	65.2	1.0	27.6	0.1
2% DMPC:DHPC	198.6±14.9	10.3±1.1	816.8±207.2	2.6±0.8	25.5±8.0	0.1±0.1
4% DMPC:DHPC	384.9±104.6	5.8±1.2	232.0±87.4	1.3±0.6	20.6±6.5	0.1±0.1
8% DMPC:DHPC	641.4±28.3	3.3±0.1	55.6±2.2	0.3±0.1	8.1±4.1	0.0
2% PS (70:30)	201.5±7.1	11.2±1.3	996.7±265.8	3.4±0.6	29.6±2.1	0.1±0.0
4% PS (70:30)	307.8±13.9	6.8±0.1	292.3±12.7	1.1±0.1	16.5±2.0	0.0
8% PS (70:30)	370.6±5.7	5.4±0.1	1721±3.5	0.7±0.2	13.2±2.7	0.0
2% PA (70:30)	222.2±10.9	9.9±1.6	769.4±292.2	2.7±0.9	26.1±4.6	0.1±0.1
4% PA (70:30)	327.2±18.2	6.7±0.4	290.6±42.1	1.7±0.1	26.5±3.7	0.1±0.1
8% PA (70:30)	373.8±4.1	5.7±0.1	194.4±7.9	1.4±0.1	24±1.6	0.1 ± 0.1
2% PS (50:50)	252.2±33.8	9.8±1.9	794±375.1	2.7±0.5	27.5±1.8	0.1±0.1
4% PS (50:50)	279.6±21.6	7.4±0.3	369±31.2	1.1±0.3	15±3.4	0.0
8% PS (50:50)	380±21.5	5.4±0.3	177.8±22.4	1.2±0.1	22.8±2.7	0.1±0.1
2% PS+PA(70:30)	230.4±21.1	9.7±1.4	742.4±244.	2.7±0.6	26.5±2.6	0.1±0.1
4% PS+PA(70:30)	297.0±15.9	7.3±0.3	350.2±31.0	1.6±0.1	21.6±0.7	0.1±0.1
8% PS+PA(70:30)	387.5±6.1	5.4±0.1	171.7±5.9	1.4± 0.1	26.4±1.5	0.1±0.1
2% PS+PA(60:40)	197.5±24.2	11.6±2.4	1188±574.7	3.0±1.0	24.2±3.5	0.1±0.1
4% PS+PA(60:40)	309.9±17.6	6.8±0.3	300.5±33.9	1.6±0.2	23.6±3.9	0.1±0.1
8% PS+PA(60:40)	386±3.4	5.4±0.1	171.4±1.7	1.5±0.1	28.7±1.3	0.1±0.1

[a]All bicelle samples were prepared in extra MII assay buffer (50 mM HEPES pH 8.0, 100 mM NaCl, 1 mM MgCl$_2$). 2 mg/mL Conalbumin (75 kDa) and 0.5 mM DDM (70 kDa) were prepared as positive controls. Hydrodynamic radii were determined by Dynamics V5 software with light scattering data collected at 18-22 °C on a DynaPro detector. The final concentration of phospholipids was 2%, bicelles was 4 or 8%. The ratio of neutral to negatively charged phospholipids is indicated within the parentheses in the table. Results are means ± S.E.M. of at least 25 scans with three independent experiments.

measured the affinity of this complex using the extra MII assay comparing ROS membranes, DDM detergent, and various bicelle compositions (**Figure 16**). Consistent with previous studies (164), the EC$_{50}$ value of G$_t$ for rhodopsin in ROS membranes was 0.64 ± 0.09 µM (**Table 3**). As anticipated, DDM-solubilized rhodopsin exhibited a significant decrease in the affinity between rhodopsin and G$_t$, with an increased EC$_{50}$
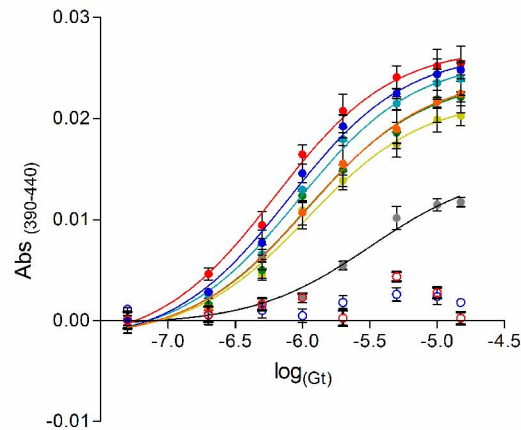
Figure 16: Effect of Negatively-charged Bicelles on the Affinity of G_t for Rhodopsin. Concentration-response curves of MII signal stabilized by G_t in the presence of different mixtures of bicelles at a final concentration of 8 % (lipid:rhodopsin ratio of approximately 12800:1). The concentration-response curves were measured at 4 °C and curves are presented for (red) ROS, (empty red circle) ROS + 150 μM GTPγS, (grey) soluble rhodopsin (DDM), (light green) PS (70:30), (green) PS (50:50), (orange) PA (70:30), (light blue) PA+PS (70:30), (dark blue) PA+PS (60:40), (empty dark blue circle) PA+PS (60:40) + 150 μM GTPγS. Solid curves are best fits from a four parameter logistic equation. See Table 3 for estimated EC_{50} values. Results are mean ± S.E.M. from of at least three independent experiments.

value of 3.14 ± 0.05 μM (**Table 3**). Bicelle-solubilized rhodopsin exhibited an intermediate affinity for G_t. In the presence of either PA (70:30) or PS (70:30) bicelles, G_t had an EC_{50} value for rhodopsin of 1.08 ± 0.12 μM and 1.08 ± 0.09 μM, respectively. Increasing the negative charge density by using PS (50:50) bicelles did not alter this affinity (EC_{50} of 1.07 ± 0.07 μM). Heterogeneity of the negatively charged lipid content improved the affinity of G_t for rhodopsin, and the EC_{50} value decreased to 0.94 ± 0.05 μM in the presence of PA+PS (70:30) bicelles. However, the affinity of G_t for rhodopsin was most comparable to that measured in ROS membranes in the presence of heterogeneous PA+PS (60:40) bicelles, where the EC_{50} value was 0.79 ± 0.05 μM. This suggests that variations in both phospholipid head group and charged density of bicelles affect the affinity between rhodopsin and G_t.

Table 3. The affinity of G_t for Rhodopsin in the Presence or Absence of Bicelles[a]

	$EC_{50} \pm$ S.E.M. (μM)	n
ROS	0.64 ± 0.09	6
DDM	3.14 ± 0.05	4
PA(70:30)	1.08 ± 0.12	3
PS(70:30)	1.08 ± 0.09	3
PS(50:50)	1.07 ± 0.07	4
PA+PS(70:30)	0.94 ± 0.06	3
PA+PS(60:40)	0.79 ± 0.05	3

[a]The concentration response curves were measured at 4 °C in the presence of different amount of G_t. Final concentration of bicelle was 8% (lipid:rhodopsin ratio of approximately 12800:1). The ratio of neutral to negatively charged phospholipids is indicated with parenthesis in the table. The concentration-response curves were analyzed using a four parameter logistic equation. Results are mean ± S.E.M. values from at least three independent experiments.

The rhodopsin-G_t(empty) complex rapidly disassociates when GTP binds to the empty nucleotide binding pocket, which is observed as a decrease in the extra MII signal. As a control for formation of functional complexes in bicelles, rhodopsin-G_t(empty) complexes from the previous experiment were incubated with excess GTPγS. As expected, a loss in the extra MII signal was observed (**Figure 16, open circles**), confirming that the rhodopsin-G_t complex was functional.

Half-life of the Rhodopsin-G_t(empty) Complex in Bicelles

The half-life of rhodopsin-G_t(empty) in the presence of negatively charged bicelles was next measured as a function of extra MII decay over time and compared to the half-life of the complex in ROS membranes and DDM. The half-life of rhodopsin-G_t(empty) was 0.63 ± 0.01 days in ROS membranes versus 0.07 ± 0.01 day in DDM

micelles at pH 8.2 and 4°C. This confirms that detergent solubilization not only affects the formation efficiency of rhodopsin-G_t complexes, but also their stability. A remarkable increase in the half-life of rhodopsin-G_t(empty) complexes was observed in the presence of several bicelle compositions at pH 8.2 and 4°C (**Figure 17A, Table 4**). PA (70:30), PS (70:30), and PS (50:50) bicelles extended the half-life to 5.4 ± 0.2, 5.8 ± 0.3 and 5.8 ± 0.3
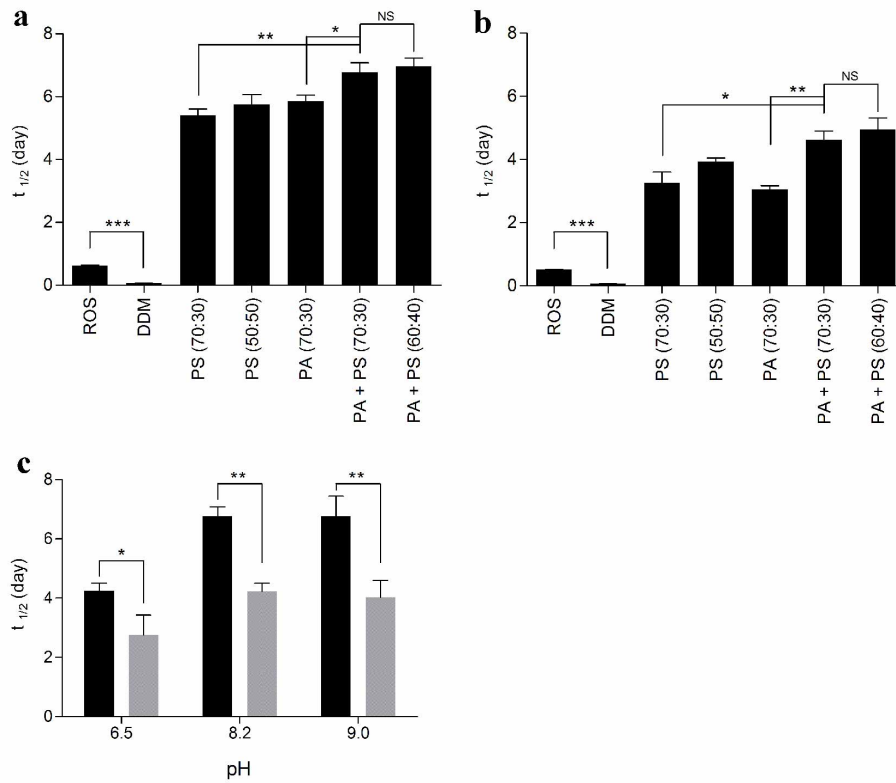
Figure 17: Stability of Rhodopsin-G_t(empty) Complex in the Presence of Negatively-charged Bicelles. The effect of negatively charged bicelles on complex stability was evaluated at **A)** 4 °C and **B)** 15 °C. **C)** The effect of pH on complex stability at 4 °C (black bars) and at 15 °C (grey bars) in the presence of PA+PS (70:30) bicelles. Final concentrations of PA+PS (70:30) bicelles were held constant at 8% (lipid:rhodopsin ratio of approximately 12800:1). The ratio of neutral to negatively charged phospholipids is indicated within the parentheses in the graph. The half-life of extra MII signal was calculated by using an exponential decay equation. Results are mean ± S.E.M. values from at least three independent experiments (* $p < 0.05$; ** $p < 0.01$; *** $p < 0.001$; NS, Not Significant).

Table 4: The Rate of Extra MII Decay in the Presence of Negatively-charged Bicelles[a]

	4 °C, pH 8.2	15 °C, pH 8.2
	$t_{1/2} \pm$ S.E.M. (day)	$t_{1/2} \pm$ S.E.M. (day)
ROS	0.6 ± 0.01	0.5 ± 0.01
DDM	0.1 ± 0.01	0.1 ± 0.5
PS(70:30)	5.4 ± 0.2	3.3 ± 0.3
PS(50:50)	5.8 ± 0.3	3.9 ± 0.1
PA(70:30)	5.9 ± 0.2	3.1 ± 0.1
PA+PS(70:30)	6.8 ± 0.3	4.6 ± 0.3
PA+PS(60:40)	7.0 ± 0.3	4.9 ± 0.4

[a]The extra-metarhodopsin II decay was measured at 4 °C and 15 °C. The final concentration of each bicelle mixture is 8% (lipid:rhodopsin ratio of approximately 12800:1). The ratio of neutral to negatively charged phospholipids is indicated within parentheses. The half life of extra MII signal was calculated using an exponential decay equation. Results are mean ± S.E.M. values from at least three independent experiments.

days, respectively. The half-life of the rhodopsin-G_t(empty) complex increased further to

6.8 ± 0.3 days in PA+PS (70:30) bicelles and 7.0 ± 0.3 days for PA+PS (60:40) bicelles.

This result was not surprising, because while not statistically significant, we did observe

a trend towards greater extra MII formation using the mixture of negatively charged

lipids, and over the time span of decay experiments, the mixture of negatively charged

lipids were found to be significantly enhanced over that seen using either negatively

charged lipid alone. As a control, we incubated the samples at the end of the decay

experiments in GTPγS (**Figure 18**), confirming that rhodopsin and G_t are both functional

and form a reversible complex within these bicelles. The differences observed in the

affinity and stability experiments reflect differences between how these experiments are
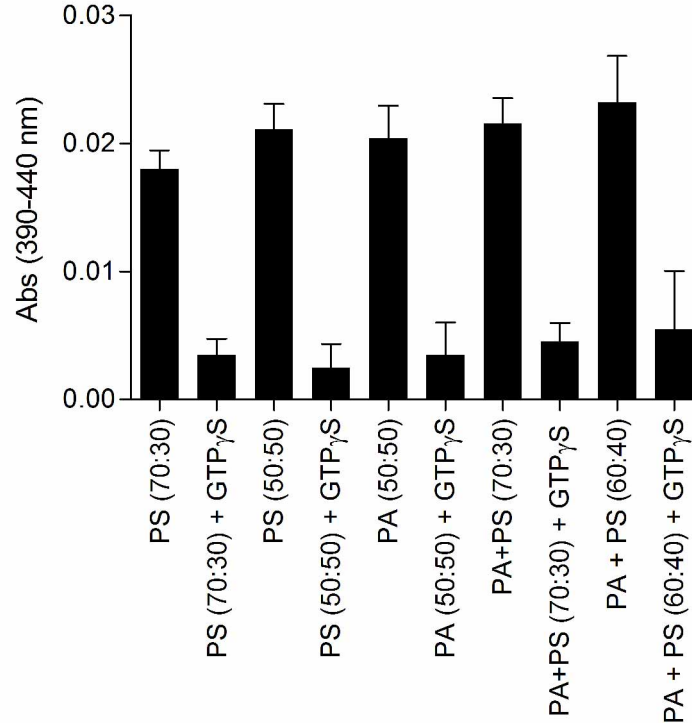
Figure 18: Extra MII Decay Measured at 4 °C and pH 8.2. To test Receptor-G protein coupling, we added excess GTPγS which terminates receptor-G protein interaction, and we measured this loss of coupling as the loss of the extra-MII signal. We added 150 μM GTPγS 48 hours after starting from the decay experiment. Then, after 5 min. incubation with GTPγS, we measured extra-metarhodopsin signal again. The final bicelle concentration is 8%. Results are mean ± S.E.M. values of at least three independent experiments.

performed; while affinity assays roughly reflect EC_{50} values, stability assays are conducted using greater than EC_{90} values of Gt. Furthermore, affinity assays employ rhodopsin that is 10-15% bleached, versus 100% bleached rhodopsin used in decay assays. Nevertheless, both experiments provide important information regarding the affinity and stability of the rhodopsin-G_t(empty)complex.

Since the MII state of rhodopsin is the physiologically relevant binding partner of G_t (141), stabilization of MII is likely to improve the half-life of the rhodopsin-G_t(empty) complex. Previous studies have demonstrated that temperature and pH influence the half-

life of the rhodopsin-G_t complex (140,141,194), perhaps reflecting changes in stability of MII and/or changes in membrane fluidity and protein dynamics. Increasing the temperature decreased the half-life of the rhodopsin-G_t(empty) complexes formed in the presence of all compositions of bicelles tested by at least 1.5-fold, as compared to results obtained at 4 °C (**Figure 17B**, **Table 4**).

The effect of bicelle concentration on the stability of rhodopsin-G_t(empty) complex was tested in the presence of both 2% phospholipids and 8% negatively charged bicelles at different temperatures. The half life of the rhodopsin-G_t(empty) complex was decreased when the concentration of phospholipids decreased from 8% to 2% (**Figure 19**). This result, taken together with the DLS data, suggests that that membrane structure is an important factor for rhodopsin-G_t(empty) complex stability.
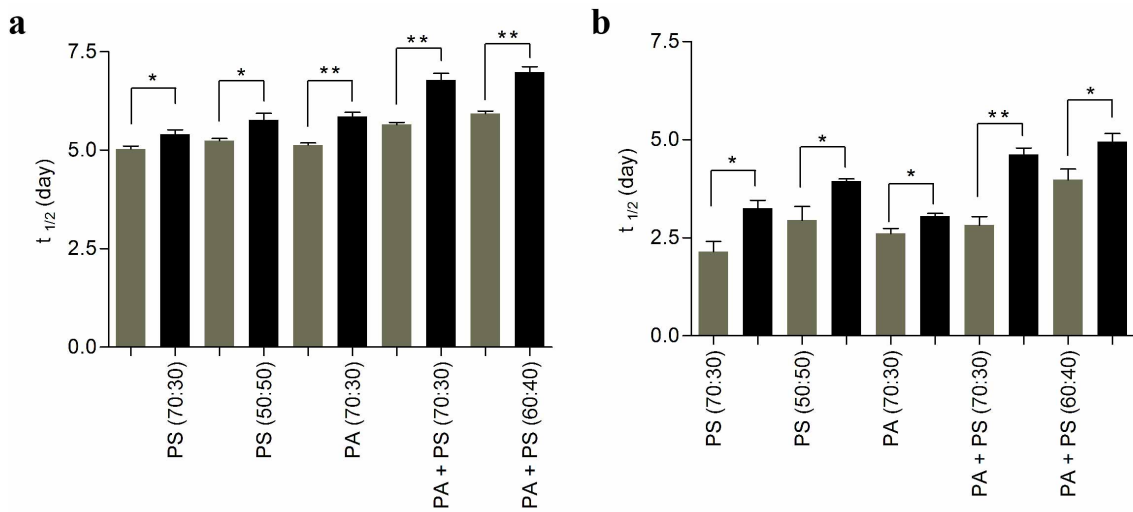
Figure 19: Stability of Rhodopsin-G_t(empty) Complex in the Presence of Negatively-charged Bicelles. The effect of negatively charged bicelles on complex stability was evaluated at **a)** 4 °C and **b)** 15 °C. The final concentration of phospholipids was 2% (grey bars), bicelles was 8% (black bars). The lipid:rhodopsin ratio was approximately 12800:1. The ratio of neutral to negatively charged phospholipids is indicated within the parentheses in the graphs. The half-life of the extra MII signal was calculated by using an exponential decay equation. Results are mean ± S.E.M. values from at least three independent experiments (* $p < 0.05$; ** $p < 0.005$).

The stability of rhodopsin-Gt(empty) complexes in PA+PS (70:30) bicelles was additionally tested for pH-dependence (Figure 7C). A decrease in pH from 8.2 to 6.5 at 4 °C resulted in a 1.5 fold decrease in the complex half-life. This was much longer than the half-life of the complex in ROS membranes (164), suggesting that extra MII instability at pH 6.5 is not a property of extra MII only but of the native membrane environment. While increasing the pH from 8.2 to 9.0 at 4 °C had a negligible effect on stability (**Figure 17C**, **black bars**), increasing the temperature had a more pronounced effect. Increasing the temperature from 4 to 15 °C resulted in a nearly 1.5 fold decrease in the half-life of the complex, regardless of pH value tested (**Figure 17C, grey bars**).

It is well established that the addition of excess ATR to rhodopsin can activate rhodopsin and stabilize the MII state (195,196). Accordingly, we measured the half-life of rhodopsin-G_t(empty) complex in the presence of 1.5 fold molar excess of ATR in both ROS and in a negatively charged phospholipid preparation. Not surprisingly, the half life of complex increased from 0.62 ± 0.01 to 0.97 ± 0.03 days at 4 °C in presence of ROS membranes, and in our 2% PA+PS (60:40) phospholipid preparation, addition of ATR increased the half life of the complexes to 4.0 ± 0.5 days at 15 °C. Lowering the temperature to 4 °C further extended the half life to 7.2 ± 0.2 days in this lipid preparation. These data are consistent with ATR's ability to stabilize the rhodopsin-G_t(empty) complex, similar to reported effects of ATR on MII stability.

Receptor-catalyzed Nucleotide Exchange in the Presence of Bicelles

Previous studies have shown that the addition of phosphatidylcholine, phosphatidylserine or phosphatidylethanolamine exerts differential effects on receptor-

catalyzed nucleotide exchange in the Gα subunit of the G protein, with G$_t$ activation rates altered specifically by the presence of phosphatidylserine (145). To evaluate the effect of our optimized bicelle compositions on G$_t$ function, the receptor-catalyzed nucleotide exchange rate was determined using an intrinsic tryptophan fluorescence assay (**Figure 20**), which reflects the ability of an activated receptor to stimulate GDP-GTP exchange on the G protein. The nucleotide exchange rates in PA (70:30), PS (70:30), or PS (50:50) bicelles were similar to those observed in ROS membranes (**Table 5**). Additionally, heterogeneity of negatively charged bicelles enhanced rates of G protein activation. The nucleotide exchange rate in the presence of PA+PS (70:30) and PA+PS (60:40) were measured 4.62 ± 0.30 and 4.48 ± 0.51 (1/sec x 10^{-2}), respectively (**Figure 20, Table 5**).
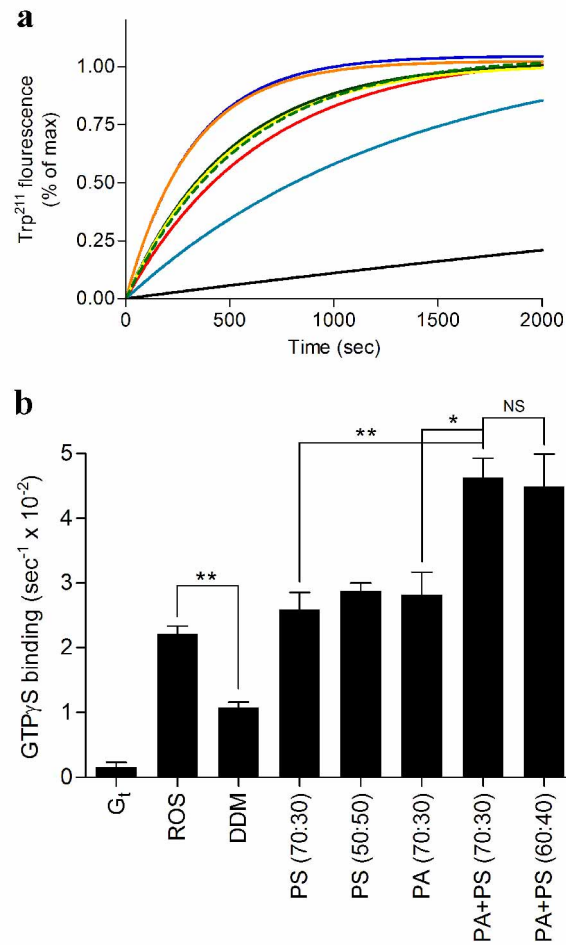
Figure 20: Intrinsic Fluorescence Changes in G_t. Basal or receptor mediated nucleotide exchange in G_t was measured in the presence or absence of different bicelles as described in the materials and methods section. Final bicelle concentration in each sample is 8% (lipid:rhodopsin ratio of approximately 12800:1). **A)** Basal or receptor mediated Trp^{211} fluorescence change of G_t. Fluorescence curves are presented for G_t in the presence of ROS (red), detergent solubilized rhodopsin (DDM) (teal), G_t alone (black), PS (70:30) (green dash), PS (50:50) (green), PA (70:30) (yellow), PA+PS (70:30) (orange), PA+PS (60:40) (blue). Data were collected at 21 °C for 40 min. **B)** Quantitation of the initial rates of basal or rhodopsin-catalyzed nucleotide exchange for G_t. The ratio of neutral to negatively charged phospholipids is indicated within the parentheses in the graph. Results are mean ± S.E.M. values of at least three independent experiments (* $p < 0.05$; ** $p < 0.01$; NS, Not Significant).

Table 5: Basal and Receptor-mediated Nucleotide Exchange Rates of G_t in the Presence of Different Bicelles[a]

	Initial rates ± S.E.M. (1 / sec x 10^{-2})
G_t	0.15 ± 0.06
ROS	2.21 ± 0.12
DDM	1.08 ± 0.07
PS (70:30)	2.59 ± 0.26
PS (50:50)	2.88 ± 0.13
PA (70:30)	2.82 ± 0.34
PA+PS (70:30)	4.62 ± 0.30
PA+PS (60:40)	4.48 ± 0.51

[a]Final concentration of bicelles was 8% (lipid:rhodopsin ratio of approximately 12800:1). The ratio of neutral to negatively charged phospholipids is indicated within parentheses. The initial nucleotide exchange rates are shown in sec^{-1} x 10^{-2} for G_t. The exchange rate was determined by fitting the data to an exponential association equation $F\lambda = F\lambda_{max}(1-e^{-kt})$. Results are mean ± S.E.M. values from at least three independent experiments.

Discussion

Early studies on receptor-G protein coupling indicate that temperature, pH, and the presence of lipids each influence complex formation (140,141,143,194), but our understanding of the contribution of membrane lipids to complex stabilization has been limited to experiments performed in detergent micelles, mixed micelles, and other undefined lipid preparations. Findings in recent years have increased our appreciation of the importance of membrane morphology and composition on receptor structure and function. Unlike spherical detergent micelles, bicelles usually adopt a disk-like shape, which NMR studies indicate are similar in morphology to native membranes (155,174). Bicelles have also previously demonstrated an ability to support folding and thermal

stability of rhodopsin and opsin (149). Here, we investigated the formation and stabilization of a receptor-G protein complex by incorporating negatively charged phospholipids into a neutral bicelle preparation.

Biochemical and biophysical studies have demonstrated that the lipid bilayer is important for the assembly, stability, and function of membrane proteins (197-199). In ROS membranes, rhodopsin is also surrounded by a specific phospholipid composition that likely facilitates visual transduction processes, and contain roughly ~2.5 % phosphatidylinositol, ~13% phosphatidylserine, ~41% phosphatidylethanolamine, ~45 % phosphatidylcholine (177-179). Since rhodopsin-G_t coupling is significantly less efficient in detergent micelles than in ROS membranes or neutral or negatively-charged bicelles, this specific lipid environment may contribute to visual signaling by optimizing the stability of this complex. Our studies confirm the previously observation that negatively charged lipids improve the efficiency of rhodopsin activation and G protein interaction (145,200-203). We have found that the overall charge of the specific bicelles influenced formation and stability of the high affinity receptor-G protein complex, likely through a combination of electrostatic and physical effects, as electrostatics are known to play a role in receptor-G protein interaction (180,181). In our experiments, increasing the density of negatively charged phospholipids in bicelles enhanced the complex formation, stability, and rates of receptor-mediated G protein activation, supporting a role for electrostatics in stabilizing optimal receptor-G protein coupling (180). The physical properties of bicelles most likely stabilize the receptor-G protein complex structure better than ROS membranes through enhanced G protein docking and membrane anchoring than what is available in the native lipid environment. Here we present evidence of

functional rhodopsin-G_t complexes in an artificial membrane environment that incorporates negatively charged phospholipids into a neutral bicelle.

Bicelle morphology and phase properties are extremely sensitive to changes in temperature, phospholipid concentration in solution, and q ratio. In the case of neutral bicelles, decreasing the total concentration below a critical percentage results in formation of large unilamellar vesicles (174). In terms of neutral bicelles, decreasing final concentration of bicelles or increasing q ratios and temperatures is known to induce a phase transition from disc-like bicelles to an extended network of interconnected lipids called the perforated lamellar phase, or "swiss cheese"-like phase, characterized by high sample viscosity (157,174). Here we observed similar effects on bicelle morphology and phase properties. Hydrodynamic radii dramatically increased when the total phospholipid concentration was decreased to 2% at ambient temperatures, which suggests formation of large vesicles (174) at temperatures above those used in our functional studies. All compositions of negatively charged bicelles were temperature sensitive, and became highly viscous above 24°C, which is the phase transition temperature for DMPC (174). Interestingly, the stability of negatively charged bicelle phase, as assessed by color and fluidity, appeared to be the greatest at below 20°C.

Lipids are known to be important for optimal function of many trans-membrane proteins. Disruption of the membrane phospholipid composition during protein purification can affect the folding of membrane proteins, and consequently, signaling capabilities. For example, changes in temperature can lead to increased phospholipid dynamics and membrane fluidity, which contribute to receptor destabilization. Temperature also has observable effects on bicelle properties, as changes in temperature

59

result in phase transitions. When the temperature is increased from 4 to 15 °C, we noted a decrease in the decay half-life of the complex in bicelles, consistent with results in other systems (140,204). Taken together, we suggest that bicelle preparations containing negatively charged phospholipids facilitate stabilization of receptor-G protein complexes, and this effect is most evident at lower temperatures, compatible with temperatures used in most functional studies.

The metarhodopsin I/metarhodopsin II, (MI/MII) equilibrium of rhodopsin governs the productive coupling of receptor with G proteins, with coupling to MII being substantially more efficient (141). Knierim *et al.* showed that more than one proton is released from the MII state when rhodopsin binds to the C-terminal peptide of Gα (91). Sato *et al.* reached a similar conclusion using a computational approach, wherein an initial decrease in extra MII was predicted as the pH was raised, followed by an increase in extra MII at even higher pH's. Similarly, we observe that increasing the pH from 6.2 to 8.5 in the presence of negatively charged phospholipid compositions enhances the half-life of the high affinity complex. These results suggest that negatively charged bicelles contribute to the stability of the complex by both enhancing MII formation, as well as facilitating the G protein orientation at the membrane necessary for productive interactions with receptors.

Further studies are planned to determine the effect of bicelles containing other negatively charged phospholipids commonly found in membranes, such as phosphatidylinositols, on stability of the receptor-G protein complex. This study will include effects of varying acyl chain length and saturation of the phospholipids, which can have effects on both receptor activation and receptor-G protein coupling (146-

148,205). While 14:0 fatty acids are not a major acyl chain constituent of lipids in ROS membranes, 14:0 lipids have been used successfully in other bicelle systems to stabilize receptor structure (150,151,153). The addition of cholesterol, as well as phospholipids which vary in head group size and charge, have also been shown to have effects on receptor-G protein interaction and G protein activation (143,145,206), suggesting this may be another factor requiring further study.

Summary and Conclusions

A highly complex lipid environment allows the adaptability and flexibility in membrane structure required for the cellular signaling. Our data demonstrate that rhodopsin-G_t interactions and G protein activation is strongly dependent on phospholipid composition and charge density. We developed an optimized system that included PA+PS (60:40) bicelles, which increased the half-life of the rhodopsin-G_t(empty) complex to one week. This system provides a powerful tool for the study of GPCR-G protein complexes, and the fundamental approaches described here may be applicable to other complexes between membrane proteins and their soluble signaling partners.

CHAPTER IV

CRYSTALLIZATION OF THE RHODOPSIN-TRANSDUCIN COMPLEX

Introduction

Rhodopsin represents a unique member of the GPCR superfamily of signaling proteins that has proven to be quite ideal for structural studies. Unlike many of the 800 or so additional receptors of the superfamily that exhibit basal activity related to multiple, conformationally diverse signaling states capable of engaging G proteins in the absence of receptor stimulation, the activation of rhodopsin is tightly regulated by its covalent ligand (70,71). In the absence of light, the inverse agonist, 11-*cis* retinal, locks rhodopsin into its inactive conformation. Only when light is sensed and a photon is absorbed does rhodopsin transition to the activated state competent for binding intracellular heterotrimeric G proteins (92). This structural rigidity and specificity of interaction is a highly desirable feature for crystallization experiments that depend on conformational homogeneity to produce high-quality, isotropic crystals. Indeed, this system was the first GPCR to have had its structure determined, and thus represents one of the best-characterized receptors to date (207). Despite the amenability of the receptor and its cognate signaling partner, the heterotrimeric G protein transducin, to structural studies, there exists one last structural frontier in the rhodopsin-transducin system remaining to be explored: the nucleotide-free, high-affinity GCPR-G protein complex. Successful determination of such a complex would provide critical insight into the specific mechanism of receptor-mediated allosteric G protein activation.

Recent advances in technology available for studying structure-function relationships in membrane proteins have paved the way for the successful crystallization of a number of GPCR structures, including the β_2AR-G$_s$ structure (70). While this latest structure has illuminated a number of interesting and surprising details of the receptor-G protein interaction, work on the nucleotide-free G protein state is not yet done. Many questions still exist regarding the GPCR-G protein interaction. For example, determinants of GPCR-G protein specificity and the structural and sequence elements that contribute to the diverse range in nucleotide exchange rates observed in G proteins have yet to be fully understood (2,46,52,208). Related to these is also the question of how the allosteric mechanism of G protein activation differs among the various combinations of GPCR-G protein pairs. These questions can be answered by structural studies on additional nucleotide free states of receptor-bound G protein subtypes. Comparative analysis is a powerful tool for understanding how related proteins evolve to become unique entities. In GPCRs, the diversity of the receptor-G protein interaction necessitates multiple, separate studies investigating additional structure-function relationships. Given its homology to the G$_i$ family of signaling G proteins, investigations into the transducin G protein system and its interactions with rhodopsin will provide further insights into general mechanisms of allosteric receptor-mediated G protein activation.

As evidenced by the wealth of structural information available, rhodopsin is an excellent model system for investigations into the complexed state of GPCRs and G proteins. The rod cells of mammalian retina are highly enriched in the visual receptor. In fact, purification of the receptor from an endogenous source such as bovine eyeballs can yield up to 80 mg of rhodopsin per every 200 retinas harvested. Often bovine retinas can

be obtained for mere dollars from local slaughterhouses, whereas the expression systems employed for recombinant GPCR and G protein expression can cost upwards of thousands of dollars per mg of protein. Similarly, abundant amounts of transducin in its fully functional form can also be purified from the same source as rhodopsin. Thus, an optimized "expression system" is readily available for the visual transduction receptor-G protein pair.

A variety of technical approaches for determining membrane protein structures presently exist. Solubilization and structure determination of membrane proteins in detergent micelles predates all of the other techniques, and over 300 membrane protein structures have been determined using this approach. More recently, phospholipids and the *in meso* method of membrane protein crystallization have come into popularity. The utility of bicelles as a model membrane for structural work on membrane proteins was first made popular nearly two decades ago when it was discovered that they had the ability to magnetically align for solid and solution state NMR (155,209). The morphology of bicelles is disc-like, much like native membranes (**Figure 11A, B**), and spontaneously form in the presence of phospholipids mixed with amphiphiles or detergent (210). Based on the ratio between phospholipid and detergent (q ratio), bicelles dimensions can be tightly controlled, thus rendering them an extremely versatile tool for studying dissimilar membrane proteins of all types. Perhaps the most impressive feature is the ability of membrane proteins to retain their native functions in phospholipid bicelles, whereas detergent micelles often cause proteins to lose their functionality (211,212). Crystal structures of the proton pump bacteriorhodopsin (172), xanthorhodopsin (152), the

voltage-dependent anion channel 1(153), rhomboid protease (213), and the GPCR β_2-adrenergic receptor (151) have all been determined in phospholipid bicelles.

Crystallization of membrane proteins in lipidic mesophases, or the lipidic cubic phase (LCP), was first introduced by Landau and Rosenbusch who demonstrated the ability of such a matrix to facilitate the formation of crystals of bacteriorhodopsin (214). Like bicelles, the cubic phase is marked by a native membrane-like morphology. This morphology is referred to as a lyotropic liquid crystal, and it consists of a curved lipid bilayer with a midplane that adopts cubic symmetry (215). In its crystalline form, the cubic mesophase forms aqueous and bilayer segments that are continuous in all three dimensions (**Figure 21**). This bicontinous property has been found to promote type I crystal packing, which is marked by the formation of crystal contacts between both the polar and non-polar regions of membrane proteins, versus the singular polar contacts observed in type II crystal packing (216). Type I packing results in improved crystal order, and thus diffraction quality. Caveats of membrane protein crystallization by the *in meso* method utilizing lipidic mesophases are the apparent curvature of the bilayer, which, like detergent micelles, can be deleterious to protein stability and the limitations, and the limited size of solvent channels permeating the bilayer which can make the crystallization of larger complexes difficult (217). However, extensive characterization and investigations into the physical properties of cubic phase lipids (218,219) have revealed a battery of reagents and precipitants, such as low molecular weight PEGS and non-volatile alcohols, that alleviate some of the membrane curvature and swell the solvent channels to produce a sponge phase for accommodating larger soluble domains such as the one associated with a GPCR-G protein complex. Notably, the field of GPCR structural

biology has had incredible success in determining structures from crystals grown in the lipidic cubic and sponge phases. Of the 119 structures determined by this method, 38 of these are of unique membrane proteins, and 17 are of GPCRs (Cherezov Group website).

Using both phospholipid bicelles and the rapidly advancing LCP technology, structural studies on the rhodopsin-transducin complex were pursued. The results from the preliminary characterizations presented in this chapter offer insights into determinants of not only GPCR-G protein stability, but also instability. This data hopefully forms the basis from which future structural studies on the rhodopsin-transducin system will be continued.
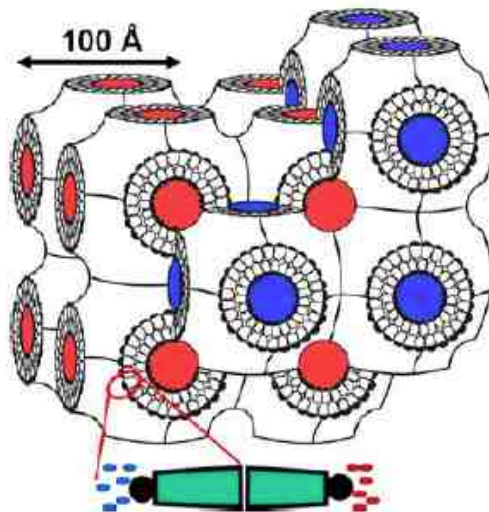
Figure 21. Cartoon Representation of a Bicontinuous Lipidic Cubic Mesophase. Figure adapted from (215).

Methods

Preparation of ROS Membranes

All steps of the purification were performed on ice or at 4 °C. For preparation of dark-adapted ROS membranes, all steps were additionally performed under dim red light. Bovine retinas obtained from 200 bovine eyes were used for each purification batch. Retinas were thawed on ice and diluted to a final volume of 200 mL in a 30% Sucrose Solution (30% w/v sucrose, 90 mM KCl, 30 mM NaCl, 2 mM $MgCl_2$, 10 mM MOPS, 0.1 mM EDTA, pH 8.0, 1 mM DTT, 50 μM PMSF). The retina slurry was stirred for 1 hr at 4 °C to separate the outer segments from the rod cell inner segments and basolateral membrane. The retina slurry was then evenly distributed into eight Oak Ridge centrifuge tubes and centrifuged for 4 minutes at 4°C in a Sorvall SS-34 rotor at 4,000 rpm. The supernatant from the spin step was set aside on ice while the cell pellet was resuspended with a small volume of 30% Sucrose Solution. The centrifugation step was then repeated for the resuspended pellets by centrifugating at 4°C for 4 minutes in a Sorvall SS-34 rotor at 6,000 rpm. The supernatants from both centrifugation cycles were pooled and the cell pellets discarded. The pooled supernatant was evenly distributed into Oak Ridge centrifuge tubes and centrifuged for 20 minutes at 4°C in a Sorvall SS-34 rotor at 19,000 rpm. The supernatant was then discarded and the cell pellets resuspended with 1 mL of 26% Sucrose Solution (26% w/v sucrose, 90 mM KCl, 30 mM NaCl, 2 mM $MgCl_2$, 10 mM MOPS, 0.1 mM EDTA, pH 8.0, 1 mM DTT, 50 μM PMSF) for every two pellets. The resuspended pellet slurry was pooled and set aside on ice while sucrose gradients were prepared.

The sucrose gradients consisted of three separate solutions: Gradient Solution 1 (0.84 M sucrose, 10 mM MOPS, 60 mM KCl, 30 mM NaCl, and 2 mM $MgCl_2$), Gradient Solution 2 (1.0 M sucrose, 10 mM MOPS, 60 mM KCl, 30 mM NaCl, and 2 mM $MgCl_2$), and Gradient Solution 3 (1.14 M sucrose, 10 mM MOPS, 60 mM KCl, 30 mM NaCl, and 2 mM $MgCl_2$). Each gradient was prepared by layering 7 mL each of the Sucrose Gradient Solutions in six 36 mL Sorvall AH629 swinging bucket centrifuge tubes (or similar). A large needle or pipette was used to carefully layer Sucrose Solution 1 on the bottom of each centrifuge tube. Sucrose Solution 2 was dispended into the tubes by inserting the pipette tip containing the solution through Sucrose Solution 1 and touching the bottom of the centrifuge tube. Dispensing Sucrose Solution 2 in this manner will cause Sucrose Solution 1 to rise. Using the same technique, Sucrose Solution 3 was dispensed below Sucrose Solution 2. Dispensing Sucrose Solution 3 will cause Sucrose Solutions 1 and 2 to rise. The final order of the solutions was Sucrose Solution 3 on the bottom, Sucrose Solution 2 in the middle, and Sucrose Solution 1 on top.

Once the sucrose gradients were prepared, the pellet slurry was carefully layered on top of each tube, balanced with 26% Sucrose Solution, and centrifuged at 4°C for 30 minutes in a Sorvall AH-629 swinging bucket rotor at 25,000 rpm. This step of the protocol resulted in a gradient separation of the slurry components with each gradient adopting various degrees of opacity. The bottom layer was somewhat clear, the next layer was orange, and the top layer, again, was clear. The orange layer in the center contained the ROS membranes and was carefully recovered. The pooled ROS membrane layers were distributed evenly into Oak Ridge centrifuge tubes and centrifuged for 20 minutes at 4 °C in a Sorvall SS-34 rotor at 19,000 to pellet the ROS membranes. The supernatant

from this spin step was discarded and each membrane pellet washed with 1 mL of freshly prepared Isolation Buffer (90 mM KCl, 30 mM NaCl, 2 mM $MgCl_2$, 10 mM MOPS, 0.1 mM EDTA, pH 8.0) containing 2.5 μg/mL Pepstatin, 10 μg/mL Aprotinin, and 10 μg/mL Leupeptin. Resuspended membranes were thoroughly homogenized by vigorously pipetting and transferred to a 15 mL conical tube. The final volume of the ROS membrane homogenate was adjusted to 15 mL with Isolation Buffer and the conical tube carefully wrapped in aluminum foil for storage at -80 °C.

Preparation of Urea-washed ROS Membranes

All steps were performed under dim red light and on ice or at 4°C. Dark-adapted ROS membranes prepared as previously described were thawed and transferred to a glass dounce homogenizer embedded in ice. The homogenizer was then partially filled with EDTA Buffer (10 mM Tris-Cl, 1 mM EDTA, 1 mM DTT, pH 7.5) and the ROS membranes gently homogenized to facilitate separation of peripheral proteins from the rhodopsin-enriched membranes. The homogenate was then transferred to Oak Ridge tubes and centrifuged for 30 minutes in a Ti-70 rotor at 30,000 rpm. Supernatant from the centrifugation step was then discarded and each pellet resuspended with 1 mL EDTA Buffer. The resuspended pellets were pooled and homogenized again in EDTA Buffer to further wash the membranes. The homogenate was then transferred into ultracentrifuge tubes and centrifuged again for 30 minutes in a Ti-70 rotor at 30,000 rpm. Following the second centrifugation step, the supernatant was discarded and each cell pellet resuspended with 1 mL of Urea Buffer (10 mM Tris-Cl, 1 mM EDTA, 1 mM DTT, 6 M urea, pH 7.5). The pellet resuspension was then homogenized in Urea Buffer. Membranes

were pelleted by centrifugation for 30 minutes in a Ti-70 rotor at 45,000. To remove excess urea, the membrane pellets were resuspended with Buffer A (10 mM MOPS pH 7.5, 2 mM $MgCl_2$, 200 mM NaCl, 1 mM DTT, 0.1 mM PMSF) and further homogenized. The homogenate was then centrifuged for 30 minutes in a Ti-70 rotor at 30,000 rpm to again pellet the membranes. Following this final spin step, the supernatant was discarded and each pellet resuspended with 1 mL of Buffer A. The concentration of rhodopsin was determined by measuring the absorbance of an aliquot of membranes diluted 25-fold with 20 mM HTAC at 500 nm before and after photobleaching. The difference in the absorbance and a molar extinction coefficient of 42,000 $M^{-1}cm^{-1}$ were then used to calculate the rhodopsin concentration using Beer's Law (220). The dark-adapted, urea-washed ROS membranes were stored at -80°C as 100 µL aliquots in black opaque microcentrifuge tubes or wrapped in foil.

Purification of Rhodopsin by Concanavalin A Affinity Chromatography

All steps were performed under dim red light and on ice or at 4°C. Approximately 400 µL of dark-adapted ROS membranes were thawed and resuspended with an equal volume of ConA Binding Buffer (20 mM Tris-Cl pH 7.4, 250 mM NaCl, 1 mM $MgCl_2$, 1 mM $CaCl_2$, 1 mM $MnCl_2$). The membranes were then pelleted by centrifugation for 25 minutes at top speed (20,000×g) in a benchtop Eppendorf Centrifuge. The supernatant was discarded and the membrane pellet resuspended with 400 µL Rhodopsin Solubilization Buffer (20 mM Tris-Cl pH 7.4, 250 mM NaCl, 1 mM $MgCl_2$, 1 mM $CaCl_2$, 1 mM $MnCl_2$, 80 mM DDM (SOL-grade)). The resuspension was mixed by pipetting until no longer cloudy. The membranes were then incubated on ice and mixed by

pipetting every 15 minutes for 45 minutes to fully extract rhodopsin from the native ROS membranes and solubilize into DDM detergent micelles. After 45 minutes, the solubilized protein was again centrifuged for 25 minutes at top speed in a benchtop Eppendorf Centrifuge. The supernatant was then carefully collected and remaining pellet discarded.

To further purify detergent-solubilized rhodopsin, a light-protected "ConA Purification Hutch" was first assembled in a 4°C environment to protect the purification apparatus from light. The hutch contained a clamp stand for securing a ConA Sepharose column, a peristaltic pump, and a tube rack for holding samples (see **Figure 22**). A 30 mL syringe was carefully attached to the top of a 1 mL ConA column and 10 mL of Wash Buffer 1 (20 mM Tris-Cl pH 7.4, 250 mM NaCl, 1 mM $MgCl_2$, 1 mM $CaCl_2$, 1 mM $MnCl_2$, 0.5 mM DDM (Anagrade)) eluted over the column to wash off the ethanol-containing storage buffer in which the column was packed. The column was then equilibrated with 30 mL of Wash Buffer 1 in a continuous loop using a peristaltic pump flowing at 0.3 mL/min for at least 48 hours.

Once the ConA column had been sufficiently equilibrated, the detergent-extracted rhodopsin was diluted to 10 mL with ConA Binding Buffer (20 mM Tris-Cl pH 7.4, 250 mM NaCl, 1 mM $MgCl_2$, 1 mM $CaCl_2$, 1 mM $MnCl_2$) and loaded onto the equilibrated ConA column. The protein load fraction was flowed over the column in a continuous loop 0.3 mL/min for at least 4 hours. The load fraction was then eluted and the column washed with 10 mL of Wash Buffer 1, 5 mL of Wash Buffer 2 (20 mM Tris-Cl pH 7.4, 100 mM NaCl, 0.5 mM DDM (Anagrade), pH 7.4), 50 mL of Elution Buffer 1 (20 mM Tris-Cl pH 7.4, 100 mM NaCl, 0.5 mM DDM (Anagrade), 400 mM α-DM, pH 7.4), and
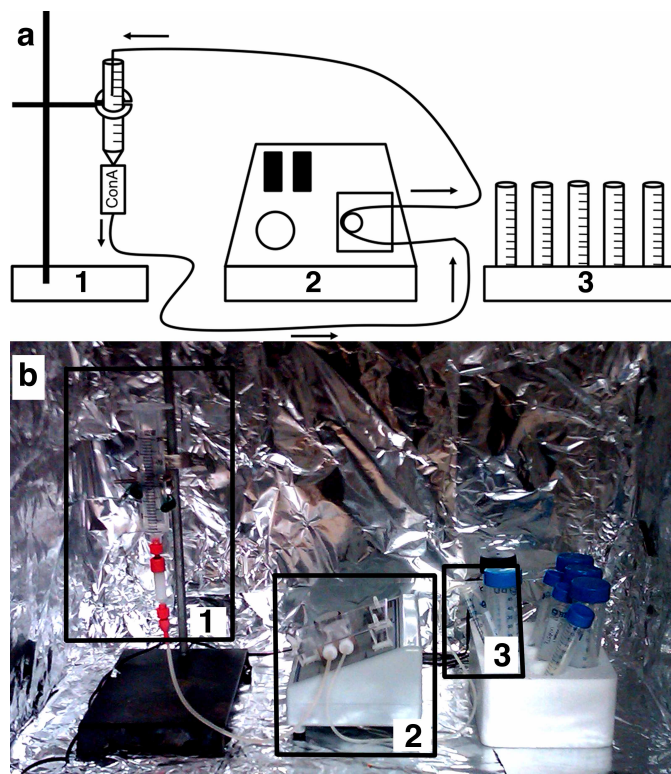
Figure 22: Concanavalin A Affinity Purification Hutch. A simple cardboard box lined with aluminum foil and sealable flaps is sufficient for creating a dark-adapted environment for conA purification of rhodopsin. *Box 1* highlights the 1 mL ConA Sepharose Column (GE Healthcare) attached to a 30 mL syringe. Both are held to a ring stand with a standard clamp. *Box 2* shows the peristaltic pump with two leads, one of which remains connected to the bottom end of the ConA Sepharose Column. Depending on the requirement of the protocol, the second lead can either rest in a collection tube (*Box 3*) or can be secured in place inside of the syringe (*Box 1*) for flowing solutions over the column in a continuous loop (i.e. while loading the column with rhodopsin or while pre-equilibrating the column with detergent). A photograph of the hutch and appartus shown as a schematic in **A)** is shown in **B)**.

5 mL of Elution Buffer 2 (20 mM Tris-Cl pH 7.4, 100 mM NaCl, 0.5 mM DDM (Anagrade), 500 mM sucrose, pH 7.4). Fractions from the Elution Buffer 1 and Elution Buffer 2 wash steps contained rhodopsin and were pooled. The pooled eluent was concentrated by centrifugation in a dark-adapted 10 kDa molecular weight cutoff Amicon concentrator at 4°C at 1,600 rcf(max) in 20 minute intervals until the total volume reached approximately 2 mL. The concentrated sample was then diluted to 50 mL with Extra Meta II Exchange Buffer and subject to rounds of serial centrifugation at 4°C and

1,600 rcf(max) in 20 minute intervals. The protein sample was concentrated to a final volume of ~200-500 µL and stored on ice until further use. The rhodopsin concentration was again determined by measuring the absorbance at 500 nm as previously described (220). For detergent-solubilized rhodopsin, however, the molecular extinction coefficient used was 40,600 $M^{-1}cm^{-1}$.

Preparation of Transducin

The rhodopsin-transducin complex was purified from light-adapted bovine ROS membranes prepared as previously described. Membranes were then washed four times with Isotonic Buffer (5 mM Tris-Cl, 130 mM KCl, 0.6 mM $MgCl_2$, 1 mM EDTA, 1 mM DTT, pH 8.0) and two times with Hypotonic Buffer (5 mM Tris-Cl, 0.6 mM $MgCl_2$, 1 mM EDTA, 1 mM DTT, pH 8.0). Transducin was released into the supernatant by resuspending ROS membrane pellets with Hypotonic Buffer containing 0.1 mM GTP. The membranes were pelleted by centrifugation and the supernatant containing transducin was dialyzed against Transducin Storage Buffer (20 mM Tris-Cl, 200 mM NaCl, 10 µM GDP, 5 mM β-ME, 10% glycerol, pH 7.5). Purified transducin was stored at -80°C.

Preparation of Gβγ

Gβγ was purified as previously described with slight modification (221). Purified transducin was first incubated with 40 mM $MgSO_4$ to dissociate the $G\alpha_t$ and $G\beta_1\gamma_1$ subunits. The protein was then loaded onto a HiTrap Blue HP sepharose column and the Gβγ fraction eluted in the flow-through in Buffer C (10 mM Tris-Cl pH 7.5, 150 mM

NaCl, 20 mM MgSO$_4$, 1 mM EDTA, 10% glycerol, 5 mM βME). Eluted protein was concentrated in a 10 kDa Amicon concentration at 4 °C at 1,600 rcf(max) and buffer exchanged into Gβγ Storage Buffer (10 mM Tris-Cl pH 7.5, 100 mM NaCl, 5 mM βME, 10% glycerol). Purified protein was stored at -80°C.

Extra Meta II Assay

The formation of extra metarhodopsin II (meta II) in ROS membranes was measured on an Aminco DW2000 spectrophotometer in the presence of increasing concentrations of G protein. Heterotrimeric G protein was reconstituted from purified wild-type or K345L Gα$_{i1}$ in the same manner as used for receptor-mediated nucleotide exchange measurements. 2 μM of rhodopsin in dark-adapted urea-washed ROS membranes were incubated with varying concentrations of wild-type or K345L Gα$_{i1}$β$_1$γ$_1$ in meta II buffer (50 mM HEPES, 100 mM NaCl, 1 mM MgCl$_2$, 1 mM DTT, pH 8.0) on ice for approximately 10 min. Absorption spectra for both dark and light-adapted samples were then collected at 4°C. Following collection of a dark-adapted spectrum, samples were exposed to 2 quick flashes of light approximately 30 s apart. The light-adapted spectrum was then immediately collected. The extra meta II signal was calculated as the change in meta II formation (difference between absorption at 390 nm and 440 nm) upon light activation. Dose response curves were generated by nonlinear regression using a sigmoidal dose-response (variable slope) equation as previously described (222).

Preparation of Phospholipid Bicelles

Bicelles composed of saturated, long-chain (14:0) DMPC, DMPA, DMPG or DMPS and the detergents (6:0) DHPC, CHAPS, or CHAPSO were prepared as a 35% stock solution with a 2.8:1 lipid to detergent ratio (q ratio) using a procedure modified from (172). Neutral bicelles were composed of DMPC and DHPC, CHAPS, or CHAPSO to form DMPC:DHPC, DMPC:CHAPS, or DMPC:CHAPSO bicelles. Negatively charged bicelles were prepared by substituting a percentage of the total molar lipid content of the neutral bicelles with negatively charged DMPA, DMPG, or DMPS, while maintaining an overall 2.8:1 phospholipid to detergent ratio. The ratio of neutral to negatively charged phospholipids is indicated within the parentheses in **Figure 11B**. A custom extrusion apparatus was used for mixing bicelles. The apparatus was constructed by connecting two 1 mL glass syringes with tubing capped with luer locks. To prepare a 1mL, 35% stock of DMPC:DHPC bicelles, 282.50 mg DMPC was added to one syringe. 337.5 μL of a 20% DHPC solution was mixed with 312.5 μL of water. 200 μL of the DHPC solution was then added to the syringe containing DMPC. The remaining DHPC solution was added to the other syringe. The bicelle mixtures were cycled through their phase transitions 4 times by incubating the entire apparatus at 4 °C and 55 °C. Bicelles were homogenized by extrusion after each incubation. Homogeneous bicelles were transferred into a microcentrifuge tube and centrifuged at 10,000 x g for 1 minute to remove excess air bubbles. Correctly formed bicelles appeared clear at 4 °C and were stored at -20 °C.

Preparation of Negatively-charged Cubic Lipids

The majority of *in meso* crystallization experiments utilize *cis*-monounsaturated fatty acids. The most commonly used lipid is the monoacylglycerol, monoolein (MO), also known as 9.9 MAG. A simplistic view of MAGs can be described as a head attached to a neck separated from its tail by a *cis* double bond. The glycerol head group forms the head connected by an ester linkage to the region of the following acyl chain forming the neck. The remaining portion of the acyl chain extending beyond the *cis* double bond is the tail. The total number of carbons in the neck and tail are denoted in the MAG notation. Thus, 9.9 MAG consists of an 18-carbon acyl chain where 9 carbons belong to the neck and 9 carbons belong to the tail. Additional MAGs screened in the crystallization of RhoGt included 7.7 MAG and 7.8 MAG consisting of 14 and 15 carbon acyl chains (**Table 6**), respectively. These cubic lipids were purchased from NuCheck prep (monoolein) or Avanti Polar Lipids (7.7 MAG and 7.8 MAG). The latter was received as a powder, thus the protocol for preparing LCP host lipids supplemented with DOPS negatively charged phosopholipid was slightly different for the two sets of MAG.

Table 6: LCP Host Lipid Compositions Screened for RhoGt Crystallization

Host Lipid	% Hydration	Temperature (°C)	Drop Size (nL)
Monoolein	40%	20	50 + 800
Monoolein + 5% DOPS	40%	20	50 + 800
7.7 MAG	50%	20	50 + 800
7.7 MAG + 5% DOPS	50%	20	50 + 800
7.8 MAG + 5% DOPS	40%	20	50 + 800

DOPS at a final concentration of 5 mol% was selected based on findings that this concentration was sufficient to stabilize the appropriate cubic phase for *in meso*

crystallization (223). For MO containing 5 mol% DOPS we first melted the frozen MO at 55°C to return the lipid to its viscous, molten phase. While MO was melting, the appropriate amount of DOPS needed for a stock containing 5 mol% DOPS was measured. Using the density of MO (0.895 g/mL), the volume of MO required for a stock containing 95 mol% MO was calculated and mixed with the DOPS in an opaque glass vial. For the powder MAGs, the amount of lipid needed for 95 mol% stocks was determined using the molecular weight and the necessary amounted needed weighed with an analytical balance. Both the MAG and DOPS were then mixed together in a sample vial. Methanol was then added to the mixtures to fully dissolve the lipids in one another and dried in a vacuum desiccator or by vacufuge to evaporate the excess methanol. If dried in a vacuum dessicator, leave the sample tube covered in a thin foil punctured with three or 4 holes to allow the methanol to evaporate. The incubation time for methanol evaporation by vacufuge depends on the speed and model of the instrument, and should be determined empirically. Though, 10-20 minutes is a good approximation for the time it will take for a 200 µL stock dissolved with 200 µL of methanol. Once dried, gently run a slow stream of nitrogen over the vial to evaporate any residual methanol. Prepared samples can be capped and stored at -20°C until ready for use in crystallization experiments. The protocol described by Caffrey and Cherezov (216) was used during sample preparation. Briefly, three parts melted cubic lipids (at 55°C) were mixed with two parts protein sample gently brought to room temperature. This was done by transferring the appropriate amount of cubic lipid to one gas-tight syringe attached to a custom coupler fitted with an 18-guage extrusion channel. The protein sample was transferred to a second gas-tight syringe. Being sure to expunge both syringes of excess air, and using a wet

77

connection, both syringes were connected to the coupler and sample extruded until optically clear. This process can be time consuming, but under the correct conditions, will most likely be obtained withing 100- to 200- manual cycles of extrusion. Once in the mesophase, the sample can be dispended for crystallization trials using the Zinsser Xantus LCP robot. Excess sample, if stable, can be stored at 20°C and under 60% humidity to maintain the phase most amenable to crystallization.

RhoGt Crystallization Trials

Rhodopsin and transducin were extracted from bovine retinas as previously described. For crystallization, proteins were used as is or further purified to homogeneity by affinity chromatography and/or size exclusion chromatography to isolate homogenous populations of the receptor-G protein complex for crystallization.

RhoGt complexes were reconstituted using 1) rhodopsin in urea-washed native ROS membranes or 2) ConA-purified, detergent-solublized rhodopsin extracted from urea-washed ROS membranes. Proteins where then mixed in stoichiometric ratios and incubated on ice for at least 30 minutes under dark-adapted conditions prior to light activation for inducing complex formation. Both proteins were quantified by the bicinchoninic acid assay (BCA assay) to determine the precise amounts of each sample needed for either 1:1 or 2:1 Rho:Gt complex formation.

For RhoGt complexes reconstituted using rhodopsin in native ROS membranes, dark-adapted membranes were first pelleted by centrifugation at 18,000 x g in a benchtop microcentrifuge for 30-45 minutes. Supernatant was discarded and membrane pellet resuspended in ROS buffer (50 mM Hepes pH 8.0, 100 mM NaCl, 1 mM $MgCl_2$) and

subject to another round of centrifugation to remove any residual urea. Rhodopsin in membranes resuspended in ROS buffer after the second round of centrifugation was quantified by determining absorbance at 500 nm, mixed in equimolar amounts with Gt to reconstitute the RhoG$_t$ complex, and samples immediately dispensed into crystallization trials following light activation by exposure to ambient light.

For ConA-purified rhodopsin extracted from urea-washed ROS membranes (protocol as previously described), purified protein was quantified, mixed in equimolar amounts with G$_t$, light activated under ambient light, and immediately passed over a Superdex S200 10/300GL column equilibrated with a minimum of 2 column volumes of RhoGt buffer (50 mM Hepes pH 8.0, 100 mM NaCl, 1 mM MgCl$_2$, 40 μM all-trans retinal (ATR)) supplemented with Anagrade quality detergent at a final concentration of 1.5-2X over the CMC value. Protein was collected from peaks corresponding to homogeneous populations, concentrated in 30 kDa cutoff concentrations, and immediately used for crystallization trials in either phospholipid bicelles or by the *in meso* method using cubic lipids. Concentrations of the purified complex used in crystallization trials varied between 2-10 mg/mL of total protein, as measured by the BCA assay.

Crystallization screening was performed for purified RhoG$_t$ exchanged into a number of different bicelle compositions (**Table 7**) or LCP host lipids (**Table 6**). LCP host lipid compositions were prepared as previously described (216,223). Crystallization conditions for RhoGt in native membranes and bicelle-solubilized RhoGt were screened in duplicate at 4°C and 18-20°C. LCP crystallization trials were all performed at 20°C. Purified samples of RhoGt were highly sensitive to freeze-thaw cycles, thus excess

amounts of the purified complex were discarded. **Figure 23** summarizes the primary

experimental approach used here for RhoGt structure determination.

Table 7: Bicelle Compositions Screened for RhoGt Crystallization

Bicelle Composition	Temperature (°C)	Drop Size (nL)
2% PS+PA (70:30)	4, 18-20	400 + 400
4% PS+PA (70:30)	4, 18-20	400 + 400
8% PS+PA (70:30)	4, 18-20	400 + 400
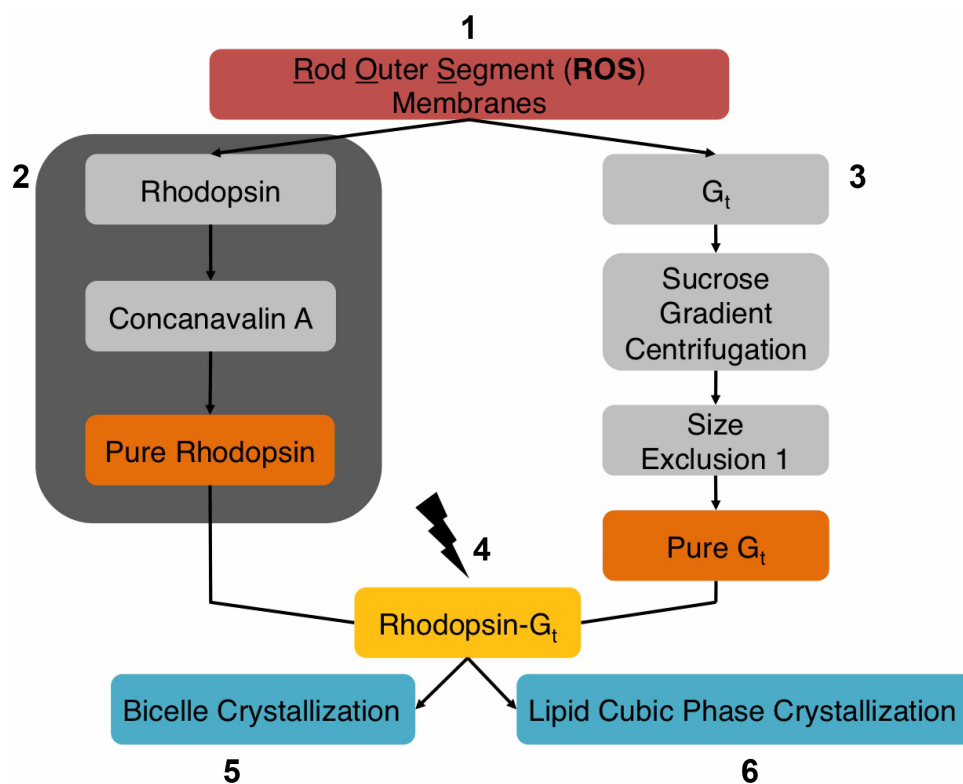
Figure 23. Experimental Approach for Crystallization and Structure Determination of the Rhodopsin-Transducin GPCR-G protein Complex. A two-pronged approach was utilized for screening RhoGt crystallization conditions. First, **1)** Endogenous rhodopsin and transducin extracted from bovine retinas were purified to homogeneity. **2)** Dark-adapted rhodopsin was purified by Concanavalin A chromatography under dim red light. **3)** Transducin was purified to homogeneity by a 2-step purification utilizing sucrose gradient centrifugation to separated G protein from the components of the ROS membranes harvested from bovine retina, followed by further separation of aggregate by size exclusion chromatography. 4) Separately purified proteins were mixed *in vitro*, light activated to form the high affinity complex, purified by a second size exclusion step, and either directly solubilized into phospholipid bicelles for **5)** bicelle-mediated crystallization (**Table 7**) or **6)** mixed with LCP host lipids (**Table 6**) for LCP crystallization.

Results

Rhodopsin Monodispersity in Detergent Micelles

A critical step in the primary experimental approach to crystallizing the RhoGt complex called for rhodopsin extraction from native urea-washed ROS membranes and solubilization in detergent. Membrane protein stability varies widely in the presence of different detergents, and identifying a suitable detergent system is an important component in membrane protein structural studies. Thus, the stability of rhodopsin was screened in a number of common, nonionic detergents by monitoring changes in mondispersity using size exclusion chromatography. Monodispersity was assessed at three wavelengths corresponding to distinct activation states of the receptor: 280 nm (total protein), 340 nm (meta I), and 380 nm (meta II). Of the five detergents screened, none appeared to produce a singular, Gaussian peak suggestive of a homogenous population of protein (**Figure 24**). However, DDM and LDAO appeared promising, such that the peaks corresponding to meta II absorption constituted a majority of the the total populations observed.

Meta II Stability in DDM and LDAO

The meta II assay was used to quantify the stability of rhodopsin in DDM and LDAO. In this assay, productive coupling between receptor and G protein reinforces the meta II state, which engages the G protein in a high affinity interaction. Thus, the extent of meta II formation can be used to assess receptor and complex stability. The meta II signal in the presence of DDM was nearly twice of that observed for LDAO-solubilized rhodopsin (**Figure 25**).
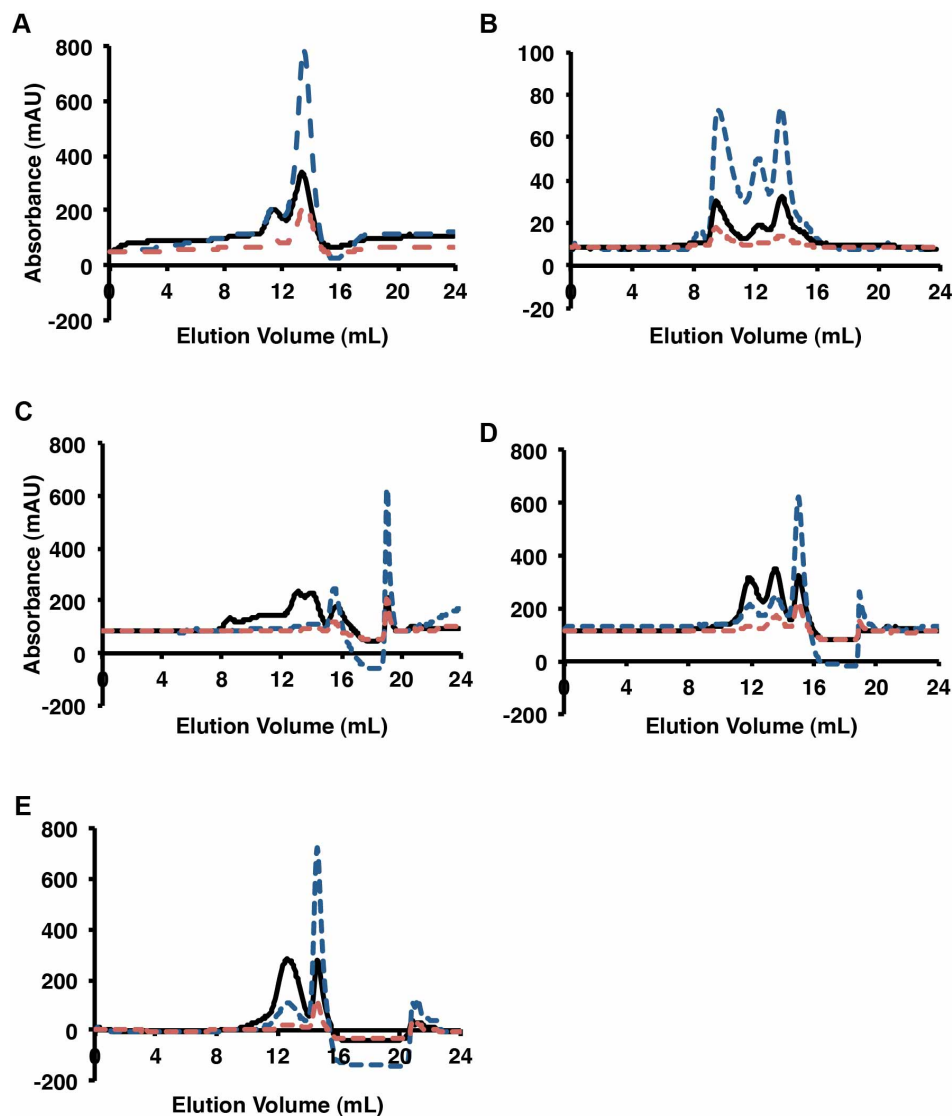
Figure 24. Rhodopsin Stability in Detergent Micelles. A Superdex 200 10/300 GL column was equilibrated with two column volumes of RhoGt buffer containing **A)** 0.02% DDM, **B)** 0.02% MNG-3, **C)** 1% OG, **D)** 0.2% DM, and **E)** 0.1% LDAO. Rhodopsin was extracted from native ROS membranes by incubating with a solution containing one of each of these detergents at a concentration 40-fold higher than their respective CMC values. This detergent-solubilized sample was then loaded onto the column and the elution profile monitored. The black trace corresponds to absorption at 280 nm (total protein). The blue trace corresponds to the 340 nm wavelength (meta I), and the red trace represents the 380 nm (meta II) wavelength.

The apparent stability of rhodopsin in the presence of DDM did not inform on the

on the half-life of the complex, thus a multi-angle light scattering experiment coupled to

size exclusion chromatography (SEC-MALS) was performed. This experiment revealed
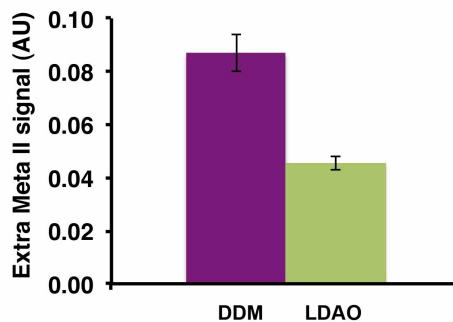
Figure 25. Comparison of Extra Meta II Signals in the Presence of DDM or LDAO. Results shown represent the mean ± S.E.M. for three independent experiments performed on each sample.

that the majority of the complex, unsurprisingly, existed in its dissociated state, as shown by the presence of multiple peaks (**Figure 26**) eluted over the time course of the experiment. The elution profiles of each of the peaks corresponded to a RhoGt complex (peak 1), free heterotrimer (peak 2), and free rhodopsin (peak 3).
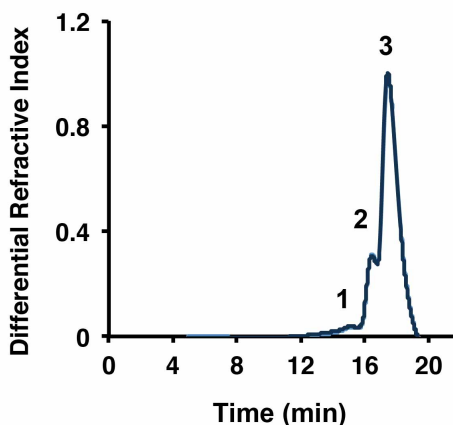
Figure 26. SEC-MALS Profile of DDM-solubilized RhoGt Complexes. DDM-solubilized rhodopsin was mixed with transudcin and loaded onto an Superdex S200 10/300 GL column equilibrated in RhoGt buffer containing 0.025 mM DDM. Each peak corresponds to a different population of protein. Based on the elution volume and differential refractive index, which is a function of molecular size, peak 1 corresponds to RhoGt, peak 2 corresponds to free heterotrimer, and peak 3 corresponds to free rhodopsin. The majority of the complex eluted in its dissociated state.

RhoGt Crystallization in Phospholipid Bicelles

The limited stability of rhodopsin-transducin complexes in detergent micelles presents a significant barrier to structural studies of the GPCR-G protein complex. A number of factors likely contribute to the instability and range from unfavorable detergent-protein interactions resulting in precipitation, membrane-curvature induced destabilization of the protein-protein interaction, and even instability imposed by the loss of lateral pressure applied from a bilayer-like environment. Fortunately, phospholipid bicelles represent a tractable membrane mimetic for stabilizing receptor-G protein complexes such as rhodopsin-transducin (211). Further, a number of membrane protein structures, including those of GPCRs (151,224), have been successfully determined in phospholipid bicelles Thus, attempts to crystallize the RhoGt complex were initially focused on bicelle-solubilized receptor. Negatively-charged bicelles were shown to be especially amenable to RhoGt complex formation and could extend the half-life of the activated complex to nearly one week (211). Bicelle sample preparation is described in the Methods sections of Chapter II and in Chapter III. Selection of the bicelle compositions used for crystallization was based on the results of a dynamic light scattering study characterizing the physical properties of each composition (211). In this study, the hydrodynamic radii were calculated as a function of the diffusion translation coefficient (**Figure 27**). Homogenous phospholipid structures with small variations in their average radii were selected for crystallization screening. Using two approaches for purifying the stable RhoGt complex (**Figure 28**), crystallization trials were then performed for bicelle-stabilized protein samples of the rhodopsin-transducin complex. The compositions screened are listed in **Table 7**. A number of promising preliminary
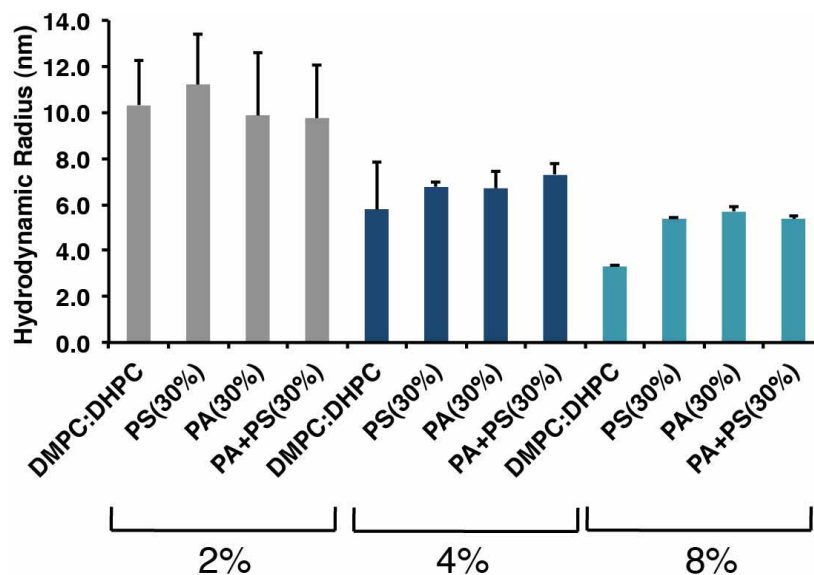
Figure 27: Phospholipid Composition Characterization by Dynamic Light Scattering. The hydrodynamic radii are plotted for neutral and negatively charged phospholipid compositions. Final concentrations of each composition in solution ranged from 2-8%. Results shown are the mean ± S.E.M. values of at least three independent experiments.

crystallization conditions were identified for RhoGt complexes solubilized in various negatively-charged bicelle compositions. A 70:30 mixture of neutral DMPC and the negatively charged DMPA and DMPS phospholipids (PS+PA(70:30)) was quite favorable for producing crystals. Some of these conditions are shown in **Figure 29**.

Although initial crystals were readily obtained, their overall quality was quite poor and attempts at reproduction and optimization were rather unsuccessful. The best attempt at optimization yielded broom-like crystals (**Figure 29A**) for which diffraction was limited to approximately 12 Å (**Figure 29B, C**).
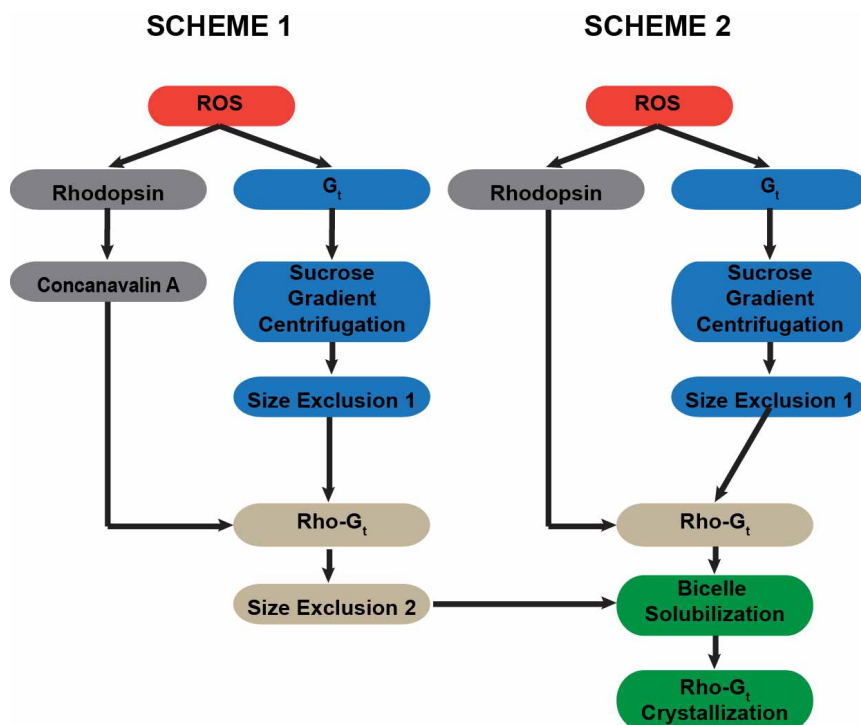
Figure 28: Optimization of RhoGt Purification for Crystallization in Phospholipid Bicelles. The protocol outlined in Scheme 1 takes advantage of the resolving power of size exclusion chromatography and Superdex columns for isolating homogenous populations of protein for crystallization trials. The protocol presented in Scheme 2 bypasses additional rhodopsin purification in order to take advantage of the stabilizing effects of native lipids on the rhodopsin-transducin interaction for crystallization.
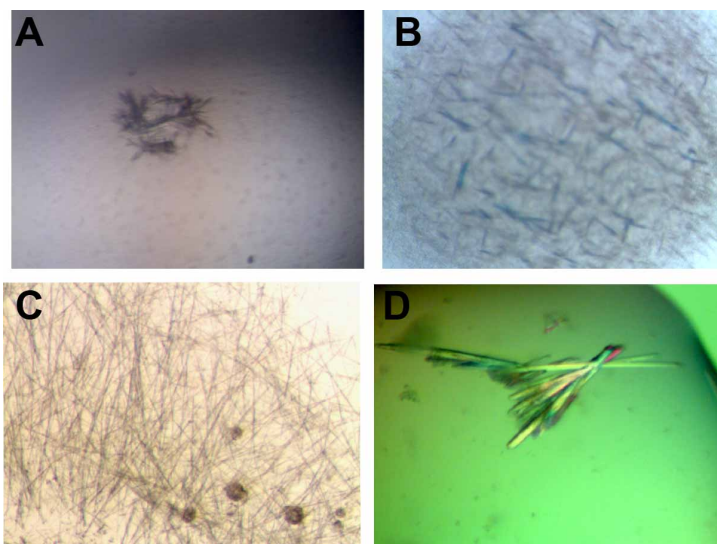
Figure 29. Preliminary Crystals of Bicelle-solubilized RhoGt. The following crystals were obtained for protein samples mixed with **A-B)** 2% PS+PA (70:30) and **C-D)** 2% PS+PA (70:30) supplemented with ATR.
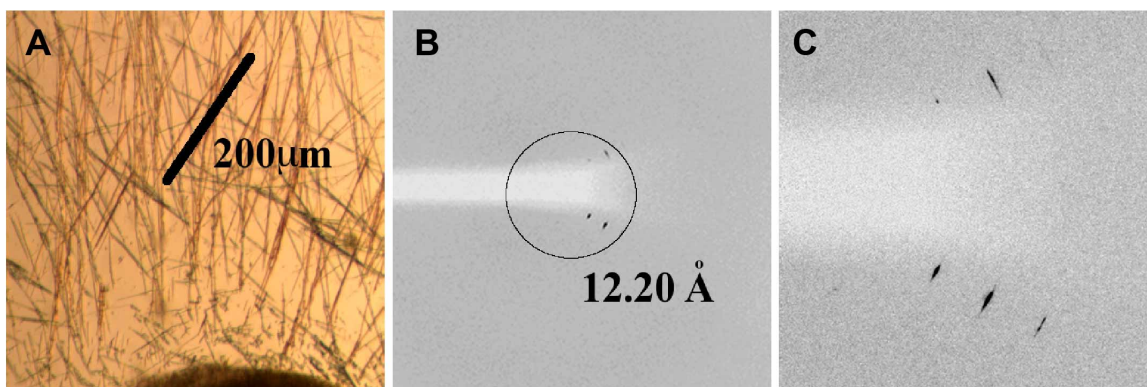
Figure 30. Sample Diffraction from Crystals Grown in the Presence of 2% PS+PA(70:30) Bicelles. Crystals were grown by the hanging drop method. Well solution (1 μL) containing 50 mM Sodium Acetate pH 4.5, 1.26M $(NH_4)_2SO_4$, and 200 mM NaCl was mixed with 1 μL of 5-7 mg/mL protein in 50 mM HEPES pH 8.0, 100 mM NaCl, 1 mM $MgCl_2$, 0.5 mM DDM, 40 μM all-trans retinal, and 2% PA+PS(70:30) bicelles.

$RhoG_t$ Crystallization by the in meso Method

LCP crystallization, or the *in meso* method, has become an increasingly powerful tool for membrane protein crystallization (215). Like bicelles, this method also provides a lipid bilayer similar to the native cell membrane in which proteins are stabilized. The added benefit of this approach is the bicontinuous nature of the membrane that facilitates classically difficult packing interactions between membrane proteins that promote diffraction to higher resolution than has been typically observed in macromolecular membrane protein crystallography (214). The high-throughput nature of the technique is especially attractive for systems limited by their expression or purification yields. Thus, crystallization of the $RhoG_t$ complex by the *in meso* method was attempted. Like phospholipid bicelles, LCP host lipids can be readily supplemented with additives that contribute properties of the native membrane environment, such as cholesterol and charge (223). Given the influence of the electrostatic environment on $RhoG_t$ complex formation,

negatively charged phospholipids compatible with cubic host lipids were also screened in LCP crystallization trials (**Table 6**).

The chemical space sampled for LCP crystallization trials was much more defined than for other techniques. Volatiles that facilitate lipid solubilization were eliminated from all screens. This included most alcohols. Further, the PEG classes screened were limited to PEG400 and PEG4000. The former has been shown to stabilize the cubic phase and acts as a swelling agent to increase the size of the solvent channels permeating the bicontinuous membranes to facilitate protein diffusion, which is especially amenable to the crystallization of larger receptor complexes with soluble domains such as those of GPCR-G protein complexes (216).

The availability of a high-magnification microscope with the capacity to image UV fluorescence in addition to cross-polarized light greatly facilitated the screening process and allowed for the identification of microcrystal formation such as that shown in **Figure 31**. Under regular light, crystals appeared invisible to the naked eye (**Figure 31A;** *left*). The polarized image (**Figure 31A**; *right*), revealed the presence of microcrystals, which were subsequently successfully optimized and adopted a morphology that appeared quite promising (**Figure 31B**).
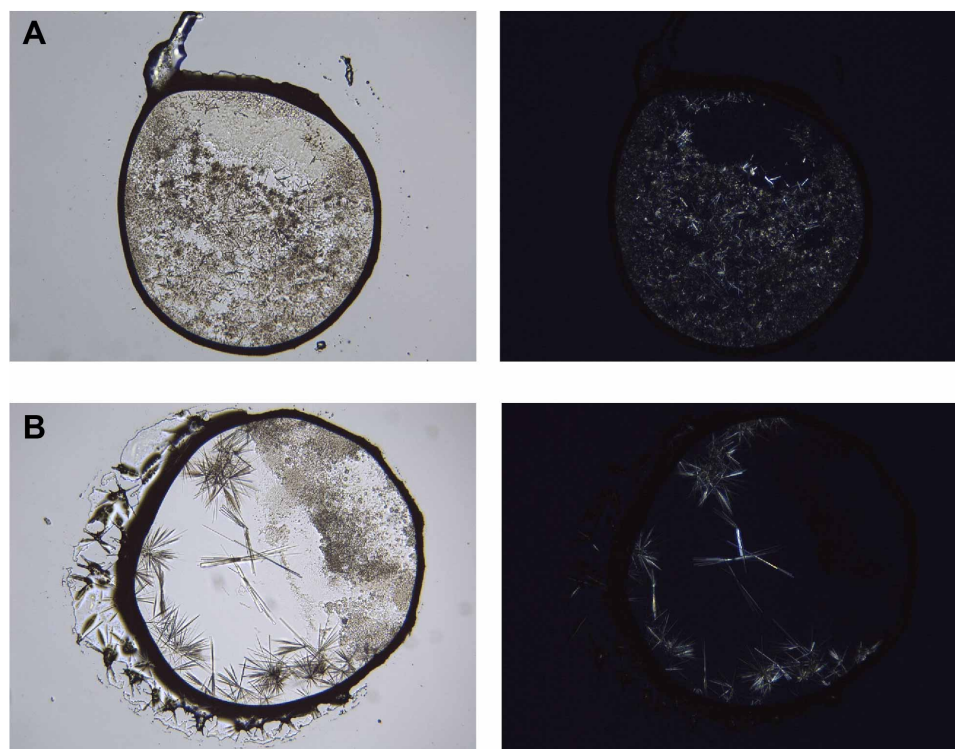
Figure 31. Microcrystals of RhoG$_t$ Obtained by the *in meso* Method. A) Initial morphology of RhoGt crystals obtained from 7.8 MAG + 5% DOPS. RhoGt (4 mg/mL) was mixed in a 60:40 v/v ratio with 7.8 MAG + 5% DOPS. A 50 nL bolus of the lipid/protein mixture was bathed in a solution (500 nL) consisiting of 50 mM Acetate pH 4.5, 0.2 M CaCl$_2$, and 15% PEG400. **B)** The optimized crystals were obtained 50 mM Acetate pH 4.5, 0.2 M CaCl$_2$, and 35% PEG400.

Despite the striking morphology of the optimized crystals, diffraction data proved that the quality of the crystals was worse than that observed for RhoGt crystallized in bicelles. Even the use of a microfocus beam (GMCAT ID-21) was unsuccessful at producing isotropic data of sufficient quality and resolution for determining a structure.

Conclusions

Phospholipid bicelles stabilization of RhoG$_t$ complexes was highly successful for *in vitro* biochemical characterizations and allowed for investigations of global features of the transient interaction between rhodopsin and transducin. Structural studies, however, were less successful in the presence of phospholipid bicelles. Inspection of the crystals

and the conditions from which they were obtained revealed a propensity for the formation of bicelle crystals depleted of protein, or at the least, containing very little protein. Interestingly, the addition of ATR as a means for extending the half-life of the complex appeared to facilitate formation of empty bicelle crystals. This was deduced from a series of negative controls on a number of different phospholipid compositions. Because the biochemical properties suggest a favorable environment for the receptor, the inability to crystallize the complex is likely due to some inherent, endogenous feature of these proteins.

While the rhodopsin-transducin system is an attractive GPCR-G protein system for structural studies because of its ease of purification, abundance in native membranes, and the lack of basal activity in the receptor, other features of the native complex may just be the limiting factor in obtaining the crystal structure of this highly coveted G protein state. Endogenous mammalian proteins such as rhodopsin and transducin come with post-translational modifications, which are very well characterized in both proteins. In this study, these modifications were left unaltered and crystallization trials were performed in their presence. Crystallization of the transducin heterotrimer (43) required proteolytic digest of such moieties, as did the structure of β_2AR-G_s (1). Heterogeneous distribution of post-translational modifications, which actually facilitate purification of rhodopsin, may have formed a barrier to the reproduction and optimization of crystallization conditions. Future crystallization attempts might require that this feature of the native proteins be addressed.

Biochemical studies were performed at concentrations significantly below those used for structural studies where G protein stability is likely uncompromised. Despite

being able to obtain highly pure, homogenous samples of activated RhoG$_t$, the limited ability to concentrate RhoGt samples above 15 mg/mL is likely a deterrent to crystal formation in both bicelle crystallization and the LCP method of membrane protein crystallization. Other GPCR crystals were grown using protein concentrations in excess of 50 mg/mL (225). While rhodopsin can be substantially concentrated in the absence of G protein, the addition of its cognate signaling partner caused significant precipitation at high concentrations of protein. This is likely due to some instability imposed on the G protein by the protein or buffer environment. It is also possible that the post-translational modifications themselves are what limit transducin solubility.

Differential scanning fluorimetery for measuring protein thermostability would be a useful experiment for identifying conditions that contribute to transducin stability and those that contribute to its instability. In this way, one can contribute to the optimization of crystallization conditions by screening protein buffers. While extensive effort was placed on screening detergents, purification methods, crystallization temperatures, and bilayer properties, less attention was given to the effect of buffer composition in this study. This is a common technique used in macromolecular crystallography for improving the diffraction quality of crystals, and the RhoG$_t$ system would likely benefit from similar treatment (226).

While the current protocol for obtaining rhodopsin from retinas using urea washing is a highly efficient method for obtaining large quantities of >90% pure receptor, there is some concern that the presence of the urea negatively alters the receptor and contributes to its heterogeneity. Further, any residual urea that may stick to the protein or the membranes could further disrupt the stability of the RhoGt interaction. A purification

91

protocol developed by Okada et al. utilizing Zn^{2+} precipitation of the receptor is a feasible alternative to the current protocol and has been shown to also be highly effective at isolating pure receptor (227). Further, crystallization of rhodopsin purified in this manner improved the quality of rhodopsin crystals (3). Recently, both protocols were used to purify phosphorylated rhodopsin. Comparison of the results from each revealed a significant difference in the monodispersity of the receptor as assessed by size exclusion chromatography (unpublished data, Qiuyen Chen). The purity and monodispersity of the receptor was significantly improved for rhodopsin purified by Zn^{2+} precipitation. Further, this alternative protocol eliminated the need for the time-consuming secondary ConA purification step, which significantly decreases the total handling time of the receptor and likely results in better quality protein for crystallization trials. Given this information, it would be worthwhile to revisit the method of rhodopsin purification from bovine retina.

Lastly, in light of recent structural and biophysical characterizations, we now know the extent to which the Gα helical domain facilitates receptor-mediated nucleotide exchange in G proteins. Computational, biophysical, and structural studies have revealed significant conformational changes that accompany receptor binding. Flexible protein regions have often prevented crystallization of even polar soluble proteins. In the context of a large, hydrophobic, and unstable signaling complex, the dynamic nature of the helical domain most likely interferes with isotropic crystal packing that is necessary for x-ray diffraction. Indeed, a stabilizing "nanobody" used to determine the structure of the β_2AR-G_s complex formed a plug between the GTPase and helical domains of the $G\alpha_s$ subunit in the structure. A similar "antagonist" against G protein activation that stabilizes the receptor-bound conformation of $G\alpha_t$ and limits the flexibility of the helical domain

will most likely be extremely advantageous to structural studies of the rhodopsin-transducin complex.

This work was has been adapted with permission from:

Thaker, T.M., Kaya A.I., Preininger, A.M., Hamm, H.E., Iverson, T.M. (2012) Allosteric Mechanisms of G protein-Coupled Receptor Signaling: A Structural Perspective. Methods in Molecular Biology. 796: 133-74.

CHAPTER V

CROSSTALK BETWEEN ALLOSTERIC NETWORKS INVOLVED IN THE
ACTIVATION OF Gα$_{i1}$

Introduction

Heterotrimeric G proteins, Gαβγ, function as molecular switches to elicit cellular responses (100). In the Gα subunit, the signaling activity is regulated by the identity of bound guanine nucleotide. Structural studies demonstrated that in the Gα subunit, the nucleotide identity is encoded in the conformations of three distinct loops termed Switch I, Switch II, and Switch III adjacent to the nucleotide-binding site (4,13,43,55) (**Figure 32A**). For example, crystal structures of the GDP-bound Gα$_{i1}$ subunit in the absence of the Gβγ subunits lacked interpretable electron density in Switches II and III, suggesting that these are disordered (2,4). In contrast, crystal structures of Gα$_{i1}$ bound to the GTP analogs, GDP-AlF$_4^-$ and GTPγS, demonstrated that the Switch regions adopt ordered conformations (4,13,40,43,55) that are proposed to be important for mediating protein-protein interactions with downstream effectors (17,228). Co-structures of Gα with adenylyl cyclase or GRK2 (53,229) have indeed revealed that Switch II composes a part of these effector-binding sites.

G protein coupled receptor (GPCRs) are key for converting the Gα subunit from its GDP- to GTP-bound forms and thus activating it for interaction with effectors regulation, as first identified from investigations of β$_2$-adrenergic receptor signaling in rat liver cells (19,20,23,28). Subsequent studies into photoreceptor activation and phosphodiesterase regulation in retinal disc membranes showed a direct interaction
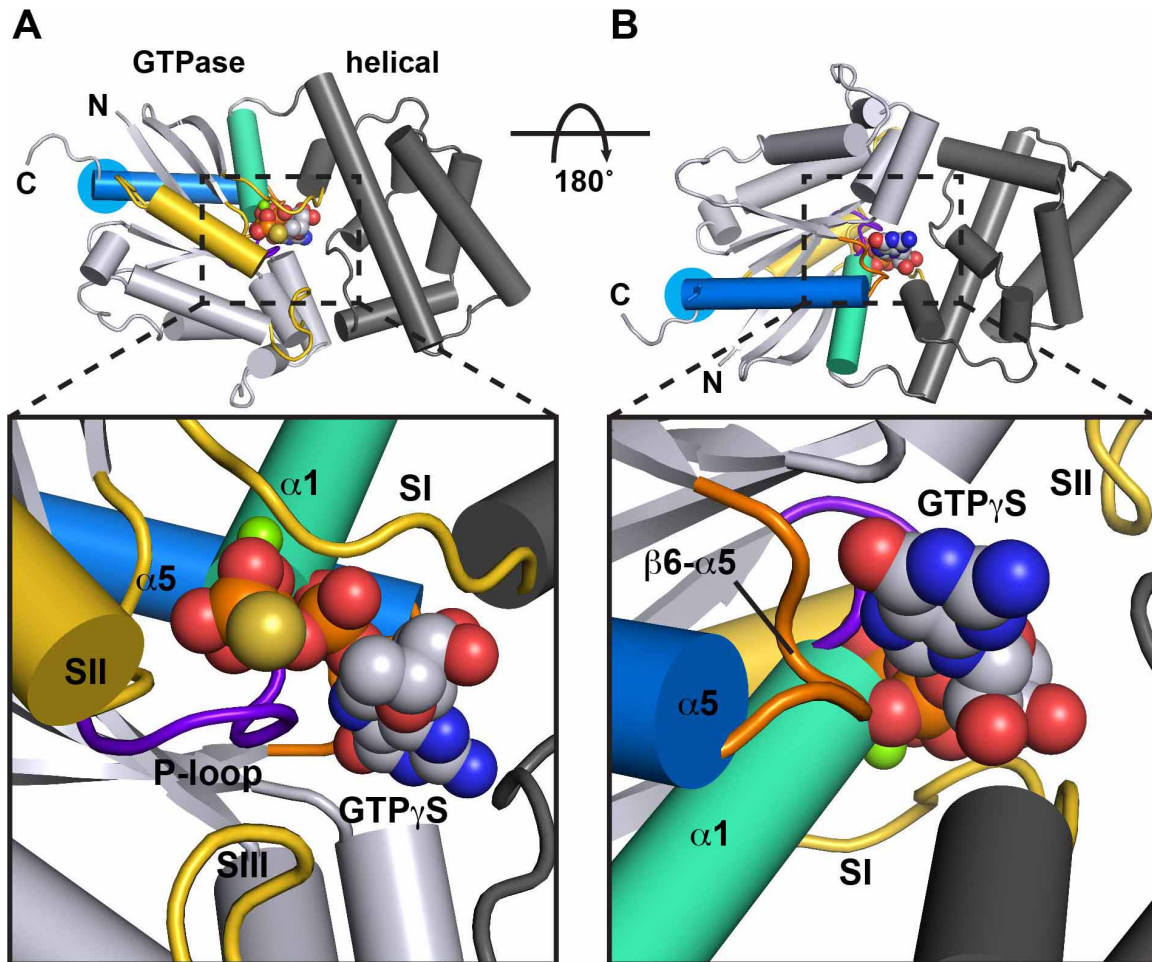
Figure 32: Overview of Structural and Functional Motifs of Gα$_{i1}$. Functional elements of Gα$_{i1}$ are shown mapped onto the structure of GTPγS-bound K345L Gα$_{i1}$. The GTPase and helical domains are labeled. The location of the K345L mutation on the α5 helix is highlighted with a *blue* circle. The N-terminus is truncated and only density following residue 32 is resolved in the structure shown. **A)** Conformations of the P-loop (*purple*) and Switch regions (SI, SII, SIII; *gold*) around the bound nucleotide. **B)** View rotated 180˚ to highlight the α1/α5 interaction and the β6-α5 loop orientation relative to GTP.

between rhodopsin and its cognate G protein, transducin, catalyzed the exchange of GDP for GTP in the Gα$_t$ subunit (32,34,230). Receptor-mediated GDP release has since been demonstrated to be the rate-limiting step of G protein activation (22,231). Biochemical, kinetic, and structural characterizations of Gα have been used to identify the sequence and structural elements of Gα that interact with receptor in order to propose a mechanism for guanine nucleotide exchange in the Gα subunit. For example, the Gα N-terminus

(123-125,128,232), the α4-β6 loop (118-120,233-235), the α3-β5 loop (121), and the C-terminus of Gα (128) have all been shown to mediate receptor-G protein interactions. Crystal structures of heterotrimeric G protein complexes have revealed that these regions formed a contiguous surface approximately 30 Å from the nucleotide-binding site (1,2,46,52).

Of the many receptor-interacting elements of Gα, perhaps the best studied is the Gα C-terminus. The importance of this Gα region in receptor-mediated nucleotide exchange was first revealed through interaction mapping using peptide mimetics of various regions of the G protein (128). In this study, changes in metarhodopsin II (meta II) formation upon binding of either transducin or a peptide derived from residues 340-350 of the Gαt C-terminus were monitored to determine the relative receptor affinities (128). Meta II is one of the activated states of rhodopsin and when in the meta II state, rhodopsin has high affinity for cognate G protein. Interestingly, competent G protein can stabilize the meta II state and conversely, meta II bound to G protein can stabilize the nucleotide-free state of Gα. The peptide corresponding to the C-terminus of Gα competed with transducin in binding rhodopsin and contributed to the stability of meta II (128) suggesting that C-terminal peptides of Gα could act as mimetics of the intact protein for stabilizing activated GPCRs. Further investigation using combinatorial libraries of peptide mimetics of the Gαt C-terminus containing systematic sequence substitutions identified mutations that resulted in peptides with improved affinity for rhodopsin over the parent sequence (236). Indeed a near 300-fold improvement in affinity was associated with a substitution in the peptide equivalent to a lysine to leucine substitution in the intact protein (K341L) (236). Similarly, the peptide mimetic of the Gαi1 C-terminus containing

the equivalent K345L mutation exhibited nearly two orders of magnitude improvement in affinity over peptide with the wild-type sequence (222). This enhanced affinity was important for stabilization of opsin and rhodopsin in activated forms for structure determination (80-82,237). Herrmann et al. examined the effects of a subset of the affinity-enhancing mutations in intact G proteins comprised of $G\beta_1\gamma_1$ and recombinant $G\alpha_{i1}$ engineered to express the C-terminal sequence of $G\alpha_t$ (238). Surprisingly, the K341L mutation on the chimeric $G\alpha_t/\alpha_{i1}$ protein background did not significantly improve the affinity for receptor as compared to the wild-type $G\alpha_t$ sequence (238). One possibility that was not considered at the time is the potential influence such a mutation may have on the assembly of allosteric networks within $G\alpha$ that communicate receptor recognition events into a nucleotide exchange response.

Complementary biophysical and structural experiments strongly suggest that the C terminus of the $G\alpha$ subunit drives allosteric guanine nucleotide exchange in the $G\alpha$ subunit. Specifically, these studies have focused on the α5 helix, an extension of the $G\alpha$ C-terminus that forms a direct connection from the receptor-binding surface of the G protein to its nucleotide-binding pocket. For example, site-directed spin labeling (SDSL) combined with electron paramagnetic resonance (EPR) spectroscopy measurements (131,239) revealed unique changes in both mobility and solvent accessibility of various spin label modifications along the α5 helix upon receptor activation (131). These changes were attributed to a rigid-body rotation and translation motion adopted by the helix. Uncoupling of this motion from receptor interactions by the insertion of a glycine linker into the α5 helix abolished nucleotide exchange within $G\alpha_{i1}$ (131,240). In complementary studies, cysteine mutagenesis stabilizing the position of the α5 helix in an activated

97

conformation demonstrated a dramatic increase in nucleotide exchange in the absence of receptor and suggested that the α5 helix dipole could contribute to GDP release (15). Van Eps et al. expanded upon these studies and again used SDSL and double electron-electron paramagnetic resonance to show that receptor interactions with the Gα C-terminus facilitated separation of the GTPase and helical domains (136). Crosslinking of the GTPase and helical domains by engineering cysteine disulfides further established that the domain separation was a necessary component of receptor-enhanced nucleotide exchange (136). The recent crystal structure of the β$_2$-adrenergic-Gα$_s$ has since corroborated the presence of extensive receptor-α5 helix interactions, as well as the presence of a significant reorientation of the helical domain (1).

While the α5 helix is a major determinant of Gα activation, a number of additional studies using mutagenesis (241,242), biophysical (131,136), and computational approaches (243,244) have identified conformational changes that accompany those exhibited by the α5 helix during G protein activation. Molecular dynamics simulations have proposed models that suggest receptor recognition stabilizes the αN-β1 junction and the β2-β3 hairpin, in addition to the α5 helix, in Gα proteins to relay receptor interactions into a GDP dissociation response (243,244). Fluorescently labeled Gα$_{i1}$ exhibited receptor-dependent changes in the environments of Switch I and Switch II, supporting a global effect of receptor binding on the structural organization of Gα proteins (137). Similarly, EPR studies revealed receptor-mediated changes in the mobility of spin labels on the β1, β2, and β6 strands of Gα$_{i1}$ (109,131). These strands form extensions of Switch I, the P-loop, and the α5-β6 loop, all of which are active site elements that have also been shown by EPR to exhibit conformational variability (131,136). Biochemical and

structural studies on the $G\alpha_{i1}$ variants altering the P-loop (5,27) and $\alpha5$-$\beta6$ loop (15,25,29) and linker (29) have revealed the importance of protein-nucleotide interactions (**Figure 32B**) mediated by residues of these structural elements in facilitating nucleotide exchange. These findings suggest that the allosteric mechanism of Gα activation likely involves precise coordination between each of the aforementioned components.

Despite these significant efforts, the mechanism of receptor-mediated allosteric activation of Gα subunits is not fully understood. Based upon the previous findings that the K341L mutation of $G\alpha_t$ displays substantially different biochemical behavior in the intact protein than it does in a peptide, we hypothesized that this mutation altered the allosteric activation network. Accordingly, we used the equivalent K345L variant of $G\alpha_{i1}$ as a tool to probe transient allosteric properties of receptor-mediated guanine nucleotide exchange. Our results combine receptor-binding studies, high-resolution crystallographic studies, and stability measurements to demonstrate how the presence of the K345L mutation alters the allosteric network in the $G\alpha_{i1}$ subunit. These results allow us to propose a mechanism for how various structural elements within Gα proteins likely coordinate to facilitate allosteric G protein activation.

Methods

Experimental methods for ROS membrane preparation, rhodopsin purification, transducin purification, nucleotide exchange assay, and the rhodopsing binding assay (extra meta II stabilization assay) are described in the Methods section of Chapter II. Assays and methods unique to the subject matter presented in this chapter are described below.

Expression and Purification of Ga Subunits

Gα$_{i1}$ was expressed as a fusion protein from a single colony of transformed *E. coli* BL21-Gold (*DE3*). Transformed *E. coli* was grown in a 2mL starter culture of 2X YT media with 50 µg/mL at 37 °C for 8 hours. The culture was then transferred to 150 mL of 2X YT media with 50 µg/mL kanamycin A and grown at 37 °C overnight. Large-scale cultures (980 mL of 2X YT media with 50 µg/mL kanamycin A) were inoculated with 20 mL of the overnight culture and grown at 37°C until the cells reached an OD$_{600}$ of approximately 0.6. Expression was induced with 30-60 µM of IPTG for 18 hrs at 22°C. After induction, the cells were harvested by centrifugation and frozen at -80°C.

Prior to purification, cell pellets were thawed and resuspended in ice-cold Lysis Buffer (50 mM NaHPO$_4$, 300 mM NaCl, 2 mM MgCl$_2$, 5 mM βME, 20 µM GDP, pH 8.0) supplemented with 0.1 mM PMSF or 1 mM pefabloc (Lysis Plus Buffer) and 1 µg/mL aprotinin, leupeptin, and pepstatin. The resuspended cells were disrupted by sonication and the lysate clarified by centrifugation for 1 hr at 220,000 × *g*. The supernatant was treated with 10 µg/mL DNase and RNase, filtered, and added in batch to a 50% slurry of TALON Cobalt affinity resin equilibrated in Lysis Plus Buffer. Supernatant was bound to resin by rotating for 1 hour at 4°C. Protein-loaded resin was transferred to a gravity flow column and the column washed with 20 column volumes of Lysis Plus Buffer, then 6 column volumes of Lysis Plus Buffer supplemented with 5 mM imidazole pH 8.0, The protein was eluted with 5 column volumes of Lysis Plus Buffer supplemented with 100 mM imidazole pH 8.0. The eluted protein was concentrated using an Amicon 10 kDa MWCO centrifugal concentrator at 2,000 × *g*. The concentrated sample was then diluted 20-fold with Lysis Buffer, and thrombin was added at a

concentration of 1 U per 1 mg of purified protein. The sample was then incubated overnight on ice at 4°C to allow for cleavage of the N-terminal affinity tag. The protein sample was further purified by passing over a column of TALON Cobalt affinity resin equilibrated in Lysis Buffer to trap uncleaved product, and by size exclusion chromatography on a Superdex S200 10/300GL column equilibrated in Storage Buffer (50 mM Tris-Cl, 200 mM NaCl, 2 mM $MgCl_2$, 1 mM EDTA, 1 mM dithiothreitol (DTT), 20 µM GDP, pH 8.0) to remove aggregate. The cleaved protein contains two additional N-terminal residues (Gly-Ser) derived from the thrombin recognition sequence. Purified $G\alpha_{i1}$ was concentrated to 10 mg/mL and glycerol added to 10% (v/v) prior to storage at -80°C. $G\alpha$ concentrations were determined by the BCA assay (245) for all crystallization and biochemical characterizations.

Rhodopsin and Transducin Purification

Endogenous rhodopsin and transducin were purified as previously described (220). Briefly, dark-adapted rhodopsin was stored as aliquots of urea-washed rod outer segment (ROS) membranes, which were prepared by washing retinas twice with EDTA Buffer (10 mM Tris-Cl, 1 mM EDTA, 1 mM DTT, ph 7.5) and once with Urea Buffer (10 mM Tris-Cl, 1 mM EDTA, 1 mM DTT, 7 M urea, pH 7.5). Pelleted membranes were then resuspended in 10 mM MOPS, 200 mM NaCl, 2 mM $MgCl_2$, 1 mM DTT, 100 µM PMSF, pH 7.5 and aliquots stored at -80°C.

The rhodopsin-transducin complex was purified from light-adapted bovine ROS membranes. Membranes were washed four times with Isotonic Buffer (5 mM Tris-Cl, 130 mM KCl, 0.6 mM $MgCl_2$, 1 mM EDTA, 1 mM DTT, pH 8.0) and two times with

Hypotonic Buffer (5 mM Tris-Cl, 0.6 mM $MgCl_2$, 1 mM EDTA, 1 mM DTT, pH 8.0). Transducin was then released into the supernatant by resuspending ROS membrane pellets with Hypotonic Buffer containing 0.1 mM GTP. The membranes were pelleted by centrifugation and the supernatant containing transducin was dialyzed against Transducin Storage Buffer (20 mM Tris-Cl, 200 mM NaCl, 10 μM GDP, 5 mM β-ME, 10% glycerol, pH 7.5). Purified transducin was stored at -80°C.

Basal and Receptor-mediated Nucleotide Exchange

The rate of GDP exchange for GTPγS in Ga_{i1} was determined by monitoring the increase in intrinsic tryptophan fluorescence (λ_{ex}= 290 nm, λ_{em}= 340 nm) using a Varian Cary Eclipse fluorescence spectrometer. The fluorescence signal from basal nucleotide exchange was measured at 21°C for 90 min after addition of 10 μM GTPγS to 500 nM wild-type or mutant Ga_{i1} in 50 mM Tris-Cl, 200 mM NaCl, 2 mM $MgCl_2$, 1 mM DTT, pH 7.5. Receptor-mediated nucleotide exchange was monitored for heterotrimeric G protein, $Ga_{i1}\beta_1\gamma_1$, reconstituted by incubating wild-type or mutant Ga_{i1} with $G\beta_1\gamma_1$ purified from endogenous transducin in a 1:1 molar ratio. 2 μM of dark rhodopsin in urea-washed rod outer segment (ROS) membranes was added to 500 nM heterotrimeric G protein sample prepared in assay buffer and incubated in the dark. Immediately upon the addition of 10 μM GTPγS, samples were light activated and mixed by pipetting. The fluorescence signal from receptor-mediated nucleotide exchange was monitored for 60 min at 21°C. Nucleotide exchange rates were calculated from data for 3 independent experiments with 4 replicates per experiment and fit using a one-site exponential association equation in Prism.

102

Rhodopsin Binding Assay

Wild-type and K345L $G\alpha_{i1}$ binding to rhodopsin in urea-washed ROS membranes was measured as previously described (15). $G\alpha_{i1}$ (5 μM) was incubated with $G\beta\gamma$ (10 μM) and rhodopsin (50 μM) in binding buffer (50 mM Tris-Cl, 100 mM NaCl, 2 mM MgCl2, pH 8.0) for 30 min at 4°C and assessed under three different conditions: dark-adapted, after light activation, and after light activation with the addition of GTPγS (100 μM). Supernatants were separated from membranes by centrifugation at 200,000 × g for 1 hr. Dark-adapted fractions were protected from light during centrifugation and supernatants removed under dim red light. Isolated fractions were boiled, visualized by Coomasie-stained SDS-PAGE gel, and quantified by densitometery using a Bio-Rad Multimager. Quantities of 37 kDa $G\alpha_{i1}$ in either the soluble or insoluble fraction are expressed as a percentage of the total protein in both. Data reported are the average of at least three independent experiments.

Extra Metarhodopsin II Formation

The formation of meta II in ROS membranes was measured on an Aminco DW2000 spectrophotometer in the presence of increasing concentrations of G protein as previously described (123). Heterotrimeric G protein was reconstituted from purified wild-type or K345L $G\alpha_{i1}$ in the same manner as used for receptor-mediated nucleotide exchange measurements. Rhodopsin (2 μM) in dark-adapted urea-washed ROS membranes were incubated with varying concentrations of wild-type or K345L $G\alpha_{i1}\beta_1\gamma_1$ in meta II buffer (50 mM HEPES, 100 mM NaCl, 1 mM MgCl$_2$, 1 mM DTT, pH 8.0) on ice for approximately 10 min. Absorption spectra for both dark and light-adapted samples

were then collected at 4°C. Following collection of a dark-adapted spectrum, samples were exposed to 2 quick flashes of light approximately 30 s apart. The light-adapted spectrum was then immediately collected. The extra meta II signal was calculated as the change in meta II formation (difference between absorption at 390 nm and 440 nm) upon light activation. Dose response curves were generated by nonlinear regression using a sigmoidal dose-response (variable slope) equation as previously described (222).

Differential Scanning Fluorimetry (DSF)

DSF was performed as described (226). Protein samples were diluted to a final concentration of 5 μM in assay buffer containing 5× SYPRO Orange (BioRad) and 50 μM GDP or GTPγS. Thermostability was screened in both the extra meta II (EMB) assay buffer and nucleotide exchange (NEB) assay buffer. Triplicate samples were prepared in 20 μL volumes and transferred to a clear low-profile 96-well PCR plate (BioRad) and equilibrated at 25 ˚C for 2 min in a BioRad CFX96 Real-time system (C1000 Thermal Cycler) prior to a temperature ramp from 25˚C to 95˚C in 0.2˚C increments at a rate of 1˚C/min. Data were analyzed using DSF analysis tools version 3.0.2 (226).

Crystallization, Data Collection, Structure Determination and Refinement

Crystals of GDP- and GTPγS-bound forms of the K345L $G\alpha_{i1}$ variant protein were grown by hanging-drop vapor diffusion using previously reported conditions (10). Prior to crystallization, purified protein was diluted into 80 mM HEPES, 120 mM succinic acid, 8 mM DTT, pH 8.0 and concentrated to 11 mg/mL in an Amicon 10 kDa MWCO centrifugal concentrator. Protein was incubated with 1 mM GTPγS for at least 1

hour or briefly with 20 μM GDP, 40 μM AlCl$_3$, and 16 mM NaF. Crystals were grown from hanging drops consisting of 4.8 μL protein (10 mg/mL) and 1.2 μL reservoir solution (2.0 – 2.2 M ammonium sulfite pH 8.0, 5 – 20 mM MgSO$_4$) equilibrated against 1 mL of reservoir solution at 20°C. Crystals were cryo-protected by briefly soaking in reservoir solution containing glycerol at a final concentration of 17.5% and flash-cooled by plunging in liquid nitrogen.

Diffraction data were collected at the Advanced Photon Source (APS) beamlines 21-ID-D and 21-ID-G. All data were collected at 100 K and recorded on a Mar 300 detector. Crystals formed in two different space groups: P3$_2$21 for GTPγS-bound K345L Gα$_{i1}$ and I4 GDP-bound K345L Gα$_{i1}$. All data were indexed, integrated, and scaled using HKL2000 (246). Crystallographic data processing and refinement statistics are reported in **Table 8.**

The structure of GTPγS-bound K345L Gα$_{i1}$ was determined by molecular replacement in Phaser (247) using the structure of K349P Gα$_{i1}$ as a search model (PDB ID: 2ZJY) (10). The structure of GDP-bound K345L Gα$_{i1}$ was determined by molecular replacement in Phaser using the GTPγS-bound K345L Gα$_{i1}$ structure as a search model. Iterative rounds of refinement in Phenix (248) and model building in Coot (249) were performed to improve model quality. Geometry was assessed in Procheck (250) and Molprobity (251). Figures 1, 3, 4, 5, 6 and 7 were prepared using PyMOL (247).

Table 8. K345L Gα$_{i1}$ Crystallographic Data Collection and Refinement statistics

	GDP-bound	*GTPγS-bound*
Data collection		
Beamline	21-ID-D	21-ID-G
Wavelength	1.078 Å	0.979 Å
Space group	I 4	P 3$_2$ 2 1
Unit cell dimensions	a=121.5 Å	a=79.6 Å
	b=121.5 Å	b=79.6 Å
	c=68.2 Å	c=104.8 Å
	α=β=γ=90°	α=β=90°, γ=120°
Resolution Range	50 - 2.10 Å (2.18 - 2.10 Å)[a]	50 - 1.55 Å (1.61 - 1.55 Å)
Number of reflections	143,580	419,345
Unique reflections	29,073	55,216
R$_{sym}$[b]	5.3% (35.0%)	6.9% (38.6%)
<I>/<σ>[c]	24.0 (5.0)	22.8 (3.7)
Completeness	99.7% (100%)	97.7% (92.0%)
Refinement		
R$_{cryst}$[d]	17.9%	15.6%
R$_{free}$[e]	21.5%	18.7%

[a]Values in parentheses are for the highest resolution shell.

[b]R$_{sym}$= $\Sigma_{hkl} \Sigma_j \mid I_j - \langle I \rangle \mid / \Sigma_{hkl} \Sigma I_j$, where j is the jth measurement and <I> is the weighted mean of I.
[c]<I>/<σ> is the mean intensity divided by the mean error.

[d]R$_{cryst}$= $\Sigma_{hkl} \mid\mid F_o \mid -k \mid F_c \mid\mid / \Sigma_{hkl} \mid F_o \mid$, where F_o and F_c are the observed and calculated structure factor amplitudes, and k is a weighting factor.
[e]R$_{free}$ is the same as R$_{cryst}$ calculated on 5% of the reflections in GDP-bound K345L Gα$_{i1}$ (1507 reflections) and GTPγS-bound K345L Gα$_{i1}$ (2806 reflections).
[f]Ramachandran analysis from PROCHECK (250).

Results

Basal and Receptor-mediated Nucleotide Exchange

Basal and receptor-mediated nucleotide exchange rates were measured for recombinant Gα$_{i1}$ as a function of the increase in intrinsic tryptophan fluorescence upon the addition of the nonhydrolyzeable GTP analog, GTPγS. The K345L Gα$_{i1}$ exchange rates were approximately 30% and 20% slower under basal and receptor-mediated conditions, respectively, than wild-type Gα$_{i1}$ (**Figure 33A; Table 9**).

Binding and Activation of Rhodopsin by the K345L Gα$_{i1}$β$_1$γ$_1$

Reconstituted Gα$_{i1}$β$_1$γ$_1$ binding to rhodopsin in ROS membranes was used to assess the effect of the K345L mutation on the ability of Gα$_{i1}$ to bind activated receptor (**Figure 33B,C**). Quantifying the percent recovery of Gα$_{i1}$ protein in the pellet fraction or the soluble fraction revealed that the amount of K345L Gα$_{i1}$ bound upon light activation (LP) was decreased compared to wild-type Gα$_{i1}$. Conversely, the quantity of Gα$_{i1}$ released into the soluble fraction upon light activation was greater for K345L Gα$_{i1}$. This suggests that the presence of the K345L mutation alters the receptor-binding site in Gα$_{i1}$.

The extra meta II assay was used to quantify the affinity between receptor and wild-type or K345L Gα$_{i1}$β$_1$γ$_1$ (**Figure 33C; Table 9**). Using this method, the affinity measured between rhodopsin and wild-type Gα$_{i1}$β$_1$γ$_1$ (EC$_{50}$ = 0.89 ± 0.02 μM) was found to be comparable to that determined by kinetic light scattering (EC$_{50}$ = 0.72 ± 0.05 μM)(238). However, the K345L Ga$_{i1}$b$_1$g$_1$ (EC$_{50}$ = 2.03 ± 0.05 μM) had a modestly reduced affinity. *In silico* modeling of the K345L Gα$_{i1}$ bound to rhodopsin was based upon the Gα$_s$- β$_2$ adrendergic receptor costructure (1) and did not offer a trivial explanation for this reduction in affinity (not shown).
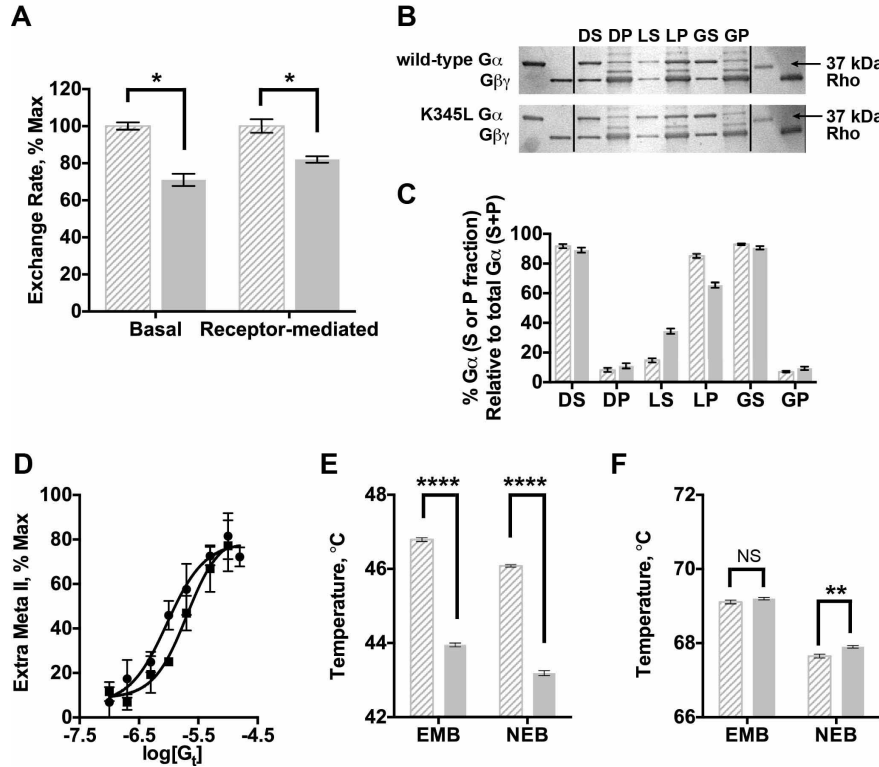
Figure 33: Biochemical Properties of Gα$_{i1}$ Variants. Data for wild-type ( ) and K345L ( ) Gα$_{i1}$. **A)** Basal and receptor-mediated nucleotide exchange rates measured as a function of intrinsic fluorescence (λ_{ex} = 280 nm, λ_{em} = 340 nm). The change in fluorescence was monitored at 21 °C for 500 nM wild-type and K345L Gα$_{i1}$β$_1$γ$_1$ upon the addition of 10 μM GTPγS. Samples for determining receptor-mediated nucleotide exchange rates were additionally incubated with 2 μM rhodopsin. Data were fit with an equation for pseudo-first order association kinetics. Data presented here are relative to wild-type Gα$_{i1}$, which was normalized to 100%. **B)** SDS-PAGE gels of wild-type and K345L Gα$_{i1}$ proteins reconstituted with Gβγ prior to binding ROS membranes in the dark, in the light, and after light activation, following the addition of GTPγS. Abbreviations are: DS, supernatant from the dark-adapted sample; DP, pellet fraction from the dark-adapted sample; LS, light supernatant; LP, light pellet; GS, supernatant from light activated sample with GTPγS; GP, pellet from light activated sample with GTPγS. **C)** Results from densitometry quantitaiton of SDS-PAGE gels in C). **D)** Rhodopsin affinity for Gα$_{i1}$β$_1$γ$_1$ determined by the extra meta II assay. Rhodopsin (2 μM) was incubated with varying concentrations (0-15 μM) of wild-type ( ) and K345L ( ) Gα$_{i1}$β$_1$γ$_1$ and the change in meta II determined by monitoring the absorbance before and after light activation at 4°C. Data were plotted as a function of the Gα$_{i1}$β$_1$γ$_1$ concentration and fit to a 4-paramater, variable slope equation to calculate the EC$_{50}$ values. **E-F)** Fluorescence analysis of heat-induced melting of wild-type and K345L Gα$_{i1}$. Protein sample (5 μM) in NEB or EMB buffer was incubated with 10X **E)** GDP or **F)** GTPγS and SYPRO orange dye prior to melting. Changes in the fluorescence signal were monitored upon a temperature ramp from 25 °C to 95 °C. Sigmoidal regions of the data were fit with the Boltzmann equation to determine the T$_m$ values, which are plotted here as the average of three independent trials per sample. Results shown are the mean ± S.E.M. of three independent experiments (* $p < 0.05$; ** $p < 0.01$; **** $p < 0.0001$).

Table 9. Results from Biochemical Characterizations of $G\alpha_{i1}$ Proteins.

	Wild-type	K345L	E43A
Nucleotide Exchange Rates			
Basal (min^{-1})	0.0180 ± 0.0006	0.0126 ± 0.0007	0.0176 ± 0.0005
Δ rates (basal)		**-30%**	**-2%**
Receptor-mediated (min^{-1})	0.20 ± 0.01	0.164 ± 0.005	0.131 ± 0.005
Δ rates (receptor-mediated)		**-19%**	**-35%**
Rhodopsin binding affinity			
Affinity (mM)	0.89 ± 0.02	2.03 ± 0.05	0.77 ± 0.06
Δ affinity		**-2.3-fold**	**+0.9-fold**
Thermostability			
GDP-bound			
Tm (˚C) (NEB)	46.08 ± 0.02	43.19 ± 0.04	44.59 ± 0.01
ΔT_m		**-2.89**	**-1.49**
Tm (˚C) (EMB)	46.79 ± 0.03	44.00 ± 0.07	44.77 ± 0.03
ΔT_m		**-2.83**	**-2.01**
GTPγS-bound			
Tm (˚C) (NEB)	67.65 ± 0.03	67.90 ± 0.02	66.01 ± 0.04
ΔT_m		**0.25**	**-1.63**
Tm (˚C) (EMB)	69.11 ± 0.03	69.20 ± 0.02	66.80 ± 0.04
ΔT_m		**0.09**	**-2.30**

Thermostability of the K345L Ga_{i1} Variant

To identify how the K345L $G\alpha_{i1}$ mutant influences the stability of the nucleotide binding states of $G\alpha_{i1}$, we measured the thermostability of the wild-type and the K345L variant in the presence of GDP (**Figure 33E; Table 9)** or GTPγS (**Figure 33F; Table 9**). Consistent with previous studies, both wild-type and K345L $G\alpha_{i1}$ are more stable when bound to GTPγS than GDP (13,40,43). The T_m values for GTPγS-bound wild-type and K345L $G\alpha_{i1}$ were statistically identical. In comparison, the T_m of the GDP-bound K345L $G\alpha_{i1}$ variant decreased by 2.8 °C as compared to wild-type $G\alpha_{i1}$.

Structures of the GTPγS- and GDP-bound K345L Gα$_{i1}$ Subunit

To examine the architectural changes in the K345L Gα$_{i1}$ variant, crystal structures in the GDP (**Figure 34A**) and GTPγS-bound (**Figure 34B**) states were determined to 1.5 Å and 2.1 Å resolution, respectively (**Table 8**). The resolution of these structures is among the highest observed for any Gα protein with each respective guanine nucleotide. Superposition of corresponding backbone Cα atoms of GTPγS-bound K345L Gα$_{i1}$ and GTPγS-bound wild-type Gα$_{i1}$ (PDBID: 1GIA (13)) resulted in an r.m.s. deviation of 0.299 Å (310 Cα atoms aligned out of 321 total) suggesting little conformational change accompanied the mutation. However, it is noted that residues at the N- and C-termini that have not previously been resolved in crystal structures of GTPγS-bound Gα$_{i1}$ proteins were clearly observed in the electron density. At this time, it is unclear whether the observation of the residues at the termini is a direct result of the mutation or is simply a crystal-to-crystal variation.

In contrast, superposition of GDP-bound K345L Gα$_{i1}$ and GDP-bound wild-type Gα$_{i1}$ (PDBID: 1GDD (4)) resulted in a r.m.s. deviation of 0.452 Å between Cα atoms (324 aligned out of 335 total). The statistically significant conformational difference of the GDP-bound form is consistent with the biochemical assessment that the GDP-bound state of Gα$_{i1}$ has been altered by the K345L mutation. The majority of the structural differences observed in the GDP-bound K345L Gα$_{i1}$ structure occurred within functionally important motifs of the guanine nucleotide binding site located at the interface of the GTPase and helical domains of the protein. The Switch regions in the GDP-bound K345L Gα$_{i1}$ structure displayed the most significant conformational changes.
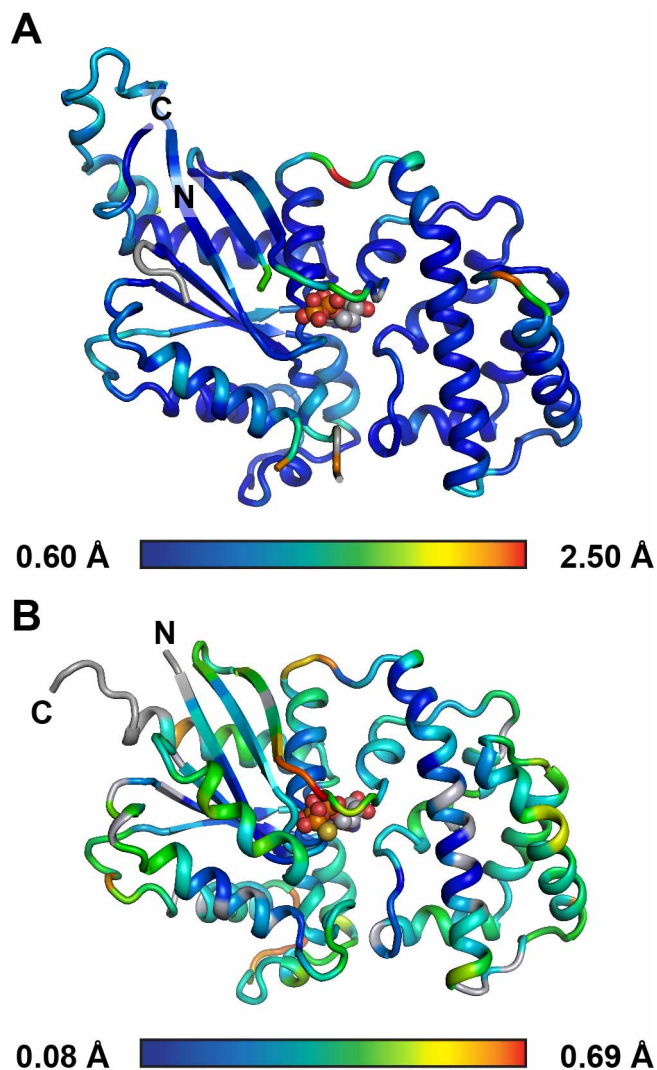
Figure 34: Structural Overview of A) GDP-bound and B) GTPγS-bound K345L Gα$_{i1}$. Structures are colored by the Cα RMS deviation calculated for K345L Gα$_{i1}$ and wild-type Gα$_{i1}$ (PDB IDs: 1GDD (GDP-bound) and 1GIA (GTPγS-bound)). Scale bars corresponding to the range in RMS deviation values are shown below.

The Switch I position was marked by an inward shift (**Figure 35A**) as compared to wild-type. This reorientation positioned Switch I in closer proximity to the α and β- phosphates of the bound GDP. Accompanying the new position of Switch I in the K345L Gα$_{i1}$ structure was the formation of a salt-bridge (2.3 Å) between Arg178 and Glu43 of the P-loop (**Figure 35B**). In previous studies, enhanced interactions between Switch I residues and bound nucleotide are correlated with reduced nucleotide exchange in Gα (46,239),
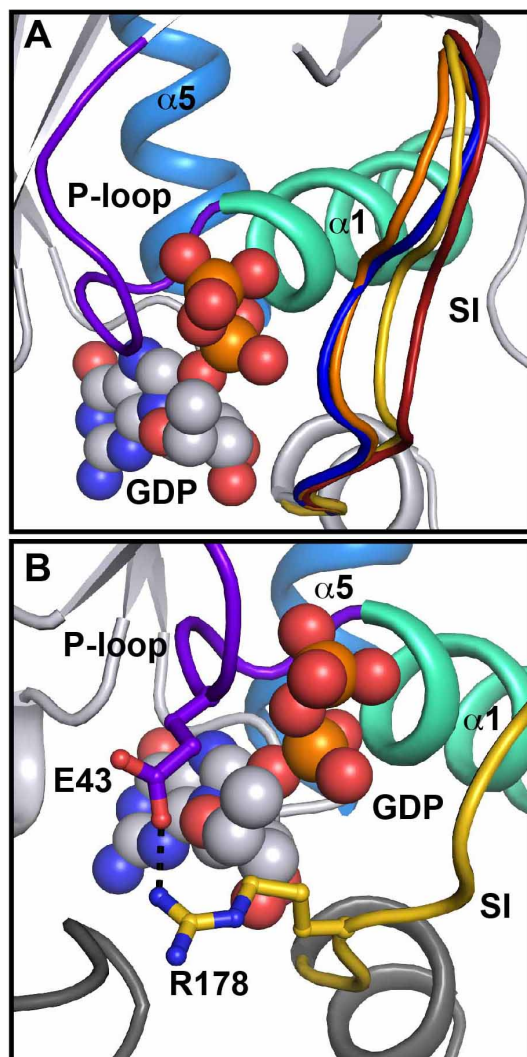
Figure 35: Switch I Conformational Changes in GDP-bound K345L Gα$_{i1}$. **A)** Relative orientation of Switch I (SI) observed in the structure of GDP-bound K345L Gα$_{i1}$ (*yellow*) compared to GDP-bound wild-type (PDBID: 1GDD; *red*), GTPγS-bound wild-type (PDBID: 1GIA; *blue*), and GDP-AlF⁻-bound Gα$_{i1}$ (PDBID: 1GFI; *orange*). **B)** The conformation of SI in the GDP-bound K345L Gα$_{i1}$ structure promotes the formation of an ionic interaction (2.3 Å) between Glu43 from the P-loop and Arg178 from SI.

suggesting that GDP is more tightly bound. Conversely, reduction of the number of Switch I interactions with bound nucleotide are correlated with an increase in the rate of nucleotide exchange in Gα subunits (6,29).

In GDP-bound K345L Gα$_{i1}$, Switch II and III differed in both structure and orientation as compared to wild-type Gα$_{i1}$. Five of the 17 Switch II residues (**Figure**

112

36A) and two of the six Switch III residues (**Figure 36B**) that were not observed in wild-type $G\alpha_{i1}$ bound to GDP (**Figure 36C**) were clearly resolved, albeit in a conformation that differed from GDP-bound $G\alpha_t$ (42) (**Figure 36D**), GDP-AlF$_4$-bound $G\alpha_{i1}$ or GTPγS $G\alpha_{i1}$. The change in Switch II may be physically propagated to the adjacent β2-β3 hairpin loop, which exhibits a 0.5 Å inward shift in the GDP-bound K345L $G\alpha_{i1}$ and a 0.5 Å outward shift in the GTPγS-bound K345L $G\alpha_{i1}$ as compared to wild-type.

Validation of the Conformational Changes as a Part of the Signaling Pathway Using Site-directed Mutagenesis

Many of the residues in regions that undergo conformational changes in the K345L $G\alpha_{i1}$ structure have been mutagenized and the altered signaling characteristics reported in the literature (6,25,29,109,131,239). To validate that the observed conformational changes are indeed important for allosteric signaling, we selected Glu43 as a target. In the GDP-bound K345L $G\alpha_{i1}$ structure, Glu43 forms a salt bridge to Arg178 that links Switch I and the P-loop. If this salt bridge is transiently formed during allosteric signaling, we anticipate that loss of the negative charge of Glu43 would result in a change in receptor-mediated nucleotide exchange rates. Biochemical analysis (**Table 9**) indeed shows a 35% reduction in receptor-mediated nucleotide exchange while basal nucleotide exchange was unaffected. The binding between the E43A $G\alpha_{i1}$ variant and rhodopsin was not affected as assessed by the meta II assay ($EC_{50} = 0.77 \pm 0.06$ mM). In addition, the T_m in GDP was statistically identical to that of wild-type, but decreased from 69.11 ± 0.03 °C (wild-type $G\alpha_{i1}$) T_m) to 66.80 ± 0.04 °C) in the presence of GTPγS.
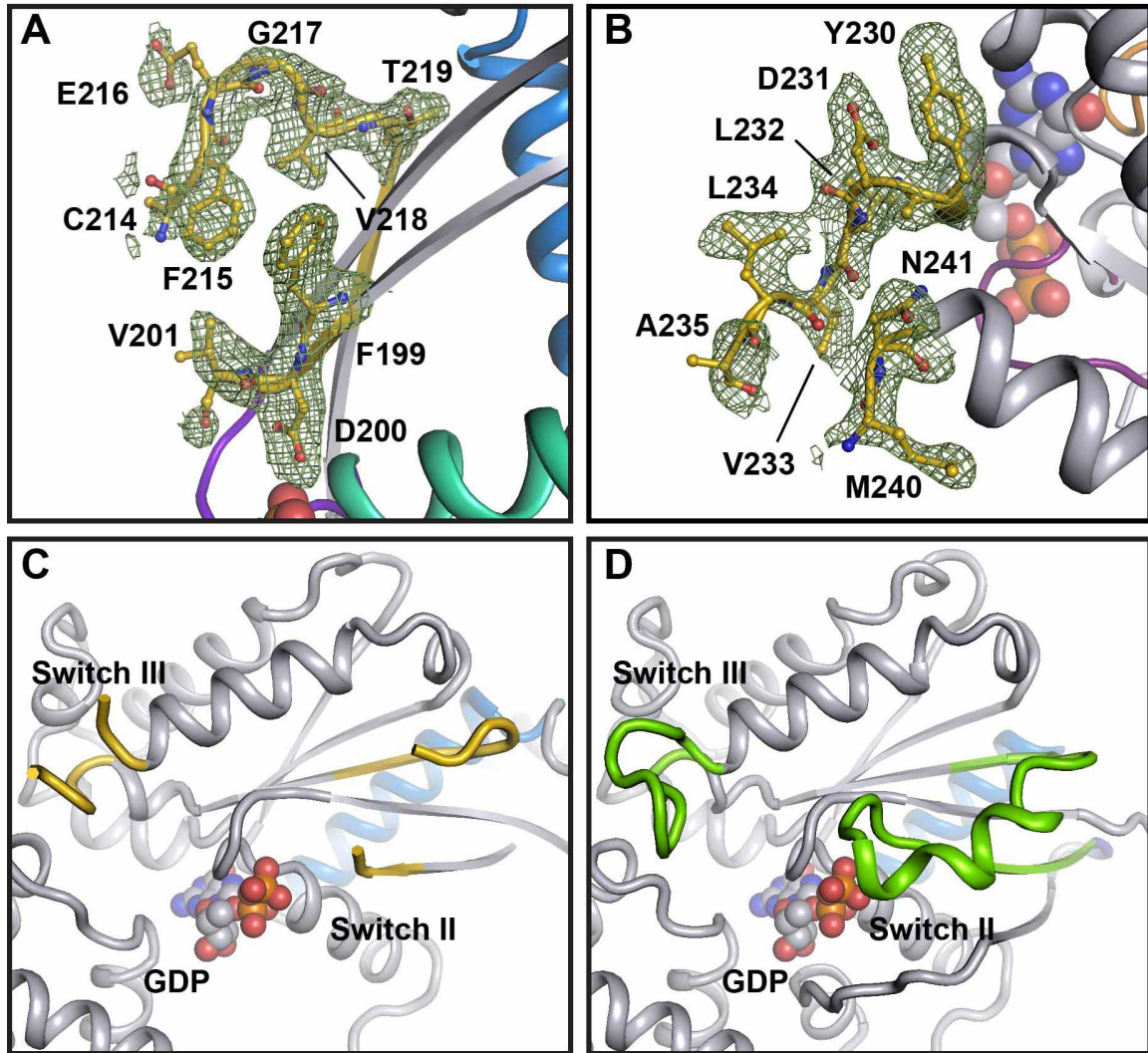
Figure 36: Conformational Variability of Switch II and III in GDP-bound Gα. A) Difference (F_o-F_c) electron density for Switch II and **B)** Switch III in GDP-bound K345L Gα_{i1} contoured to 2σ. Relevant structural elements are labeled as such. Comparison of Switch II (SII) and Switch III (SIII) conformations in **C)** GDP-bound K345L Gα_{i1} (*yellow*) and **D)** wild-type Gα_t (*green*).

That this mutation affects receptor-mediated activation but not basal nucleotide exchange or receptor binding strongly indicates that Glu43 contributes to allosteric signaling as predicted.

Discussion

The K345L Gα$_{i1}$ Shifts the Equilibrium between Nucleotide Bound States by Altering the Allosteric Network Between Receptor and Guanine Nucleotide

The majority of published Gα mutations proposed to alter allosteric signaling are associated with an increase in both intrinsic and receptor-mediated nucleotide exchange (6,25,29). This is consistent with the global destabilization of structure often associated with site-directed mutants. In contrast, a reduction in both basal and receptor mediated nucleotide exchange was observed in K345L Gα$_{i1}$. The mechanistic basis for this unusual reduction in nucleotide exchange could potentially be attributed to one of many physical changes. For example, K345L Gα$_{i1}$ might have an increase in the affinity for bound GDP, or the nucleotide-free state of K345L Gα$_{i1}$ that binds receptor might be destabilized, or the allosteric connection between receptor-binding and nucleotide release might be disrupted in K345L Gα$_{i1}$. To distinguish between these possibilities and determine whether focused study of this mutation would provide insight into the function of Gα proteins, we assessed additional biochemical properties of K345L Gα$_{i1}$. The modest loss of binding and receptor activation is in contrast to the previously reported 200-fold increase in the affinity for the Gα$_{i1}$ peptide containing the K345L mutation (222), but in agreement with studies of Gα$_t$ demonstrating similar receptor affinity as wild-type when this mutation was placed in the context of the intact protein (238).

To identify if this loss in affinity had a trivial explanation, we compared the structures of meta II (81) bound to a peptide mimetic of Gα$_{i1}$ to that of the β$_2$-adrendergic receptor bound to intact Gα$_s$ (1) and used *in silico* modeling to qualitatively assess the influence of sequence on binding in each case. It is notable for this analysis that the

peptide costructure shows a different binding mode than the C-terminus of $G\alpha_s$. This difference in conformation has previously motivated a proposal that the peptide costructure represents a pre-docked state for the C-terminus of $G\alpha$. Examination of the structure of opsin or meta II bound to peptide does not demonstrate an obvious reason why the K345L mutation would have increased affinity in the context of a peptide and decreased affinity in the context of the intact $G\alpha$.

An alternative mechanism that would result in the K345L mutation having increased receptor affinity in a peptide but reduced affinity in the context of the intact protein would be if the mutation altered the allosteric equilibrium between the nucleotide-bound states of $G\alpha$. The lack of immediate physical phenomena, such as steric clash, that would explain a lowering of receptor affinity in the presence of the intact protein supports destabilization of the nucleotide-free state of K345L $G\alpha_{i1}$. In addition, we measured a lowered T_m of the GDP-bound state of $G\alpha$. This state first associates with activated receptor in a low affinity complex, and the lowered T_m of this state in particular is consistent with a shifted nucleotide binding equilibrium in K345L $G\alpha_{i1}$.

Structural Changes in GDP-bound K345L $G\alpha_{i1}$ Localize within Functional Regions of the $G\alpha$ Subunit

It is reasonable to speculate the role of the β1-strand and the β2-β3 hairpin as additional sensors for receptor binding in addition to their role as triggers for inducing receptor-mediated conformational changes in $G\alpha$. Structural, computational, and dynamics studies have long supported the role of the β2-β3 hairpin in receptor-mediated $G\alpha$ activation. Consistent with this hypothesis, the residues Val34, Leu194, and Leu348

mediating the interactions between the β1-strand, the β2-β3 hairpin, and the α5 helix are highly conserved in Gα subunits with the exception of a histidine residue replacing Val34 in Gα$_s$. Biochemical studies on the Gα$_{o/i2}$ chimeras suggest that α5 helix interactions with the β2-β3 hairpin are important to subunit activation (252), and that the β2-β3 hairpin formed the relay in the gear-shift model for receptor-mediated nucleotide exchange (134). Parallel molecular dynamics simulations and EPR characterizations corroborated the role of the β2-β3 hairpin as a dynamic component during G protein activation (131,243). However, these studies did not offer a specific mechanism for how the β2-β3 hairpin conformational switch facilitates nucleotide exchange or how this conformational switch is even initiated. Most recently, the β$_2$-adrenergic-Gα$_s$ complex structure revealed a major receptor-G protein interaction with the β2-β3 hairpin loop mediated by the conserved intracellular loop 2 residue, Phe139. This residue was in close proximity to the Gα$_s$ residue homologous to the Leu194, which resides in the β2-β3 hairpin loop in Gα$_{i1}$ (1). Investigations into the relevance of this interaction using fluorescent probes showed that mutation of Leu194 to a cysteine uncoupled receptor interactions from G protein activation (137). In the latter, it was suggested that the Phe139-Leu194 interaction is part of a larger network completed by interactions with the α5 helix residue Phe336 for transducing receptor-interactions into conformational changes within Switches I and II during Gα activation. The results presented here elaborate on this specific mechanism by which the β2-β3 strand facilities Gα activation and subsequent conformational changes in Switch regions. The presence of the membrane-proximal hydrophobic network in which the β2-β3 hairpin takes part in likely represents one architectural aspect of the Gα state preceding the state sampled by the formation of the Phe139-Leu194 interaction.

Much less is known about the precise role of the β1-strand in facilitating Gα activation. Previously determined structures have revealed only minor differences that did not offer any conclusive insight into its functional role. Even in the K345L Gα$_{i1}$ variant structures, this region does not exhibit much if any conformational variability with the exception of Val34 participating in the membrane-proximal hydrophobic network identified here. Hydrogen-deuterium exchange experiments, on the other hand, have provided compelling evidence for the N-terminal motif as a dynamic element facilitating GDP release in Gα$_s$ proteins (253). One interpretation as to how this is mediated involves destabilization of the active site P-loop, an extension of the β1-strand, upon receptor binding and induction of β1-strand conformational changes. Thus, the integrity of these hydrophobic interactions forming the membrane-proximal network at the receptor-binding interface is likely one determinant for maintaining the Gα subunit in a state such as that observed in GDP-bound wild-type Gα$_{i1}$ proteins and here in the K345L variant. In the absence of receptor, formation of the hydrophobic interaction likely limits spontaneous Gα activation.

Productive coupling of receptors and G proteins is the physiological event that catalyzes the rate-limiting step of GDP release in Gα activation, and general consensus exists over the importance of Switch I in facilitating this event. Crystal structures of wild-type Gα proteins (13,40) showed that Switch I, which forms an extension of the β2-β3 hairpin, adopts among the most dramatic conformational changes in the various Gα activation states, and a number of studies on Gα Switch I mutants underscore the importance of this region for nucleotide release. One such study investigating the effects of the K180P mutant on the kinetics of GTP hydrolysis inadvertently revealed the

importance of the wild-type lysine residue in maintaining $G\alpha_{i1}$ in the ground state (14). In the presence of this mutation and GppNHp, $G\alpha_{i1}$ assumed an autoinhibited conformation marked by increased interactions between Switch I and the active site P-loop. Similar interactions between Switch I and the P-loop residues were also observed in the autoinhibited GppNHp-bound wild-type $G\alpha_{i1}$ structure (9) and in the GDP-bound K345L $G\alpha_{i1}$ structure. In contrast, in the T329A $G\alpha_{i1}$ variant Switch I is displaced outward to increase the active site volume, disrupt the Mg^{2+} ion coordination sphere and Switch I interactions with the P-loop, and destabilize the GDP-bound ground state (6). Consequently, nucleotide exchange rates were significantly elevated in the T329A $G\alpha_{i1}$ variant compared to those observed in wild-type and K345L $G\alpha_{i1}$. In light of these observations, the structure of the GDP-bound K345L $G\alpha_{i1}$ variant also represents a ground state that is marked by not only the membrane proximal hydrophobic network, but also a Switch I conformation engaged in a stabilizing interaction with the P-loop.

Disruption of an Active Site Salt-bridge between the P-loop Residue Glu43 and Switch I Residue Arg178 is Required for Facilitating G protein Activation

One particularly subtle hallmark of the heterotrimeric G protein is the formation of a salt bridge between the P-loop residue, Glu43, and the Switch I residue, Arg178, in the $G\alpha$ subunit, such that it is observed in both the $G\alpha_t$ (2) and the $G\alpha_{i1}$ (46) heterotrimeric complex and appears to be reinforced by the presence of the $G\beta\gamma$ subunits. Surprisingly, of the ten available GDP-bound, five GDP-AlF$_4^-$-bound, seven GTPγS-bound, and two GppNHp-bound $G\alpha_{i1}$ structures, only three unambiguously possessed this interaction. All three of these structures (GDP-bound K345L $G\alpha_{i1}$, GppNHp-bound wild-

type $G\alpha_{i1}$, and GppNHp-bound K180P $G\alpha_{i1}$) exhibited decreased capacity to transition to the activated state, and thus appear to be auto-inhibited to some extent much like heterotrimeric G protein complexes in the absence of receptor-mediated activation (9,14,46). Nucleotide-release is similarly inhibited in the $G\alpha_{i1}$ bound to the GoLoco motif of RGS14, where upon further analysis of the structure of the complex, it was revealed that the Glu43-Arg178 interaction was also conserved here (254). While Arg178 has been extensively characterized in the literature and is known to be required for stabilizing the γ-phosphate leaving group of GTP during hydrolysis, less is know about Glu43 in contrast (13,40,255). One study suggests a role for the amide atoms of the P-loop residue in facilitating Arg178 in stabilizing dissociative transition states (11,256), however, the evidence presented here suggests that the salt-bridge hinders transitions to the activated state.

Substantial deuterium exchange at the interface of the GTPase and helical domains of $G\alpha_s$ upon receptor-mediated activation has been attributed to conformational changes in the P-loop (253). Mutation of the Glu43-adjacent P-loop residue, Gly42, in $G\alpha_{i1}$ to an arginine has been previously shown to diminish Gα transitions to the activated state and nucleotide exchange rates (27). This biochemical phenotype was attributed to the inability of Arg42 to promote the active site conformational changes accompanying G protein activation. Thus, such concomitant conformational changes described for Switch I and the P-loop likely represent a driving force behind GDP release, and we speculate that the Glu43-Arg178 salt bridge observed in the GDP-bound K345L $G\alpha_{i1}$ structure acts a sensor for $G\alpha_{i1}$ interactions with activated receptor to facilitate these conformational changes. The uncoupling of receptor-binding and nucleotide exchange in the E43A $G\alpha_{i1}$

mutant shown here supports the role of the active salt bridge and the P-loop residue in the process of Gα activation.

A Model for Receptor-mediated G protein Activation

By placing the newly observed conformational intermediates and functional regions identified here within the context of known conformations of the Gα subunit, we propose a network for allosteric receptor-mediated nucleotide exchange in Gα$_{i1}$.

The C-terminal α5 helix has long been known to be of primary importance for communicating receptor binding to the guanine nucleotide-binding site. While speculative, it is possible that the well-characterized receptor-initiated α5 roto-translation further introduces conformational strain in elements of the GTPase fold itself for mediating GDP release. Indeed a twist in the central β-sheet is observed in the β$_2$-adrenergic-Gα$_s$ complex structure. Structural changes in Switch I and the P-loop are likely the result of this strain. Specifically, the α5 helix together with the β1-strand, and the β2-β3 hairpin loop, each constituting various dynamic elements of the receptor-binding site, likely contribute to the conformational strain. A route by which receptor binding could promote nucleotide exchange in Gα subunits is illustrated in **Fig. 36**, and utilizes the β1-strand and the α1 helix to communicate receptor-interactions with the β2-β3-hairpin and the α5 helix into structural changes in the active site Switch I and P-loop during Gα activation.

An ionic interaction between a glutamine residue in the base of the α1 helix and a threonine at the base of the α5 helix link the two structural elements to the P-loop. Such an interaction can be thought to limit the conformational flexibity of either structural

element. Site-directed mutagenesis to disrupt this interaction previously was shown to dramatically enhance the rate of uncatalyzed nucleotide exchange in $G\alpha_{i1}$ (6). Roto-translation of the α5 helix upon receptor binding would be expected to similarly break the ionic interaction and remove the constraints on the P-loop flexibility imposed by the α5-α1 interaction.

In addition to the α5 helix, the β1-strand in $G\alpha_s$ has been shown by hydrogen-deuterium exchange to represent a highly dynamic element of the Gα protein during receptor-mediated activation (253). The β1-strand precedes the P-loop connected to the α1 helix. It is possible that α5-mediated release of the α1 helix, and subsequent flexibility in the P-loop, contributes to the dynamic behavior of the β1-strand. Because of the intimate interactions between the β-strands of the GTPase fold, conformational changes in β1 can be thought to propagate to the adjacent β2-β3 hairpin, which acts as a conduit from the receptor-binding site to the active site Switch I loop. Indeed, conformational changes in the β2-β3 interactions with the α5 have been shown by SDSL and EPR to be important for facilitating receptor-mediated nucleotide exchange (239).

The tightly coupled nature of the interactions between the β1-α5-α1-P-loop network (**Figure 37A)** and the β2-β3-Switch I network (**Figure 37B**) suggests extensive crosstalk between the two, and the resultant conformational changes are likely occurring in concert to facilitate nucleotide exchange in the presence of receptor-stimulation (**Figure 37C**). Additional investigations of these membrane proximal elements are necessary for validating their individual contributions in the mechanism. However, the data presented here presents a framework for which such future experiments can be designed to further probe allostery in G protein signaling.
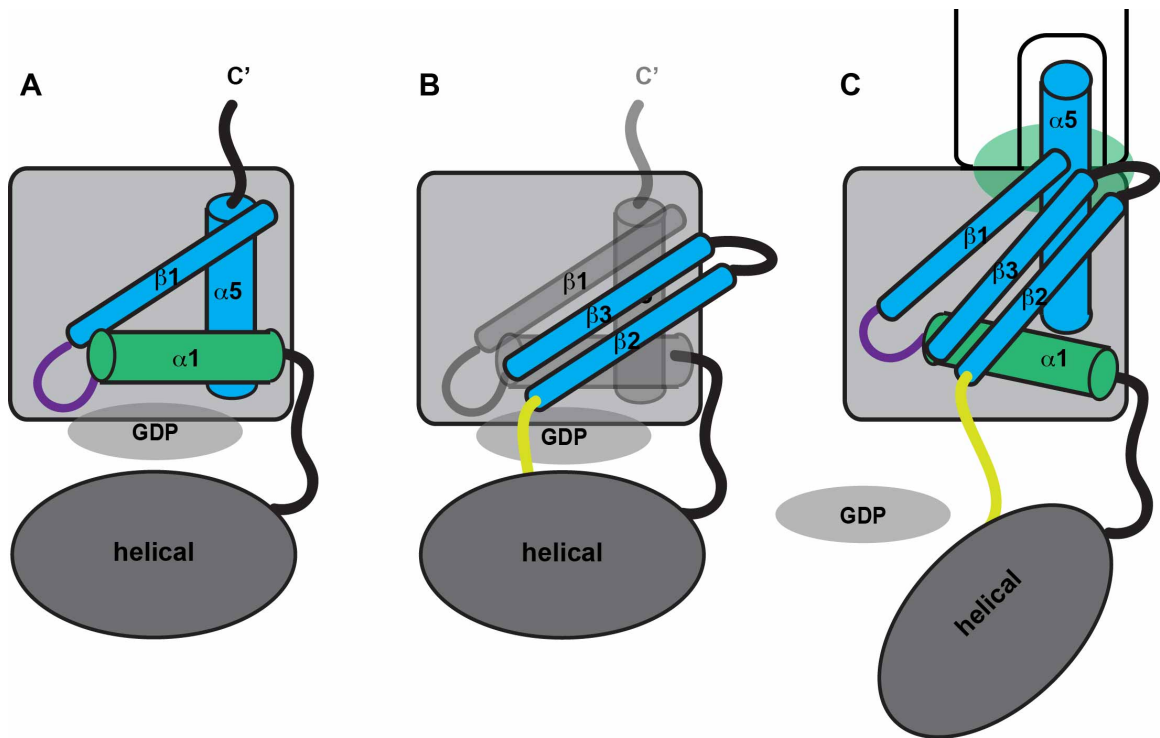
Figure 37: An Allosteric Model for Gα Activation. Gα is shown in the absence of Gβγ. **A)** The β1-P-loop-α1 helix (network 1) form a network of interactions with the α5 helix, which hold these elements in their constrained conformations in the absence of receptor binding. **B)** An adjacent motif formed by the β2-β3 hairpin-Switch I (network 2) form an additional network that is also static in the absence of receptor-coupling. **C)** Upon receptor binding to the Gα subunit, and the α5 helix, rearrangements in the interactions among elements of network 1 are communicated to network 2, and concomitant conformational changes in the P-loop (*purple*) and Switch I (*gold*) result to facilitate GDP release.

Conclusions

This study reveals the importance of subtle conformational changes in receptor-mediated G protein activation. Investigations into the well-studied C-terminal mutation, K345L (K341L in $Gα_t$), and a novel active site mutation, E43A, in the full-length $Gα_{i1}$ subunit contribute to our understanding of how N- and C-terminal motifs in Gα proteins facilitate crosstalk between allosteric networks during heterotrimeric G protein activation.

Accession Numbers

Atomic coordinates and structure factors have been deposited into the RCSB

Protein Data Bank with accession codes 4NOD and 4NOE.

CHAPTER VI

SYNOPSIS AND CONCLUSIONS

The goals of this work were to gain insight into the allosteric mechanisms of receptor-mediated G protein activation. The results presented contribute novel information on three distinct aspects of this mechanism. The first part addresses molecular determinants of complex formation and stabilization. The second part applies the findings from the first part to the structural study of the rhodopsin-transducin complex, which revealed molecular determinants of complex disassembly. In the last part of this work, structural and biochemical investigations into the local environment of the $G\alpha_{i1}$ subunit in the presence of a mutation destabilizing receptor-G protein interactions reveal the allosteric connections that likely convey receptor binding into a signal facilitating nucleotide release during G protein activation.

In the first part of this study, model membrane systems were investigated to overcome challenges of studying transient GPCR-G protein complexes, and to better understand the determinants of GPCR-G protein complex formation preceding the G protein activation step. A novel technique utilizing dynamic light scattering was developed to characterize the physical properties of phospholipid bicelles of varying compositions. Biochemical results reporting the effects of various bicelle compositions on GPCR-G protein complex formation, stabilization, and subsequent receptor-mediated G protein activation were put into the context of membrane morphology. These results underscored the importance of membrane structure in facilitating productive receptor-G

protein interactions, and offered insights into the mechanism by which detergent micelles destabilize such protein-protein interactions. In addition, the dependence on nonspecific negative charge for complex stabilization highlighted the extent to which electrostatic interactions at the membrane interface facilitate GPCR-G protein coupling. Surprisingly, the presence of the negative charge enhanced both the affinity of receptor for G protein and the rate of G protein activation. These findings, taken together, offer a rationalization for the inherent instability of such complexes *in vivo*, such that weak interactions are likely necessary for efficient G protein turnover in response to extracellular stimuli.

In the second part of this study, the findings from the first part were exploited for structural studies performed on the rhodopsin-transducin complex to gain insight into the structure of the nucleotide-free state of the G protein. Negatively charged bicelles and lipidic cubic phase phospholipids were investigated as a medium for crystallization. The results of these studies revealed that the physical properties of GPCRs and G proteins that are stabilizing *in vivo* are actually destabilizing for protein crystallization. Successful structural studies will most likely require the manipulation of protein systems with engineered stability.

Lastly, in the third part of this study, structure function investigations of the K345L $G\alpha_{i1}$ revealed how modest changes in allosteric networks can have dramatic effects on G protein activation. Further, this study reinforced the importance of productive receptor-G protein interactions for facilitating conformational changes in allosteric sites of the G protein during activation. Destabilization of the GDP-bound state in the presence of the K345L mutation revealed novel interactions between the well-characterized receptor-binding element, the $\alpha5$ helix, and proximal structural elements of

the GTPase fold that represent a conduit between the receptor and nucleotide binding site. These included the β1, β2, and β3 strands, and minor changes in their membrane proximal environment dramatically effected the conformation of the active site Switch I loop. These findings unveil a novel mechanism for conveying receptor interactions into a signal facilitating nucleotide release.

While one of the goals of this work was to characterize the global architecture of the GPCR-G protein complex to better understand the nucleotide-free state of the G protein, indirect investigations in the absence of the crystal structure were able to offer equally valuable insight into the transient G protein activation state. Thus, continued efforts towards identifying and characterizing various Gα intermediates will be necessary for painting a complete picture of the allosteric landscape in G proteins as was attempted here. These results hopefully provide a framework for additional investigations into allosteric mechanisms of G protein regulation.

Appendix A

SUBSTRATE SPECIFICITY IN ACETATE KINASE ENZYMES FROM THE
DOMAIN *EUKARYEA*

Introduction

Enzyme-catalyzed phosphoryl transfer reactions are important for a range of biological activities. Acetate kinases (ACKs) transfer a phosphoryl group to and from acetate, thus promoting the interconversion of acetate and acetyl phosphate. With this transformation, ACKs play a role in multiple, distinct bioenergetic pathways (257-259). For example, in fermentative bacteria, the ACK-catalyzed dephosphorylation of acetyl phosphate has been demonstrated to be essential for the ACK- phosphotransacetylase (ACK-PTA) bioenergetic pathway, which utilizes energy stored in acetyl-CoA (257). Similarly, ACK-dependent dephosphorylation of acetyl phosphate facilitates ATP synthesis via the pentose phosphoketolase pathway in fungi (258). Conversely, in the methanoarchaeon *Methanosarcina*, ACK activates acetate for its conversion to acetyl-CoA in the first step of acetioclastic methanogenesis (259). While the investigations into ACK enzymes have focused on bacterial and archaeal systems, ACK was identified in the eukaroyote *Entamoeba histolytica* in the early 1960s (260) and was first biochemically characterized in the 1970s (261). Genes encoding putative ACKs have since been identified within the genomes of other eukaryotic pathogens, including the basidomycete *Cryptococcus neoformans* (258). At least in *E. histolytica*, the organism does not appear to have homologs for other proteins required for the known bioenergetic pathways that use ACK (262). This suggests that the biological function of the *E. histolytica* ACK may

128

be different from that demonstrated in prokaryotes, but at present, that function remains unknown.

ACKs belong to the acetate and sugar kinase/hsp70/actin (ASKHA) superfamily (263). Members of this family use tandem RNase-H like folds as a scaffold for the optimal positioning of five signature sequence motifs, three of which (termed ADENOSINE, PHOSPHATE 1, and PHOSPHATE 2) form the ATP binding pocket (**Figure 38A, B**) (264). While the oligomeric states of ASKHA superfamily members can differ, each protomer fully houses a complete active site.
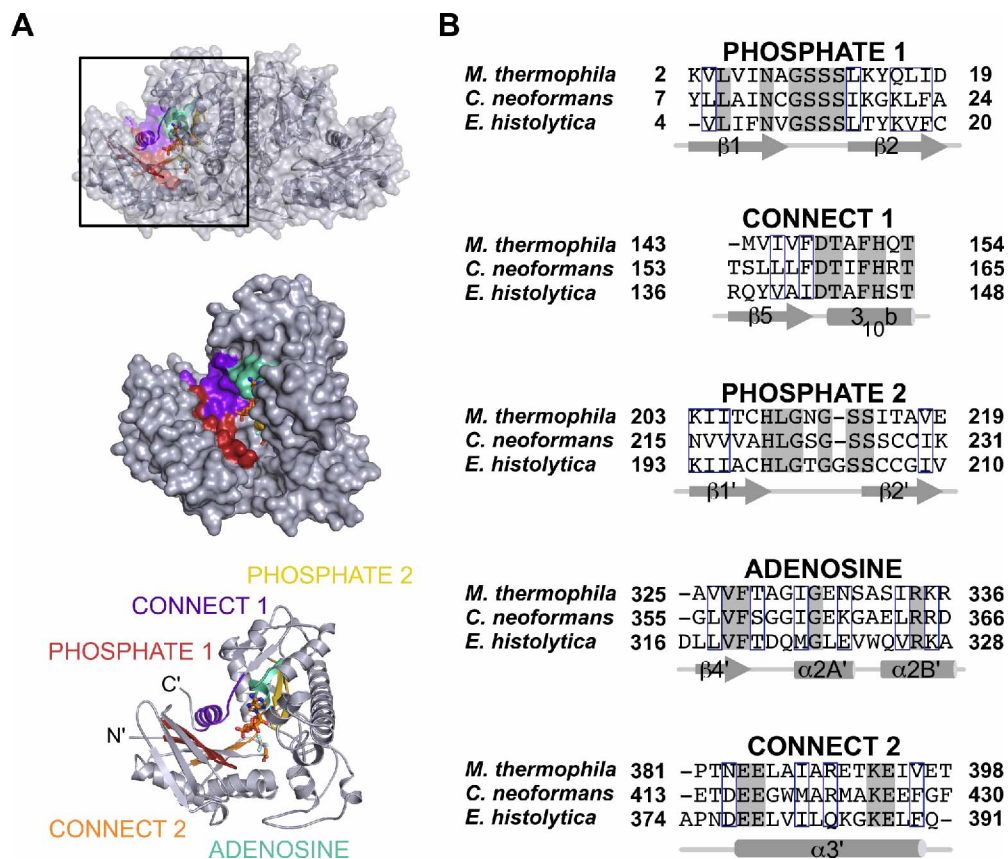
Figure 38: Conserved motifs of the ASKHA superfamily. **A**) Location of the ASKHA superfamily sequence motifs shown in a protomer of *C. neoformans* ACK. **B**) A structure-based sequence alignment of each motif shown with secondary structure elements labeled. Fully conserved residues are shaded grey and strongly conserved residues are outlined in blue.

Biochemical and structural investigations of ACK from the methanogenic archaeon *Methanosarcina thermophila* have been key in developing a mechanistic proposal for ACKs (265-271). It is now generally accepted that phosphoryl transfer between the nucleotide and the substrate occurs directly via an in-line mechanism. This is supported by a crystal structure of the *M. thermophila* ACK in complex with acetate and the nucleotide transition state analog ADP-AlF$_3$ (271), which showed the two cosubstrates bound within the active site in a linear array. The structural evidence for the in-line transfer mechanism effectively ended a long-standing debate on the role of ACK phosphoenzyme, which had originally been proposed as a catalytic intermediate.

Domain motions are proposed to facilitate catalysis in *M. thermophila* ACK by closing around the cosubstrates, which correctly aligns the g-phosphate of ATP (or pyrophosphate (PP$_i$)) with the phosphoryl acceptor (271). Fluorescence quenching experiments demonstrated that the differences in interdomain angle observed in the crystal structures of numerous ASKHA enzymes indeed convert to interdomain movement (264,272).

Mirroring the state of knowledge on the biological function of eukaryotic ACKs, few direct studies on the enzymatic mechanism of eukaryotic enzymes have been performed and it is not clear how (or if) the mechanism is modified with respect to the mechanism proposed for the *M. thermophila* enzyme (271). Interestingly, the *E. histolytica* ACK has been shown to use P$_i$/PP$_i$, rather than ADP/ATP, as the phosphoryl acceptor/donor pair for phosphoryl transfer (261,262). Further, this enzyme has a strong kinetic advantage for catalyzing the dephosphorylation of acetyl phosphate (261,262). Although a kinetic characterization has not yet been reported in the literature, *C.*

neoformans ACK has also been shown to kinetically favor acetate formation (Ingram-Smith, C., personal communication). Here, we report the crystal structures of the *E. histolytica* and *C. neoformans* ACKs at 2.4 Å and 1.9 Å resolution, respectively. These provide a structural basis for catalysis in the eukaryotic ACKs.

Materials and Methods

Protein Expression and Purification

The *E. histolytica* ACK gene cloned into the pQE30 plasmid was co-transformed with the *lacI*-containing plasmid pREP-4 into *Escherichia coli* YBS121 (a generous gift of George Bennett, Rice University). The *C. neoformans* ACK gene was cloned into the pET21b plasmid and transformed into *E. coli* Rosetta2 (*DE3*). Both were expressed and purified using similar methods to those described for *E. histolytica* ACK (262). Briefly, expression cultures were grown in LB broth containing the appropriate antibiotic at 37°C with shaking until the OD_{600} reached 0.9. Expression was induced with the addition of IPTG to a final concentration of 1 mM. Cultures were shaken overnight at ambient temperature.

Cells were harvested by centrifugation and resuspended in purification buffer (25 mM Tris, 150 mM NaCl, 20 mM imidazole, and 10% glycerol, pH 7.4). Cells were lysed using a French pressure cell and the cellular debris removed by centrifugation at 100,000 x g for 1 hour. ACK was purified from clarified lysate using a 5 mL HisTrap Ni-affinity column and eluted with a linear gradient from 20 mM to 500 mM imidazole in purification buffer. Each protein was pooled and dialyzed against buffer containing 25

mM Tris, 150 mM NaCl, and 10% glycerol, pH 7.4 and further purified by size exclusion chromatography using a Superdex S200 10/300GL column.

Crystallization, Data Collection, Structure Determination and Refinement

E. histolytica ACK was crystallized using the hanging drop vapor diffusion method by mixing 1 μL protein (8 mg/mL in 25 mM HEPES, pH 7.5) with 1 μL reservoir solution (50 mM ADA, 0.6 M potassium-sodium tartrate, 10 mM $FeCl_3$, pH 6.6) and equilibrating against 1 mL reservoir solution at 20°C. Crystals formed within 3 days and were cryo-protected in a solution containing all of the crystallization components and 30% ethylene glycol prior to flash cooling in liquid nitrogen.

C. neoformans ACK was crystallized by the hanging drop vapor diffusion method by mixing 1 μL protein (3 mg/mL in 25 mM Tris, pH 7.4) with 1 μL reservoir solution (50 mM ADA, 100 mM sodium tartrate, 18.5% PEG 2000, pH 6.2) and equilibrated against 1 mL reservoir solution at 4°C for 4 days. Crystals were cryo-protected by soaking in a solution containing all of the components of the crystallization reaction, but with the PEG 2000 concentration increased to 30% and then flash cooled in liquid nitrogen.

Crystallographic data were collected at the Advanced Photon Source LS-CAT beamlines (**Table 10**) and processed using HKL2000 (246). The structures of both eukaryotic ACKs were determined by molecular replacement using the program PHASER (247) and a polyalanine model of the *M. thermophila* ACK structure (PDB entry 1G99; (266)) as the search model. Preliminary phases for the *C. neoformans* ACK model were calculated in DM (273) and improved by solvent-flattening and two-fold

non-crystallographic symmetry (NCS) averaging. Manual model building was performed in COOT (249) and refinement was performed in CNS (274) and REFMAC (275). Tight NCS restraints applied to individual domains of the *C. neoformans* ACK model were reduced as the model quality improved. Final model quality was assessed with PROCHECK (250). Figures were prepared with PyMOL (276).

Table 10: ACK Crystallographic Data Collection and Refinement Statistics

	E. histolytica ACK	*C. neoformans* ACK
Data collection		
APS Beamline	21-ID-G	21-ID-D
Wavelength	0.979 Å	1.127 Å
Space group	I222	$P2_1$
Unit cell dimensions	a=98.8 Å	a=51.4 Å
	b=126.9 Å	b=107.6 Å
	c=145.6 Å	c=79.1 Å
	β=90	b=99.8°
Resolution Range	44 - 2.4 Å (2.46 - 2.4 Å)[a]	39 - 1.9 Å (1.97 - 1.9 Å)
Number of reflections	273,804	224,881
Unique reflections	35,682	64,297
R_{sym}[b]	13.8% (44.0%)	5.8% (30.9%)
$<I>/<\sigma>$[c]	15.6 (3.0)	27.0 (5.2)
Redundancy	7.7 (5.8)	3.5 (3.0)
Completeness	99.3% (93.7%)	95.7% (89.8%)
Refinement		
R_{cryst}[d]	21.0%	17.8%
R_{free}[e]	23.1%	21.9%
Rms deviation		
Bond Length	0.004	0.01
Bond Angle	0.93	1.2

[a]Values in parentheses are for the highest resolution shell.

[b]$R_{sym}= \Sigma_{hkl} \Sigma_j |I_j - \langle I \rangle| / \Sigma_{hkl} \Sigma_j I_j$, where j is the jth measurement and <I> is the weighted mean of I.
[c]$<I>/<\sigma>$ is the mean intensity divided by the mean error.

[d]$R_{cryst}= \Sigma_{hkl} ||F_o| - k|F_c|| / \Sigma_{hkl} |F_o|$, where F_o and F_c are the observed and calculated structure factor amplitudes, and k is a weighting factor.
[e]R_{free} is the same as R_{cryst} calculated on 5% of the reflections in *E. histolytica* ACK (1999 reflections) and *C. neoformans* ACK (3188 reflections).

Overall Structures

On a global level, the structures of both eukaryotic ACKs (**Figure 39A, B**) are similar to that of the previously reported *M. thermophila* ACK. This dimer has been described as resembling a bird with wings spread (266). The 'body' of the bird contains the C-terminal RNase-H like domain and mediates dimerization, while the 'wing' is organized around the N-terminal RNase-H like domain.
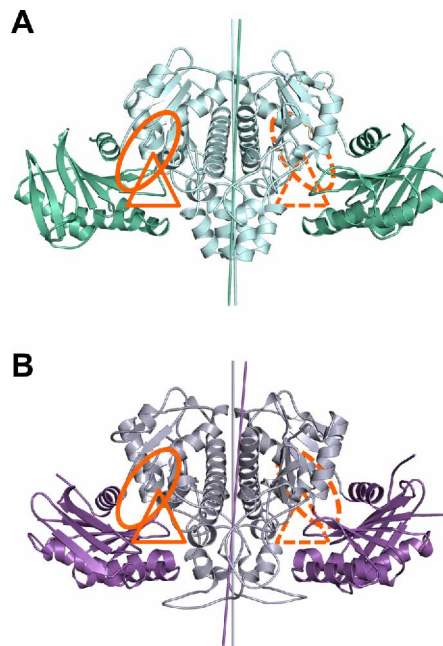
Figure 39: Structures of the eukaryotic ACKs. A) *E. histolytica* ACK with the N-terminal wing domain colored green and the C-terminal body domain colored cyan. **B)** *C. neoformans* ACK with the wing domain colored purple and the body domain colored grey. The putative acetate and nucleotide binding sites are highlighted with a triangle and a circle, respectively. The rotation axes relating each domain of the dimer are highlighted with a line colored similarly to the corresponding domain.

Superposition of each protomer of the *E. histolytica* and *C. neoformans* ACKs revealed that while each domain is folded similarly, there is a difference in the interdomain angle between the body and wing domains. This gives rise to unique rotation

axes that superimpose the body and wing domains in both structures (**Figure 39A, B**). The difference in angle was calculated using DynDom (277) and revealed a difference in interdomain angle of 9° between the two protomers of *E. histolytica* ACK and 14° between the two protomers of the *C. neoformans* ACK.

Active Site Architecture

The *M. thermophila* ACK is the closest structurally characterized homolog of the eukaryotic ACKs, and will be used for comparisons in this report. Comparison of each eukaryotic ACK to *M. thermophila* ACK determined in the presence of acetate, ADP-AlF$_3$, and thiopyrophosphate (PPS) (271) supports the assignment of the active site at the interface of the body and wing domains and suggests a binding site for the phosphoryl donor (ATP or PP$_i$) and acetate. The three signature motifs that mediate ATP binding in the ASKHA superfamily, termed ADENOSINE, PHOSPHATE 1, and PHOSPHATE 2 (278), surround the putative phosphoryl donor binding pocket in both of the eukaryotic ACKs (**Figure 38A**). Co-crystallization of the *E. histolytica* and *C. neoformans* ACKs with either PP$_i$ or nucleotide analogs, respectively, did not result in the appearance of new electron density corresponding to a bound phosphoryl donor in this site. Instead, superpositions with the structure of acetate and ADP-AlF$_3$ bound *M. thermophila* ACK (**Figure 40A, D**) were used to evaluate whether the phosphoryl donor could reasonably be accommodated in a similar location within the eukaryotic ACKs. Manual modeling of ADP-AlF$_3$ into the structure of the *C. neoformans* ACK (**Figure 40B, E**) and PPS into the structure of the *E. histolytica* ACK (**Figure 40C, F**) resulted in reasonable contacts between protein and the respective nucleotide analogs.
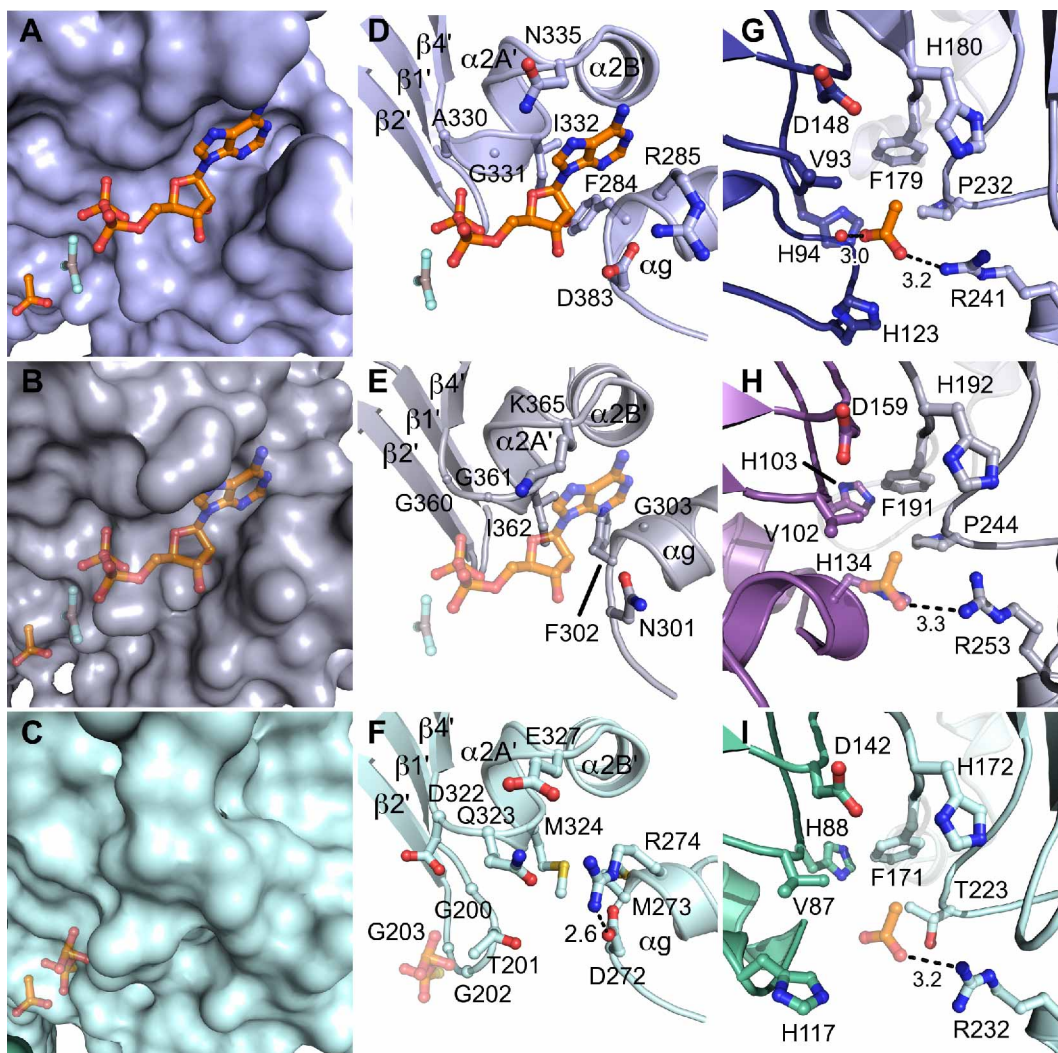
Figure 40: Active site architecture. **A)** A surface representation of the *M. thermophila* ACK (PDB ID 1TUY) with the N-terminal wing domain colored dark blue and the C-terminal body domain colored light blue. **B)** A surface representation of the *C. neoformans* ACK colored as in **Figure 2**. ADP-AlF$_3$ and acetate are modeled into putative binding sites. **C)** A surface representation of the *E. histolytica* ACK colored as in **Figure 2** with PPS and acetate modeled into putative binding sites. **D-F)** Close up views of the nucleotide or PP$_i$ binding sites in ACKs. **D)** *M. thermophila* ACK, **E)** *C. neoformans* ACK, and **F)** *E. histolytica* ACK. In panels **E)** and **F)**, the position is modeled according to methods listed in the text. **G-I)** Close up views of the substrate binding site. **G)** *M. thermophila* ACK **H)** *C. neoformans* ACK, and **I)** *E. histolytica* ACK. The acetate is modeled in panels **H)** and **I)**.

The ADENOSINE motif normally positions the protein side chains into conformations that promote the interaction between protein and the adenosine base of ATP in ASKHA superfamily enzymes (278). Interestingly, both the sequence and the

136

backbone structure of the ADENOSINE motif are conserved in the *E. histolytica* ACK (**Figure 38A, 40F**), which has been demonstrated to use PP_i, and not ATP, as a phosphoryl donor (Fowler et al., 2012). Inspection of the *E. histolytica* ACK structure shows that substitution of a conserved glycine to glutamine and isoleucine to methionine (Gln-323 and Met-324 on a2A') sterically occludes the ATP-binding cleft (**Figure 40C, F**). Additionally, a salt bridge between Asp-272 and Arg-274 on ag stabilizes an alternate conformation of Arg-274 which positions its guanidino group into the ATP-binding cleft further contributing to the occlusion. These features may be important in the conversion of phosphoryl donor selectivity from ATP to PP_i.

The structure of the *M. thermophila* ACK in complex with its substrate acetate (**Figure 49A, G**) revealed a hydrophobic substrate-binding pocket between the wing and body domains (271). Manual modeling of acetate into both the *C. neoformans* (**Figure 40B, H**) and *E. histolytica* ACKs (**Figure 40C, I**) again resulted in reasonable contacts between protein and substrate. Indeed, the residues surrounding the acetate-binding pocket are almost completely conserved in the eukaryotic ACKs with the exception of a proline to threonine substitution at position 223 in the *E. histolytica* enzyme (**Figure 40I**). However, site-directed mutagenesis studies of Thr-223 in *E. histolytica* ACK did not reveal a specific role for this side chain (262).

Mechanistic Implications

Given the similarities observed within the active sites of the *M. thermophila, C. neoformans*, and *E. histolytica* ACKs, it is reasonable to use the mechanism proposed for the *M. thermophila* enzyme as a starting proposal for eukaryotic ACKs. Each of the

enzymes has an active site that would support binding of the acetate and the phosphoryl donor (either ATP or PP_i) in a linear arrangement (**Figure 40A-C**). This binding mode is consistent with the in-line transfer mechanism proposed for *M. thermophila* ACK, where the phosphoryl transfer occurs directly between the two properly aligned cosubstrates (271).

The biological role of ACK in *M. thermophila* is to produce acetyl phosphate (and ADP) from acetate and ATP during methanogenesis (266). The reaction is therefore commonly discussed in the acetyl phosphate forming direction, although *in vitro,* the *M. thermophila* enzyme catalyzes the reverse reaction at a similar rate (262,269). In contrast, kinetic characterization of both the *E. histolytica* ACK (261,262) and the *C. neoformans* ACK (Ingram-Smith, C. and Smith, K.S., manuscript in preparation) revealed faster turnover in the acetate-forming direction. It is unclear from the structures why the reaction is favored in one direction while the *M. thermophila* enzyme appears to catalyze the same reaction bidirectionally with comparable efficiency (269). Nevertheless, it is conceivable that the in-line transfer could work in reverse. In this scenario, acetyl phosphate and P_i/ADP would bind in a linear array within the active site, and the phosphoryl group would be transferred from the acetyl phosphate to the P_i/ADP.

The difference in interdomain angle observed in both the *E. histolytica* and *C. neoformans* ACKs mirrors that observed in other ASKHA superfamily members (264). Enzymes with a global architecture similar to ACKs commonly employ domain closure to facilitate catalysis (for example, see (279)). The ability to adopt multiple interdomain angles in the eukaryotic ACKs suggests that interdomain motions could similarly contribute to catalysis, as has been shown for the *M. thermophila* enzyme (272).

138

Accession Numbers

Coordinates and structure factors have been deposited with the RCSB Protein Data Bank with accession numbers 4H0O (*E. histolytica* ACK) and 4H0P (*C. neoformans* ACK).

This work was has been reprinted with permission from:

Thaker, T.M., Tanabe, M., Ingram-Smith, C., Fowler, M., Smith K.S., Preininger, A.M., and Iverson, T.M. (2013) Crystal Structures of Acetate Kinases from the Eukaryotic Pathogens *Entamoeba histolytica* and *Cryptococcus neoformans*. Journal of Structural Biology. 181(2): 185-189.

REFERENCES

1. Rasmussen, S. G., Devree, B. T., Zou, Y., Kruse, A. C., Chung, K. Y., Kobilka, T. S., Thian, F. S., Chae, P. S., Pardon, E., Calinski, D., Mathiesen, J. M., Shah, S. T., Lyons, J. A., Caffrey, M., Gellman, S. H., Steyaert, J., Skiniotis, G., Weis, W. I., Sunahara, R. K., and Kobilka, B. K. (2011) Crystal structure of the beta(2) adrenergic receptor-Gs protein complex. *Nature* **477**, 549-555

2. Lambright, D. G., Sondek, J., Bohm, A., Skiba, N. P., Hamm, H. E., and Sigler, P. B. (1996) The 2.0 angstrom crystal structure of a heterotrimeric G protein. *Nature* **379**, 311-319

3. Okada, T., Sugihara, M., Bondar, A. N., Elstner, M., Entel, P., and Buss, V. (2004) The retinal conformation and its environment in rhodopsin in light of a new 2.2 A crystal structure. *J Mol Biol* **342**, 571-583

4. Mixon, M. B., Lee, E., Coleman, D. E., Berghuis, A. M., Gilman, A. G., and Sprang, S. R. (1995) Tertiary and quaternary structural changes in Gi alpha 1 induced by GTP hydrolysis. *Science* **270**, 954-960

5. Raw, A. S., Coleman, D. E., Gilman, A. G., and Sprang, S. R. (1997) Structural and biochemical characterization of the GTPgammaS-, GDP.Pi-, and GDP-bound forms of a GTPase-deficient Gly42 --> Val mutant of Gialpha1. *Biochemistry* **36**, 15660-15669

6. Kapoor, N., Menon, S. T., Chauhan, R., Sachdev, P., and Sakmar, T. P. (2009) Structural evidence for a sequential release mechanism for activation of heterotrimeric G proteins. *J Mol Biol* **393**, 882-897

7. Lambert, N. A., Johnston, C. A., Cappell, S. D., Kuravi, S., Kimple, A. J., Willard, F. S., and Siderovski, D. P. (2010) Regulators of G-protein signaling accelerate GPCR signaling kinetics and govern sensitivity solely by accelerating GTPase activity. *Proc Natl Acad Sci U S A* **107**, 7066-7071

8. Johnston, C. A., Willard, F. S., Jezyk, M. R., Fredericks, Z., Bodor, E. T., Jones, M. B., Blaesius, R., Watts, V. J., Harden, T. K., Sondek, J., Ramer, J. K., and Siderovski, D. P. (2005) Structure of Galpha(i1) bound to a GDP-selective peptide provides insight into guanine nucleotide exchange. *Structure* **13**, 1069-1080

9. Coleman, D. E., and Sprang, S. R. (1999) Structure of Gialpha1.GppNHp, autoinhibition in a galpha protein-substrate complex. *J Biol Chem* **274**, 16669-16672

10. Morikawa, T., Muroya, A., Nakajima, Y., Tanaka, T., Hirai, K., Sugio, S., Wakamatsu, K., and Kohno, T. (2007) Crystallization and preliminary X-ray crystallographic analysis of the receptor-uncoupled mutant of Galphai1. *Acta Crystallogr Sect F Struct Biol Cryst Commun* **63**, 139-141

11. Berghuis, A. M., Lee, E., Raw, A. S., Gilman, A. G., and Sprang, S. R. (1996) Structure of the GDP-Pi complex of Gly203-->Ala gialpha1: a mimic of the ternary product complex of galpha-catalyzed GTP hydrolysis. *Structure* **4**, 1277-1290

12. Coleman, D. E., and Sprang, S. R. (1998) Crystal structures of the G protein Gi alpha 1 complexed with GDP and Mg2+: a crystallographic titration experiment. *Biochemistry* **37**, 14376-14385

13. Coleman, D. E., Berghuis, A. M., Lee, E., Linder, M. E., Gilman, A. G., and Sprang, S. R. (1994) Structures of active conformations of Gi alpha 1 and the mechanism of GTP hydrolysis. *Science* **265**, 1405-1412

14. Thomas, C. J., Du, X., Li, P., Wang, Y., Ross, E. M., and Sprang, S. R. (2004) Uncoupling conformational change from GTP hydrolysis in a heterotrimeric G protein alpha-subunit. *Proc Natl Acad Sci U S A* **101**, 7560-7565

15. Preininger, A. M., Funk, M. A., Oldham, W. M., Meier, S. M., Johnston, C. A., Adhikary, S., Kimple, A. J., Siderovski, D. P., Hamm, H. E., and Iverson, T. M. (2009) Helix dipole movement and conformational variability contribute to allosteric GDP release in Galphai subunits. *Biochemistry* **48**, 2630-2642

16. Johnston, C. A., Lobanova, E. S., Shavkunov, A. S., Low, J., Ramer, J. K., Blaesius, R., Fredericks, Z., Willard, F. S., Kuhlman, B., Arshavsky, V. Y., and Siderovski, D. P. (2006) Minimal determinants for binding activated G alpha from the structure of a G alpha(i1)-peptide dimer. *Biochemistry* **45**, 11390-11400

17. Gilman, A. G. (1987) G-Proteins - Transducers of Receptor-Generated Signals. *Annual Review of Biochemistry* **56**, 615-649

18. Limbird, L. E., and Lefkowitz, R. J. (1977) Resolution of beta-adrenergic receptor binding and adenylate cyclase activity by gel exclusion chromatography. *J Biol Chem* **252**, 799-802

19. Rodbell, M., Krans, H. M., Pohl, S. L., and Birnbaumer, L. (1971) The glucagon-sensitive adenyl cyclase system in plasma membranes of rat liver. IV. Effects of guanylnucleotides on binding of 125I-glucagon. *J Biol Chem* **246**, 1872-1876

20. Rodbell, M., Birnbaumer, L., Pohl, S. L., and Krans, H. M. (1971) The glucagon-sensitive adenyl cyclase system in plasma membranes of rat liver. V. An

obligatory role of guanylnucleotides in glucagon action. *J Biol Chem* **246**, 1877-1882

21.   Londos, C., Salomon, Y., Lin, M. C., Harwood, J. P., Schramm, M., Wolff, J., and Rodbell, M. (1974) 5'-Guanylylimidodiphosphate, a potent activator of adenylate cyclase systems in eukaryotic cells. *Proc Natl Acad Sci U S A* **71**, 3087-3090

22.   Cassel, D., and Selinger, Z. (1977) Catecholamine-induced release of [3H]-Gpp(NH)p from turkey erythrocyte adenylate cyclase. *J Cyclic Nucleotide Res* **3**, 11-22

23.   Cassel, D., and Selinger, Z. (1978) Mechanism of adenylate cyclase activation through the beta-adrenergic receptor: catecholamine-induced displacement of bound GDP by GTP. *Proc Natl Acad Sci U S A* **75**, 4155-4159

24.   Cassel, D., and Selinger, Z. (1977) Mechanism of adenylate cyclase activation by cholera toxin: inhibition of GTP hydrolysis at the regulatory site. *Proc Natl Acad Sci U S A* **74**, 3307-3311

25.   Posner, B. A., Mixon, M. B., Wall, M. A., Sprang, S. R., and Gilman, A. G. (1998) The A326S mutant of Gialpha1 as an approximation of the receptor-bound state. *J Biol Chem* **273**, 21752-21758

26.   Jones, J. C., Duffy, J. W., Machius, M., Temple, B. R., Dohlman, H. G., and Jones, A. M. (2011) The crystal structure of a self-activating G protein alpha subunit reveals its distinct mechanism of signal initiation. *Sci Signal* **4**, ra8

27.   Bosch, D. E., Willard, F. S., Ramanujam, R., Kimple, A. J., Willard, M. D., Naqvi, N. I., and Siderovski, D. P. (2012) A P-loop mutation in Galpha subunits prevents transition to the active state: implications for G-protein signaling in fungal pathogenesis. *PLoS Pathog* **8**, e1002553

28.   Northup, J. K., Sternweis, P. C., Smigel, M. D., Schleifer, L. S., Ross, E. M., and Gilman, A. G. (1980) Purification of the regulatory component of adenylate cyclase. *Proc Natl Acad Sci U S A* **77**, 6516-6520

29.   Singh, G., Ramachandran, S., and Cerione, R. A. (2012) A constitutively active Galpha subunit provides insights into the mechanism of G protein activation. *Biochemistry* **51**, 3232-3240

30.   Hildebrandt, J. D., Codina, J., and Birnbaumer, L. (1984) Interaction of the stimulatory and inhibitory regulatory proteins of the adenylyl cyclase system with the catalytic component of cyc-S49 cell membranes. *J Biol Chem* **259**, 13178-13185

31.   Wheeler, G. L., and Bitensky, M. W. (1977) A light-activated GTPase in vertebrate photoreceptors: regulation of light-activated cyclic GMP phosphodiesterase. *Proc Natl Acad Sci U S A* **74**, 4238-4242

32.   Godchaux, W., 3rd, and Zimmerman, W. F. (1979) Membrane-dependent guanine nucleotide binding and GTPase activities of soluble protein from bovine rod cell outer segments. *J Biol Chem* **254**, 7874-7884

33.   Kuhn, H. (1980) Light- and GTP-regulated interaction of GTPase and other proteins with bovine photoreceptor membranes. *Nature* **283**, 587-589

34.   Fung, B. K., Hurley, J. B., and Stryer, L. (1981) Flow of information in the light-triggered cyclic nucleotide cascade of vision. *Proc Natl Acad Sci U S A* **78**, 152-156

35.   Cassel, D., and Pfeuffer, T. (1978) Mechanism of cholera toxin action: covalent modification of the guanyl nucleotide-binding protein of the adenylate cyclase system. *Proc Natl Acad Sci U S A* **75**, 2669-2673

36.   Gill, D. M., and Meren, R. (1978) ADP-ribosylation of membrane proteins catalyzed by cholera toxin: basis of the activation of adenylate cyclase. *Proc Natl Acad Sci U S A* **75**, 3050-3054

37.   Moss, J., Manganiello, V. C., and Vaughan, M. (1977) Substrate and effector specificity of a guanosine 3':5'-monophosphate phosphodiesterase from rat liver. *J Biol Chem* **252**, 5211-5215

38.   Katada, T., Amano, T., and Ui, M. (1982) Modulation by Islet-Activating Protein of Adenylate-Cyclase Activity in C6 Glioma-Cells. *Journal of Biological Chemistry* **257**, 3739-3746

39.   Katada, T., and Ui, M. (1982) Direct Modification of the Membrane Adenylate-Cyclase System by Islet-Activating Protein Due to Adp-Ribosylation of a Membrane-Protein. *P Natl Acad Sci-Biol* **79**, 3129-3133

40.   Sondek, J., Lambright, D. G., Noel, J. P., Hamm, H. E., and Sigler, P. B. (1994) GTPase mechanism of Gproteins from the 1.7-A crystal structure of transducin alpha-GDP-AIF-4. *Nature* **372**, 276-279

41.   Bokoch, G. M., Katada, T., Northup, J. K., Ui, M., and Gilman, A. G. (1984) Purification and properties of the inhibitory guanine nucleotide-binding regulatory component of adenylate cyclase. *J Biol Chem* **259**, 3560-3567

42. Lambright, D. G., Noel, J. P., Hamm, H. E., and Sigler, P. B. (1994) Structural determinants for activation of the alpha-subunit of a heterotrimeric G protein. *Nature* **369**, 621-628

43. Noel, J. P., Hamm, H. E., and Sigler, P. B. (1993) The 2.2 A crystal structure of transducin-alpha complexed with GTP gamma S. *Nature* **366**, 654-663

44. Gloriam, D. E., Fredriksson, R., and Schioth, H. B. (2007) The G protein-coupled receptor subset of the rat genome. *BMC Genomics* **8**, 338

45. Hargrave, P. A., McDowell, J. H., Curtis, D. R., Wang, J. K., Juszczak, E., Fong, S. L., Rao, J. K., and Argos, P. (1983) The structure of bovine rhodopsin. *Biophys Struct Mech* **9**, 235-244

46. Wall, M. A., Coleman, D. E., Lee, E., Iniguez-Lluhi, J. A., Posner, B. A., Gilman, A. G., and Sprang, S. R. (1995) The structure of the G protein heterotrimer Gi alpha 1 beta 1 gamma 2. *Cell* **83**, 1047-1058

47. Okada, T., Ernst, O. P., Palczewski, K., and Hofmann, K. P. (2001) Activation of rhodopsin: new insights from structural and biochemical studies. *Trends Biochem Sci* **26**, 318-324

48. Millar, R. P., and Newton, C. L. (2010) The year in G protein-coupled receptor research. *Mol Endocrinol* **24**, 261-274

49. Bockaert, J., and Pin, J. P. (1999) Molecular tinkering of G protein-coupled receptors: an evolutionary success. *EMBO J* **18**, 1723-1729

50. Bosch, D. E., Kimple, A. J., Muller, R. E., Giguere, P. M., Machius, M., Willard, F. S., Temple, B. R., and Siderovski, D. P. (2012) Heterotrimeric G-protein signaling is critical to pathogenic processes in Entamoeba histolytica. *PLoS Pathog* **8**, e1003040

51. Lagerstrom, M. C., and Schioth, H. B. (2008) Structural diversity of G protein-coupled receptors and significance for drug discovery. *Nature Reviews Drug Discovery* **7**, 339-357

52. Nishimura, A., Kitano, K., Takasaki, J., Taniguchi, M., Mizuno, N., Tago, K., Hakoshima, T., and Itoh, H. (2010) Structural basis for the specific inhibition of heterotrimeric Gq protein by a small molecule. *Proc Natl Acad Sci U S A* **107**, 13666-13671

53. Tesmer, V. M., Kawano, T., Shankaranarayanan, A., Kozasa, T., and Tesmer, J. J. (2005) Snapshot of activated G proteins at the membrane: the Galphaq-GRK2-Gbetagamma complex. *Science* **310**, 1686-1690

54.   Kreutz, B., Yau, D. M., Nance, M. R., Tanabe, S., Tesmer, J. J., and Kozasa, T. (2006) A new approach to producing functional G alpha subunits yields the activated and deactivated structures of G alpha(12/13) proteins. *Biochemistry* **45**, 167-174

55.   Sunahara, R. K., Tesmer, J. J., Gilman, A. G., and Sprang, S. R. (1997) Crystal structure of the adenylyl cyclase activator Gsalpha. *Science* **278**, 1943-1947

56.   Vu, T. K., Hung, D. T., Wheaton, V. I., and Coughlin, S. R. (1991) Molecular cloning of a functional thrombin receptor reveals a novel proteolytic mechanism of receptor activation. *Cell* **64**, 1057-1068

57.   Slep, K. C., Kercher, M. A., Wieland, T., Chen, C. K., Simon, M. I., and Sigler, P. B. (2008) Molecular architecture of Galphao and the structural basis for RGS16-mediated deactivation. *Proc Natl Acad Sci U S A* **105**, 6243-6248

58.   Hofmann, B. A., Sydow, S., Jahn, O., van Werven, L., Liepold, T., Eckart, K., and Spiess, J. (2001) Functional and protein chemical characterization of the N-terminal domain of the rat corticotropin-releasing factor receptor 1. *Protein Sci* **10**, 2050-2062

59.   Grauschopf, U., Lilie, H., Honold, K., Wozny, M., Reusch, D., Esswein, A., Schafer, W., Rucknagel, K. P., and Rudolph, R. (2000) The N-terminal fragment of human parathyroid hormone receptor 1 constitutes a hormone binding domain and reveals a distinct disulfide pattern. *Biochemistry* **39**, 8878-8887

60.   Bazarsuren, A., Grauschopf, U., Wozny, M., Reusch, D., Hoffmann, E., Schaefer, W., Panzner, S., and Rudolph, R. (2002) In vitro folding, functional characterization, and disulfide pattern of the extracellular domain of human GLP-1 receptor. *Biophys Chem* **96**, 305-318

61.   Bjarnadottir, T. K., Fredriksson, R., Hoglund, P. J., Gloriam, D. E., Lagerstrom, M. C., and Schioth, H. B. (2004) The human and mouse repertoire of the adhesion family of G-protein-coupled receptors. *Genomics* **84**, 23-33

62.   Baud, V., Chissoe, S. L., Viegas-Pequignot, E., Diriong, S., N'Guyen, V. C., Roe, B. A., and Lipinski, M. (1995) EMR1, an unusual member in the family of hormone receptors with seven transmembrane segments. *Genomics* **26**, 334-344

63.   Krasnoperov, V. G., Bittner, M. A., Beavis, R., Kuang, Y., Salnikow, K. V., Chepurny, O. G., Little, A. R., Plotnikov, A. N., Wu, D., Holz, R. W., and Petrenko, A. G. (1997) alpha-Latrotoxin stimulates exocytosis by the interaction with a neuronal G-protein-coupled receptor. *Neuron* **18**, 925-937

64. Krasnoperov, V., Lu, Y., Buryanovsky, L., Neubert, T. A., Ichtchenko, K., and Petrenko, A. G. (2002) Post-translational proteolytic processing of the calcium-independent receptor of alpha-latrotoxin (CIRL), a natural chimera of the cell adhesion protein and the G protein-coupled receptor. Role of the G protein-coupled receptor proteolysis site (GPS) motif. *J Biol Chem* **277**, 46518-46526

65. Lin, H. H., Chang, G. W., Davies, J. Q., Stacey, M., Harris, J., and Gordon, S. (2004) Autocatalytic cleavage of the EMR2 receptor occurs at a conserved G protein-coupled receptor proteolytic site motif. *J Biol Chem* **279**, 31823-31832

66. Harmar, A. J. (2001) Family-B G-protein-coupled receptors. *Genome Biol* **2**, REVIEWS3013

67. Kunishima, N., Shimada, Y., Tsuji, Y., Sato, T., Yamamoto, M., Kumasaka, T., Nakanishi, S., Jingami, H., and Morikawa, K. (2000) Structural basis of glutamate recognition by a dimeric metabotropic glutamate receptor. *Nature* **407**, 971-977

68. Rondard, P., Liu, J., Huang, S., Malhaire, F., Vol, C., Pinault, A., Labesse, G., and Pin, J. P. (2006) Coupling of agonist binding to effector domain activation in metabotropic glutamate-like receptors. *J Biol Chem* **281**, 24653-24661

69. Liu, X., He, Q., Studholme, D. J., Wu, Q., Liang, S., and Yu, L. (2004) NCD3G: a novel nine-cysteine domain in family 3 GPCRs. *Trends Biochem Sci* **29**, 458-461

70. Katritch, V., Cherezov, V., and Stevens, R. C. (2013) Structure-function of the G protein-coupled receptor superfamily. *Annu Rev Pharmacol Toxicol* **53**, 531-556

71. Venkatakrishnan, A. J., Deupi, X., Lebon, G., Tate, C. G., Schertler, G. F., and Babu, M. M. (2013) Molecular signatures of G-protein-coupled receptors. *Nature* **494**, 185-194

72. Sakmar, T. P., Franke, R. R., and Khorana, H. G. (1991) The role of the retinylidene Schiff base counterion in rhodopsin in determining wavelength absorbance and Schiff base pKa. *Proc Natl Acad Sci U S A* **88**, 3079-3083

73. Dratz, E. A., and Hargrave, P. A. (1983) The Structure of Rhodopsin and the Rod Outer Segment Disk Membrane. *Trends in Biochemical Sciences* **8**, 128-131

74. Findlay, J. B., and Pappin, D. J. (1986) The opsin family of proteins. *Biochem J* **238**, 625-642

75. Unger, V. M., and Schertler, G. F. (1995) Low resolution structure of bovine rhodopsin determined by electron cryo-microscopy. *Biophys J* **68**, 1776-1786

76. Schertler, G. F., Villa, C., and Henderson, R. (1993) Projection structure of rhodopsin. *Nature* **362**, 770-772

77. Farrens, D. L., Altenbach, C., Yang, K., Hubbell, W. L., and Khorana, H. G. (1996) Requirement of rigid-body motion of transmembrane helices for light activation of rhodopsin. *Science* **274**, 768-770

78. Altenbach, C., Kusnetzow, A. K., Ernst, O. P., Hofmann, K. P., and Hubbell, W. L. (2008) High-resolution distance mapping in rhodopsin reveals the pattern of helix movement due to activation. *Proc Natl Acad Sci U S A* **105**, 7439-7444

79. Park, J. H., Scheerer, P., Hofmann, K. P., Choe, H. W., and Ernst, O. P. (2008) Crystal structure of the ligand-free G-protein-coupled receptor opsin. *Nature* **454**, 183-187

80. Scheerer, P., Park, J. H., Hildebrand, P. W., Kim, Y. J., Krauss, N., Choe, H. W., Hofmann, K. P., and Ernst, O. P. (2008) Crystal structure of opsin in its G-protein-interacting conformation. *Nature* **455**, 497-502

81. Choe, H. W., Kim, Y. J., Park, J. H., Morizumi, T., Pai, E. F., Krauss, N., Hofmann, K. P., Scheerer, P., and Ernst, O. P. (2011) Crystal structure of metarhodopsin II. *Nature* **471**, 651-655

82. Standfuss, J., Edwards, P. C., D'Antona, A., Fransen, M., Xie, G., Oprian, D. D., and Schertler, G. F. (2011) The structural basis of agonist-induced activation in constitutively active rhodopsin. *Nature* **471**, 656-660

83. Palczewski, K., Kumasaka, T., Hori, T., Behnke, C. A., Motoshima, H., Fox, B. A., Le Trong, I., Teller, D. C., Okada, T., Stenkamp, R. E., Yamamoto, M., and Miyano, M. (2000) Crystal structure of rhodopsin: A G protein-coupled receptor. *Science* **289**, 739-745

84. Ballesteros, J. A., Jensen, A. D., Liapakis, G., Rasmussen, S. G., Shi, L., Gether, U., and Javitch, J. A. (2001) Activation of the beta 2-adrenergic receptor involves disruption of an ionic lock between the cytoplasmic ends of transmembrane segments 3 and 6. *J Biol Chem* **276**, 29171-29177

85. Filipek, S., Stenkamp, R. E., Teller, D. C., and Palczewski, K. (2003) G protein-coupled receptor rhodopsin: a prospectus. *Annu Rev Physiol* **65**, 851-879

86. Hoffmann, C., Zurn, A., Bunemann, M., and Lohse, M. J. (2008) Conformational changes in G-protein-coupled receptors-the quest for functionally selective conformations is open. *Br J Pharmacol* **153 Suppl 1**, S358-366

87. Matthews, R. G., Hubbard, R., Brown, P. K., and Wald, G. (1963) Tautomeric Forms of Metarhodopsin. *J Gen Physiol* **47**, 215-240

88. Fahmy, K., Siebert, F., and Sakmar, T. P. (1994) A mutant rhodopsin photoproduct with a protonated Schiff base displays an active-state conformation: a Fourier-transform infrared spectroscopy study. *Biochemistry* **33**, 13700-13705

89. Vogel, R., Mahalingam, M., Ludeke, S., Huber, T., Siebert, F., and Sakmar, T. P. (2008) Functional role of the "ionic lock"--an interhelical hydrogen-bond network in family A heptahelical receptors. *J Mol Biol* **380**, 648-655

90. Janz, J. M., and Farrens, D. L. (2004) Rhodopsin activation exposes a key hydrophobic binding site for the transducin alpha-subunit C terminus. *J Biol Chem* **279**, 29767-29773

91. Knierim, B., Hofmann, K. P., Ernst, O. P., and Hubbell, W. L. (2007) Sequence of late molecular events in the activation of rhodopsin. *Proc Natl Acad Sci U S A* **104**, 20290-20295

92. Luo, D. G., Xue, T., and Yau, K. W. (2008) How vision begins: an odyssey. *Proc Natl Acad Sci U S A* **105**, 9855-9862

93. Landis, C. A., Masters, S. B., Spada, A., Pace, A. M., Bourne, H. R., and Vallar, L. (1989) GTPase inhibiting mutations activate the alpha chain of Gs and stimulate adenylyl cyclase in human pituitary tumours. *Nature* **340**, 692-696

94. Lyons, J., Landis, C. A., Harsh, G., Vallar, L., Grunewald, K., Feichtinger, H., Duh, Q. Y., Clark, O. H., Kawasaki, E., Bourne, H. R., and et al. (1990) Two G protein oncogenes in human endocrine tumors. *Science* **249**, 655-659

95. Dryja, T. P., Hahn, L. B., Reboul, T., and Arnaud, B. (1996) Missense mutation in the gene encoding the alpha subunit of rod transducin in the Nougaret form of congenital stationary night blindness. *Nat Genet* **13**, 358-360

96. Van Raamsdonk, C. D., Bezrookove, V., Green, G., Bauer, J., Gaugler, L., O'Brien, J. M., Simpson, E. M., Barsh, G. S., and Bastian, B. C. (2009) Frequent somatic mutations of GNAQ in uveal melanoma and blue naevi. *Nature* **457**, 599-602

97. Van Dop, C., Tsubokawa, M., Bourne, H. R., and Ramachandran, J. (1984) Amino acid sequence of retinal transducin at the site ADP-ribosylated by cholera toxin. *J Biol Chem* **259**, 696-698

98. Ross, E. M., Howlett, A. C., Ferguson, K. M., and Gilman, A. G. (1978) Reconstitution of hormone-sensitive adenylate cyclase activity with resolved components of the enzyme. *J Biol Chem* **253**, 6401-6412

99. Downes, G. B., and Gautam, N. (1999) The G protein subunit gene families. *Genomics* **62**, 544-552

100. Oldham, W. M., and Hamm, H. E. (2008) Heterotrimeric G protein activation by G-protein-coupled receptors. *Nat Rev Mol Cell Biol* **9**, 60-71

101. Chen, C. A., and Manning, D. R. (2001) Regulation of G proteins by covalent modification. *Oncogene* **20**, 1643-1652

102. Escriba, P. V., Wedegaertner, P. B., Goni, F. M., and Vogler, O. (2007) Lipid-protein interactions in GPCR-associated signaling. *Biochim Biophys Acta* **1768**, 836-852

103. Schmidt, C. J., Thomas, T. C., Levine, M. A., and Neer, E. J. (1992) Specificity of G protein beta and gamma subunit interactions. *J Biol Chem* **267**, 13807-13810

104. Sprang, S. R. (1997) G protein mechanisms: insights from structural analysis. *Annual Review of Biochemistry* **66**, 639-678

105. Sanford, J., Codina, J., and Birnbaumer, L. (1991) Gamma-subunits of G proteins, but not their alpha- or beta-subunits, are polyisoprenylated. Studies on post-translational modifications using in vitro translation with rabbit reticulocyte lysates. *J Biol Chem* **266**, 9570-9579

106. Ray, K., Kunsch, C., Bonner, L. M., and Robishaw, J. D. (1995) Isolation of cDNA clones encoding eight different human G protein gamma subunits, including three novel forms designated the gamma 4, gamma 10, and gamma 11 subunits. *J Biol Chem* **270**, 21765-21771

107. Lai, R. K., Perez-Sala, D., Canada, F. J., and Rando, R. R. (1990) The gamma subunit of transducin is farnesylated. *Proc Natl Acad Sci U S A* **87**, 7673-7677

108. Iniguez-Lluhi, J. A., Simon, M. I., Robishaw, J. D., and Gilman, A. G. (1992) G protein beta gamma subunits synthesized in Sf9 cells. Functional characterization and the significance of prenylation of gamma. *J Biol Chem* **267**, 23409-23417

109. Van Eps, N., Oldham, W. M., Hamm, H. E., and Hubbell, W. L. (2006) Structural and dynamical changes in an alpha-subunit of a heterotrimeric G protein along the activation pathway. *Proc Natl Acad Sci U S A* **103**, 16194-16199

110. Ross, E. M., and Wilkie, T. M. (2000) GTPase-activating proteins for heterotrimeric G proteins: regulators of G protein signaling (RGS) and RGS-like proteins. *Annual Review of Biochemistry* **69**, 795-827

111. Xie, G. X., and Palmer, P. P. (2007) How regulators of G protein signaling achieve selective regulation. *J Mol Biol* **366**, 349-365

112. Tesmer, J. J., Berman, D. M., Gilman, A. G., and Sprang, S. R. (1997) Structure of RGS4 bound to AlF4--activated G(i alpha1): stabilization of the transition state for GTP hydrolysis. *Cell* **89**, 251-261

113. Srinivasa, S. P., Watson, N., Overton, M. C., and Blumer, K. J. (1998) Mechanism of RGS4, a GTPase-activating protein for G protein alpha subunits. *J Biol Chem* **273**, 1529-1533

114. DiBello, P. R., Garrison, T. R., Apanovitch, D. M., Hoffman, G., Shuey, D. J., Mason, K., Cockett, M. I., and Dohlman, H. G. (1998) Selective uncoupling of RGS action by a single point mutation in the G protein alpha-subunit. *J Biol Chem* **273**, 5780-5784

115. Rosenthal, W., Seibold, A., Antaramian, A., Gilbert, S., Birnbaumer, M., Bichet, D. G., Arthus, M. F., and Lonergan, M. (1994) Mutations in the vasopressin V2 receptor gene in families with nephrogenic diabetes insipidus and functional expression of the Q-2 mutant. *Cell Mol Biol (Noisy-le-grand)* **40**, 429-436

116. Thompson, M. D., Percy, M. E., McIntyre Burnham, W., and Cole, D. E. (2008) G protein-coupled receptors disrupted in human genetic disease. *Methods Mol Biol* **448**, 109-137

117. Hamm, H. E., Deretic, D., Hargrave, P. A., Arendt, A., Mcdowell, J. H., Koenig, B., and Hofmann, K. P. (1988) Synthetic Peptides to G-Alpha Compete with G-Protein for Interaction with Light-Activated Rhodopsin and Monoclonal-Antibody 4a. *Biophysical Journal* **53**, A388-A388

118. Onrust, R., Herzmark, P., Chi, P., Garcia, P. D., Lichtarge, O., Kingsley, C., and Bourne, H. R. (1997) Receptor and betagamma binding sites in the alpha subunit of the retinal G protein transducin. *Science* **275**, 381-384

119. Cai, K., Itoh, Y., and Khorana, H. G. (2001) Mapping of contact sites in complex formation between transducin and light-activated rhodopsin by covalent crosslinking: use of a photoactivatable reagent. *Proc Natl Acad Sci U S A* **98**, 4877-4882

120. Mazzoni, M. R., and Hamm, H. E. (1996) Interaction of transducin with light-activated rhodopsin protects It from proteolytic digestion by trypsin. *J Biol Chem* **271**, 30034-30040

121. Grishina, G., and Berlot, C. H. (2000) A surface-exposed region of G(salpha) in which substitutions decrease receptor-mediated activation and increase receptor affinity. *Mol Pharmacol* **57**, 1081-1092

122. Hamm, H. E., Deretic, D., Arendt, A., Hargrave, P. A., Koenig, B., and Hofmann, K. P. (1988) Site of G-Protein Binding to Rhodopsin Mapped with Synthetic Peptides from the Alpha-Subunit. *Science* **241**, 832-835

123. Dratz, E. A., Furstenau, J. E., Lambert, C. G., Thireault, D. L., Rarick, H., Schepers, T., Pakhlevaniants, S., and Hamm, H. E. (1993) NMR structure of a receptor-bound G-protein peptide. *Nature* **363**, 276-281

124. Taylor, J. M., Jacob-Mosier, G. G., Lawton, R. G., Remmers, A. E., and Neubig, R. R. (1994) Binding of an alpha 2 adrenergic receptor third intracellular loop peptide to G beta and the amino terminus of G alpha. *J Biol Chem* **269**, 27618-27624

125. Itoh, Y., Cai, K., and Khorana, H. G. (2001) Mapping of contact sites in complex formation between light-activated rhodopsin and transducin by covalent crosslinking: use of a chemically preactivated reagent. *Proc Natl Acad Sci U S A* **98**, 4883-4887

126. Taylor, J. M., Jacob-Mosier, G. G., Lawton, R. G., VanDort, M., and Neubig, R. R. (1996) Receptor and membrane interaction sites on Gbeta. A receptor-derived peptide binds to the carboxyl terminus. *J Biol Chem* **271**, 3336-3339

127. Ford, C. E., Skiba, N. P., Bae, H., Daaka, Y., Reuveny, E., Shekter, L. R., Rosal, R., Weng, G., Yang, C. S., Iyengar, R., Miller, R. J., Jan, L. Y., Lefkowitz, R. J., and Hamm, H. E. (1998) Molecular basis for interactions of G protein betagamma subunits with effectors. *Science* **280**, 1271-1274

128. Hamm, H. E., Deretic, D., Arendt, A., Hargrave, P. A., Koenig, B., and Hofmann, K. P. (1988) Site of G protein binding to rhodopsin mapped with synthetic peptides from the alpha subunit. *Science* **241**, 832-835

129. Kisselev, O., Pronin, A., Ermolaeva, M., and Gautam, N. (1995) Receptor-G protein coupling is established by a potential conformational switch in the beta gamma complex. *Proc Natl Acad Sci U S A* **92**, 9102-9106

130. Kisselev, O. G., and Downs, M. A. (2003) Rhodopsin controls a conformational switch on the transducin gamma subunit. *Structure* **11**, 367-373

131. Oldham, W. M., Van Eps, N., Preininger, A. M., Hubbell, W. L., and Hamm, H. E. (2006) Mechanism of the receptor-catalyzed activation of heterotrimeric G proteins. *Nature Structural & Molecular Biology* **13**, 772-777

132. Preininger, A. M., Funk, M. A., Oldham, W. M., Meier, S. M., Johnston, C. A., Adhikary, S., Kimple, A. J., Siderovski, D. P., Hamm, H. E., and Iverson, T. M. (2009) Helix Dipole Movement and Conformational Variability Contribute to Allosteric GDP Release in G alpha(i) Subunits. *Biochemistry* **48**, 2630-2642

133. Rondard, P., Iiri, T., Srinivasan, S., Meng, E., Fujita, T., and Bourne, H. R. (2001) Mutant G protein alpha subunit activated by G beta gamma: A model for receptor activation? *Proceedings of the National Academy of Sciences of the United States of America* **98**, 6150-6155

134. Cherfils, J., and Chabre, M. (2003) Activation of G-protein G alpha subunits by receptors through G alpha-G beta and G alpha-G gamma interactions. *Trends in Biochemical Sciences* **28**, 13-17

135. Iiri, T., Farfel, Z., and Bourne, H. R. (1998) G-protein diseases furnish a model for the turn-on switch. *Nature* **394**, 35-38

136. Van Eps, N., Preininger, A. M., Alexander, N., Kaya, A. I., Meier, S., Meiler, J., Hamm, H. E., and Hubbell, W. L. (2011) Interaction of a G protein with an activated receptor opens the interdomain interface in the alpha subunit. *Proc Natl Acad Sci U S A* **108**, 9420-9424

137. Hamm, H. E., Kaya, A. I., Gilbert, J. A., 3rd, and Preininger, A. M. (2013) Linking receptor activation to changes in Sw I and II of Galpha proteins. *J Struct Biol* **184**, 63-74

138. Palczewski, K. (2006) G protein-coupled receptor rhodopsin. *Annu Rev Biochem* **75**, 743-767

139. Emeis, D., Kuhn, H., Reichert, J., and Hofmann, K. P. (1982) Complex formation between metarhodopsin II and GTP-binding protein in bovine photoreceptor membranes leads to a shift of the photoproduct equilibrium. *FEBS Lett* **143**, 29-34

140. Parkes, J. H., Gibson, S. K., and Liebman, P. A. (1999) Temperature and pH dependence of the metarhodopsin I-metarhodopsin II equilibrium and the binding of metarhodopsin II to G protein in rod disk membranes. *Biochemistry* **38**, 6862-6878

141. Parkes, J. H., and Liebman, P. A. (1984) Temperature and pH dependence of the metarhodopsin I-metarhodopsin II kinetics and equilibria in bovine rod disk membrane suspensions. *Biochemistry* **23**, 5054-5061

142. Fung, J. J., Deupi, X., Pardo, L., Yao, X. J., Velez-Ruiz, G. A., Devree, B. T., Sunahara, R. K., and Kobilka, B. K. (2009) Ligand-regulated oligomerization of beta(2)-adrenoceptors in a model lipid bilayer. *EMBO J* **28**, 3315-3328

143.   Alves, I. D., Salgado, G. F., Salamon, Z., Brown, M. F., Tollin, G., and Hruby, V. J. (2005) Phosphatidylethanolamine enhances rhodopsin photoactivation and transducin binding in a solid supported lipid bilayer as determined using plasmon-waveguide resonance spectroscopy. *Biophys J* **88**, 198-210

144.   Litman, B. J., Niu, S. L., Polozova, A., and Mitchell, D. C. (2001) The role of docosahexaenoic acid containing phospholipids in modulating G protein-coupled signaling pathways: visual transduction. *J Mol Neurosci* **16**, 237-242; discussion 279-284

145.   Jastrzebska, B., Goc, A., Golczak, M., and Palczewski, K. (2009) Phospholipids are needed for the proper formation, stability, and function of the photoactivated rhodopsin-transducin complex. *Biochemistry* **48**, 5159-5170

146.   Mitchell, D. C., Niu, S. L., and Litman, B. J. (2001) Optimization of receptor-G protein coupling by bilayer lipid composition I: kinetics of rhodopsin-transducin binding. *J Biol Chem* **276**, 42801-42806

147.   Gawrisch, K., Soubias, O., and Mihailescu, M. (2008) Insights from biophysical studies on the role of polyunsaturated fatty acids for function of G-protein coupled membrane receptors. *Prostaglandins Leukot Essent Fatty Acids* **79**, 131-134

148.   Bennett, M. P., and Mitchell, D. C. (2008) Regulation of membrane proteins by dietary lipids: effects of cholesterol and docosahexaenoic acid acyl chain-containing phospholipids on rhodopsin stability and function. *Biophys J* **95**, 1206-1216

149.   McKibbin, C., Farmer, N. A., Jeans, C., Reeves, P. J., Khorana, H. G., Wallace, B. A., Edwards, P. C., Villa, C., and Booth, P. J. (2007) Opsin stability and folding: modulation by phospholipid bicelles. *J Mol Biol* **374**, 1319-1332

150.   Faham, S., Boulting, G. L., Massey, E. A., Yohannan, S., Yang, D., and Bowie, J. U. (2005) Crystallization of bacteriorhodopsin from bicelle formulations at room temperature. *Protein Sci* **14**, 836-840

151.   Rasmussen, S. G., Choi, H. J., Rosenbaum, D. M., Kobilka, T. S., Thian, F. S., Edwards, P. C., Burghammer, M., Ratnala, V. R., Sanishvili, R., Fischetti, R. F., Schertler, G. F., Weis, W. I., and Kobilka, B. K. (2007) Crystal structure of the human beta2 adrenergic G-protein-coupled receptor. *Nature* **450**, 383-387

152.   Luecke, H., Schobert, B., Stagno, J., Imasheva, E. S., Wang, J. M., Balashov, S. P., and Lanyi, J. K. (2008) Crystallographic structure of xanthorhodopsin, the light-driven proton pump with a dual chromophore. *Proc Natl Acad Sci U S A* **105**, 16561-16565

153. Ujwal, R., Cascio, D., Colletier, J. P., Faham, S., Zhang, J., Toro, L., Ping, P., and Abramson, J. (2008) The crystal structure of mouse VDAC1 at 2.3 A resolution reveals mechanistic insights into metabolite gating. *Proc Natl Acad Sci U S A* **105**, 17742-17747

154. Bayburt, T. H., Vishnivetskiy, S. A., McLean, M. A., Morizumi, T., Huang, C. C., Tesmer, J. J., Ernst, O. P., Sligar, S. G., and Gurevich, V. V. (2011) Monomeric rhodopsin is sufficient for normal rhodopsin kinase (GRK1) phosphorylation and arrestin-1 binding. *J Biol Chem* **286**, 1420-1428

155. Sanders, C. R., and Prosser, R. S. (1998) Bicelles: a model membrane system for all seasons? *Structure* **6**, 1227-1234

156. Wu, H., Su, K., Guan, X., Sublette, M. E., and Stark, R. E. (2010) Assessing the size, stability, and utility of isotropically tumbling bicelle systems for structural biology. *Biochim Biophys Acta* **1798**, 482-488

157. Glover, K. J., Whiles, J. A., Wu, G., Yu, N., Deems, R., Struppe, J. O., Stark, R. E., Komives, E. A., and Vold, R. R. (2001) Structural evaluation of phospholipid bicelles for solution-state studies of membrane-associated biomolecules. *Biophys J* **81**, 2163-2171

158. Struppe, J., Whiles, J. A., and Vold, R. R. (2000) Acidic phospholipid bicelles: A versatile model membrane system. *Biophysical Journal* **78**, 281-289

159. Struppe, J., Komives, E. A., Taylor, S. S., and Vold, R. R. (1998) 2H NMR studies of a myristoylated peptide in neutral and acidic phospholipid bicelles. *Biochemistry* **37**, 15523-15527

160. Marcotte, I., and Auger, M. (2005) Bicelles as model membranes for solid- and solution-state NMR studies of membrane peptides and proteins. *Concepts in Magnetic Resonance Part A* **24A**, 17-37

161. Prosser, R. S., Hwang, J. S., and Vold, R. R. (1998) Magnetically aligned phospholipid bilayers with positive ordering: a new model membrane system. *Biophys J* **74**, 2405-2418

162. Mazzoni, M. R., Malinksi, J. A., and Hamm, H. E. (1991) Structural Analysis of Rod GTP-binding Protein, G_t. Limited Proteolytic Digestion Pattern of G_t with Four Proteases Defines Monoclonal Antibody Epitope. *Journal of Biological Chemistry* **266**, 14072-14081

163. Litman, B. J. (1982) Purification of rhodopsin by concanavalin A affinity chromatography. *Methods Enzymol* **81**, 150-153

164. Aris, L., Gilchrist, A., Rens-Domiano, S., Meyer, C., Schatz, P. J., Dratz, E. A., and Hamm, H. E. (2001) Structural Requirements for the Stabilization of Metarhodopsin II by the C Terminus of the a subunit of Transducin. *Journal of Biological Chemistry* **276**, 2333-2339

165. Bradford, M. M. (1976) A rapid and sensitive method for the quantitation of microgram quantities of protein utilizing the principle of protein-dye binding. *Anal Biochem* **72**, 248-254

166. Preininger, A., Funk, M., Meier, S., Oldham, W., Johnston, C., Adhikary, S., Kimple, A., Siderovski, D., Hamm, H., and Iverson, T. (2009) Helix dipole movement and conformational variability contribute to allosteric GDP release in Gi subunits. *Biochemistry* **48**, 2630-2642

167. Schleicher, A., Kuhn, H., and Hofmann, K. P. (1989) Kinetics, binding constant, and activation energy of the 48-kDa protein-rhodopsin complex by extra-metarhodopsin II. *Biochemistry* **28**, 1770-1775

168. Hoffmann, W., Siebert, F., Hofmann, K. P., and Kreutz, W. (1978) Two distinct rhodopsin molecules within the disc membrane of vertebrate rod outer segments. *Biochim Biophys Acta* **503**, 450-461

169. Emeis, D., and Hofmann, K. P. (1981) Shift in the relation between flash-induced metarhodopsin I and metarhodpsin II within the first 10% rhodopsin bleaching in bovine disc membranes. *FEBS Lett* **136**, 201-207

170. Kisselev, O. G., Meyer, C. K., Heck, M., Ernst, O. P., and Hofmann, K. P. (1999) Signal transfer from rhodopsin to the G-protein: evidence for a two-site sequential fit mechanism. *Proc Natl Acad Sci U S A* **96**, 4898-4903

171. Chen, Y., Herrmann, R., Fishkin, N., Henklein, P., Nakanishi, K., and Ernst, O. P. (2008) Synthesis and spectroscopic characterization of photo-affinity peptide ligands to study rhodopsin-G protein interaction. *Photochem Photobiol* **84**, 831-838

172. Faham, S., and Bowie, J. U. (2002) Bicelle crystallization: a new method for crystallizing membrane proteins yields a monomeric bacteriorhodopsin structure. *J Mol Biol* **316**, 1-6

173. Bayburt, T. H., Leitz, A. J., Xie, G., Oprian, D. D., and Sligar, S. G. (2007) Transducin activation by nanoscale lipid bilayers containing one and two rhodopsins. *J Biol Chem* **282**, 14875-14881

174. Sanders, C. R., and Schwonek, J. P. (1992) Characterization of Magnetically Orientable Bilayers in Mixtures of Dihexanoylphosphatidylcholine and Dimyristoylphosphatidylcholine by Solid-State Nmr. *Biochemistry* **31**, 8898-8905

175. Sanders, C. R., Kuhn Hoffmann, A., Gray, D. N., Keyes, M. H., and Ellis, C. D. (2004) French swimwear for membrane proteins. *Chembiochem* **5**, 423-426

176. Whiles, J. A., Deems, R., Vold, R. R., and Dennis, E. A. (2002) Bicelles in structure-function studies of membrane-associated proteins. *Bioorg Chem* **30**, 431-442

177. Boesze-Battaglia, K., and Schimmel, R. (1997) Cell membrane lipid composition and distribution: implications for cell function and lessons learned from photoreceptors and platelets. *J Exp Biol* **200**, 2927-2936

178. Eichberg, J., and Hess, H. H. (1967) The lipid composition of frog retinal rod outer segments. *Experientia* **23**, 993-994

179. Wiegand, R. D., Naash, M. I., Penn, J. S., Maude, M. B., and Anderson, R. E. (1986) Effect of Constant Light on Rat Retinas Deficient in Glutathione-Reductase. *Federation Proceedings* **45**, 1728-1728

180. Kosloff, M., Alexov, E., Arshavsky, V. Y., and Honig, B. (2008) Electrostatic and lipid anchor contributions to the interaction of transducin with membranes: mechanistic implications for activation and translocation. *J Biol Chem* **283**, 31197-31207

181. Lambright, D. G., Sondek, J., Bohm, A., Skiba, N. P., Hamm, H. E., and Sigler, P. B. (1996) The 2.0 A crystal structure of a heterotrimeric G protein. *Nature* **379**, 311-319

182. Bohm, A., Gaudet, R., and Sigler, P. B. (1997) Structural aspects of heterotrimeric G-protein signaling. *Curr Opin Biotechnol* **8**, 480-487

183. Saari, J. C., Nawrot, M., Stenkamp, R. E., Teller, D. C., and Garwin, G. G. (2009) Release of 11-cis-retinal from cellular retinaldehyde-binding protein by acidic lipids. *Mol Vis* **15**, 844-854

184. Ilincheta de Boschero, M. G., and Giusto, N. M. (1992) Phosphatidic acid and polyphosphoinositide metabolism in rod outer segments. Differential role of soluble and peripheral proteins. *Biochim Biophys Acta* **1127**, 105-115

185. LaLonde, M. M., Janssens, H., Rosenbaum, E., Choi, S. Y., Gergen, J. P., Colley, N. J., Stark, W. S., and Frohman, M. A. (2005) Regulation of phototransduction responsiveness and retinal degeneration by a phospholipase D-generated signaling lipid. *J Cell Biol* **169**, 471-479

186. Calvert, P. D., Govardovskii, V. I., Krasnoperova, N., Anderson, R. E., Lem, J., and Makino, C. L. (2001) Membrane protein diffusion sets the speed of rod phototransduction. *Nature* **411**, 90-94

187. Aveldano, M. I. (1995) Phospholipid solubilization during detergent extraction of rhodopsin from photoreceptor disk membranes. *Arch Biochem Biophys* **324**, 331-343

188. Nickell, S., Park, P. S., Baumeister, W., and Palczewski, K. (2007) Three-dimensional architecture of murine rod outer segments determined by cryoelectron tomography. *J Cell Biol* **177**, 917-925

189. Andersson, A., and Maler, L. (2006) Size and shape of fast-tumbling bicelles as determined by translational diffusion. *Langmuir* **22**, 2447-2449

190. Dupuy, C., Auvray, X., and Petipas, C. (1997) Anomeric effects on the structure of micelles of alkyl maltosides in water. *Langmuir* **13**, 3965-3967

191. Kozak, M., Kempka, M., Szpotkowski, K., and Jurga, S. (2007) NMR in soft materials: A study of DMPC/DHPC bicellar system. *J Non-Cryst Solids* **353**, 4246-4251

192. Botelho, A. V., Huber, T., Sakmar, T. P., and Brown, M. F. (2006) Curvature and hydrophobic forces drive oligomerization and modulate activity of rhodopsin in membranes. *Biophys J* **91**, 4464-4477

193. Botelho, A. V., Gibson, N. J., Thurmond, R. L., Wang, Y., and Brown, M. F. (2002) Conformational energetics of rhodopsin modulated by nonlamellar-forming lipids. *Biochemistry* **41**, 6354-6368

194. Sato, K., Morizumi, T., Yamashita, T., and Shichida, Y. (2010) Direct observation of the pH-dependent equilibrium between metarhodopsins I and II and the pH-independent interaction of metarhodopsin II with transducin C-terminal peptide. *Biochemistry* **49**, 736-741

195. Jager, S., Palczewski, K., and Hofmann, K. P. (1996) Opsin/all-trans-retinal complex activates transducin by different mechanisms than photolyzed rhodopsin. *Biochemistry* **35**, 2901-2908

196. Jastrzebska, B., Golczak, M., Fotiadis, D., Engel, A., and Palczewski, K. (2009) Isolation and functional characterization of a stable complex between photoactivated rhodopsin and the G protein, transducin. *FASEB J* **23**, 371-381

197. Lee, A. G. (2003) Lipid-protein interactions in biological membranes: a structural perspective. *Biochim Biophys Acta* **1612**, 1-40

198.	Shogomori, H., and Brown, D. A. (2003) Use of detergents to study membrane rafts: the good, the bad, and the ugly. *Biol Chem* **384**, 1259-1263

199.	Simons, K., and Ikonen, E. (1997) Functional rafts in cell membranes. *Nature* **387**, 569-572

200.	Gibson, N. J., and Brown, M. F. (1991) Role of phosphatidylserine in the MI-MII equilibrium of rhodopsin. *Biochem Biophys Res Commun* **176**, 915-921

201.	Gibson, N. J., and Brown, M. F. (1993) Lipid headgroup and acyl chain composition modulate the MI-MII equilibrium of rhodopsin in recombinant membranes. *Biochemistry* **32**, 2438-2454

202.	Bayburt, T. H., Vishnivetskiy, S. A., McLean, M. A., Morizumi, T., Huang, C. C., Tesmer, J. J., Ernst, O. P., Sligar, S. G., and Gurevich, V. V. (2010) Monomeric rhodopsin is sufficient for normal rhodopsin kinase (GRK1) phosphorylation and arrestin-1 binding. *J Biol Chem*

203.	Tsukamoto, H., Sinha, A., DeWitt, M., and Farrens, D. L. (2010) Monomeric rhodopsin is the minimal functional unit required for arrestin binding. *J Mol Biol* **399**, 501-511

204.	Kohl, B., and Hofmann, K. P. (1987) Temperature dependence of G-protein activation in photoreceptor membranes. Transient extra metarhodopsin II on bovine disk membranes. *Biophys J* **52**, 271-277

205.	Feller, S. E. (2008) Acyl chain conformations in phospholipid bilayers: a comparative study of docosahexaenoic acid and saturated fatty acids. *Chem Phys Lipids* **153**, 76-80

206.	Niu, S. L., Mitchell, D. C., and Litman, B. J. (2001) Optimization of receptor-G protein coupling by bilayer lipid composition II: formation of metarhodopsin II-transducin complex. *J Biol Chem* **276**, 42807-42811

207.	Hofmann, K. P., Scheerer, P., Hildebrand, P. W., Choe, H. W., Park, J. H., Heck, M., and Ernst, O. P. (2009) A G protein-coupled receptor at work: the rhodopsin model. *Trends Biochem Sci* **34**, 540-552

208.	Ferguson, K. M., Higashijima, T., Smigel, M. D., and Gilman, A. G. (1986) The influence of bound GDP on the kinetics of guanine nucleotide binding to G proteins. *J Biol Chem* **261**, 7393-7399

209.	Sanders, C. R., 2nd. (1994) Qualitative comparison of the bilayer-associated structures of diacylglycerol and a fluorinated analog based upon oriented sample NMR data. *Chem Phys Lipids* **72**, 41-57

210. Ujwal, R., and Bowie, J. U. (2011) Crystallizing membrane proteins using lipidic bicelles. *Methods* **55**, 337-341

211. Kaya, A. I., Thaker, T. M., Preininger, A. M., Iverson, T. M., and Hamm, H. E. (2011) Coupling efficiency of rhodopsin and transducin in bicelles. *Biochemistry* **50**, 3193-3203

212. Czerski, L., and Sanders, C. R. (2000) Functionality of a membrane protein in bicelles. *Anal Biochem* **284**, 327-333

213. Vinothkumar, K. R. (2011) Structure of rhomboid protease in a lipid environment. *J Mol Biol* **407**, 232-247

214. Landau, E. M., and Rosenbusch, J. P. (1996) Lipidic cubic phases: a novel concept for the crystallization of membrane proteins. *Proc Natl Acad Sci U S A* **93**, 14532-14535

215. Caffrey, M., Li, D., and Dukkipati, A. (2012) Membrane protein structure determination using crystallography and lipidic mesophases: recent advances and successes. *Biochemistry* **51**, 6266-6288

216. Caffrey, M., and Cherezov, V. (2009) Crystallizing membrane proteins using lipidic mesophases. *Nat Protoc* **4**, 706-731

217. Cherezov, V. (2011) Lipidic cubic phase technologies for membrane protein structural studies. *Curr Opin Struct Biol* **21**, 559-566

218. Cherezov, V., Clogston, J., Papiz, M. Z., and Caffrey, M. (2006) Room to move: crystallizing membrane proteins in swollen lipidic mesophases. *J Mol Biol* **357**, 1605-1618

219. Wadsten, P., Wohri, A. B., Snijder, A., Katona, G., Gardiner, A. T., Cogdell, R. J., Neutze, R., and Engstrom, S. (2006) Lipidic sponge phase crystallization of membrane proteins. *J Mol Biol* **364**, 44-53

220. Thaker, T. M., Kaya, A. I., Preininger, A. M., Hamm, H. E., and Iverson, T. M. (2012) Allosteric mechanisms of G protein-Coupled Receptor signaling: a structural perspective. *Methods Mol Biol* **796**, 133-174

221. Kleuss, C., Pallast, M., Brendel, S., Rosenthal, W., and Schultz, G. (1987) Resolution of transducin subunits by chromatography on blue sepharose. *J Chromatogr* **407**, 281-289

222. Aris, L., Gilchrist, A., Rens-Domiano, S., Meyer, C., Schatz, P. J., Dratz, E. A., and Hamm, H. E. (2001) Structural requirements for the stabilization of

metarhodopsin II by the C terminus of the alpha subunit of transducin. *J Biol Chem* **276**, 2333-2339

223. Cherezov, V., Clogston, J., Misquitta, Y., Abdel-Gawad, W., and Caffrey, M. (2002) Membrane protein crystallization in meso: lipid type-tailoring of the cubic phase. *Biophys J* **83**, 3393-3407

224. Park, S. H., Das, B. B., Casagrande, F., Tian, Y., Nothnagel, H. J., Chu, M., Kiefer, H., Maier, K., De Angelis, A. A., Marassi, F. M., and Opella, S. J. (2012) Structure of the chemokine receptor CXCR1 in phospholipid bilayers. *Nature* **491**, 779-783

225. Cherezov, V., Rosenbaum, D. M., Hanson, M. A., Rasmussen, S. G., Thian, F. S., Kobilka, T. S., Choi, H. J., Kuhn, P., Weis, W. I., Kobilka, B. K., and Stevens, R. C. (2007) High-resolution crystal structure of an engineered human beta2-adrenergic G protein-coupled receptor. *Science* **318**, 1258-1265

226. Niesen, F. H., Berglund, H., and Vedadi, M. (2007) The use of differential scanning fluorimetry to detect ligand interactions that promote protein stability. *Nat Protoc* **2**, 2212-2221

227. Okada, T., Takeda, K., and Kouyama, T. (1998) Highly selective separation of rhodopsin from bovine rod outer segment membranes using combination of divalent cation and alkyl(thio)glucoside. *Photochem Photobiol* **67**, 495-499

228. Hamm, H. E., and Gilchrist, A. (1996) Heterotrimeric G proteins. *Curr Opin Cell Biol* **8**, 189-196

229. Tesmer, J. J., Sunahara, R. K., Gilman, A. G., and Sprang, S. R. (1997) Crystal structure of the catalytic domains of adenylyl cyclase in a complex with Gsalpha.GTPgammaS. *Science* **278**, 1907-1916

230. Kwok-Keung Fung, B., and Stryer, L. (1980) Photolyzed rhodopsin catalyzes the exchange of GTP for bound GDP in retinal rod outer segments. *Proc Natl Acad Sci U S A* **77**, 2500-2504

231. Higashijima, T., Ferguson, K. M., Smigel, M. D., and Gilman, A. G. (1987) The effect of GTP and Mg2+ on the GTPase activity and the fluorescent properties of Go. *J Biol Chem* **262**, 757-761

232. Ho, M. K., Chan, J. H., Wong, C. S., and Wong, Y. H. (2004) Identification of a stretch of six divergent amino acids on the alpha5 helix of Galpha16 as a major determinant of the promiscuity and efficiency of receptor coupling. *Biochem J* **380**, 361-369

233. Lichtarge, O., Bourne, H. R., and Cohen, F. E. (1996) Evolutionarily conserved Galphabetagamma binding surfaces support a model of the G protein-receptor complex. *Proc Natl Acad Sci U S A* **93**, 7507-7511

234. Bae, H., Anderson, K., Flood, L. A., Skiba, N. P., Hamm, H. E., and Graber, S. G. (1997) Molecular determinants of selectivity in 5-hydroxytryptamine1B receptor-G protein interactions. *J Biol Chem* **272**, 32071-32077

235. Bae, H., Cabrera-Vera, T. M., Depree, K. M., Graber, S. G., and Hamm, H. E. (1999) Two amino acids within the alpha4 helix of Galphai1 mediate coupling with 5-hydroxytryptamine1B receptors. *J Biol Chem* **274**, 14963-14971

236. Martin, E. L., Rens-Domiano, S., Schatz, P. J., and Hamm, H. E. (1996) Potent peptide analogues of a G protein receptor-binding region obtained with a combinatorial library. *J Biol Chem* **271**, 361-366

237. Deupi, X., Edwards, P., Singhal, A., Nickle, B., Oprian, D., Schertler, G., and Standfuss, J. (2012) Stabilized G protein binding site in the structure of constitutively active metarhodopsin-II. *Proc Natl Acad Sci U S A* **109**, 119-124

238. Herrmann, R., Heck, M., Henklein, P., Kleuss, C., Wray, V., Hofmann, K. P., and Ernst, O. P. (2006) Rhodopsin-transducin coupling: role of the Galpha C-terminus in nucleotide exchange catalysis. *Vision Res* **46**, 4582-4593

239. Oldham, W. M., Van Eps, N., Preininger, A. M., Hubbell, W. L., and Hamm, H. E. (2007) Mapping allosteric connections from the receptor to the nucleotide-binding pocket of heterotrimeric G proteins. *Proc Natl Acad Sci U S A* **104**, 7927-7932

240. Marin, E. P., Krishna, A. G., and Sakmar, T. P. (2002) Disruption of the alpha5 helix of transducin impairs rhodopsin-catalyzed nucleotide exchange. *Biochemistry* **41**, 6988-6994

241. Marin, E. P., Krishna, A. G., and Sakmar, T. P. (2001) Rapid activation of transducin by mutations distant from the nucleotide-binding site: evidence for a mechanistic model of receptor-catalyzed nucleotide exchange by G proteins. *J Biol Chem* **276**, 27400-27405

242. Herrmann, R., Heck, M., Henklein, P., Hofmann, K. P., and Ernst, O. P. (2006) Signal transfer from GPCRs to G proteins: role of the G alpha N-terminal region in rhodopsin-transducin coupling. *J Biol Chem* **281**, 30234-30241

243. Ceruso, M. A., Periole, X., and Weinstein, H. (2004) Molecular dynamics simulations of transducin: interdomain and front to back communication in activation and nucleotide exchange. *J Mol Biol* **338**, 469-481

244. Kling, R. C., Lanig, H., Clark, T., and Gmeiner, P. (2013) Active-State Models of Ternary GPCR Complexes: Determinants of Selective Receptor-G-Protein Coupling. *PLoS One* **8**, e67244

245. Smith, P. K., Krohn, R. I., Hermanson, G. T., Mallia, A. K., Gartner, F. H., Provenzano, M. D., Fujimoto, E. K., Goeke, N. M., Olson, B. J., and Klenk, D. C. (1985) Measurement of protein using bicinchoninic acid. *Anal Biochem* **150**, 76-85

246. Otwinowski, Z., and Minor, W. (1997) Processing of X-ray diffraction data collected in oscillation mode. *Method Enzymol* **276**, 307-326

247. McCoy, A. J., Grosse-Kunstleve, R. W., Adams, P. D., Winn, M. D., Storoni, L. C., and Read, R. J. (2007) Phaser crystallographic software. *J Appl Crystallogr* **40**, 658-674

248. Adams, P. D., Afonine, P. V., Bunkoczi, G., Chen, V. B., Davis, I. W., Echols, N., Headd, J. J., Hung, L. W., Kapral, G. J., Grosse-Kunstleve, R. W., McCoy, A. J., Moriarty, N. W., Oeffner, R., Read, R. J., Richardson, D. C., Richardson, J. S., Terwilliger, T. C., and Zwart, P. H. (2010) PHENIX: a comprehensive Python-based system for macromolecular structure solution. *Acta Crystallogr D* **66**, 213-221

249. Emsley, P., and Cowtan, K. (2004) Coot: model-building tools for molecular graphics. *Acta Crystallogr D* **60**, 2126-2132

250. Laskowski, R. A., Macarthur, M. W., Moss, D. S., and Thornton, J. M. (1993) Procheck - a Program to Check the Stereochemical Quality of Protein Structures. *J Appl Crystallogr* **26**, 283-291

251. Chen, V. B., Arendall, W. B., 3rd, Headd, J. J., Keedy, D. A., Immormino, R. M., Kapral, G. J., Murray, L. W., Richardson, J. S., and Richardson, D. C. (2010) MolProbity: all-atom structure validation for macromolecular crystallography. *Acta Crystallogr D Biol Crystallogr* **66**, 12-21

252. Denker, B. M., Boutin, P. M., and Neer, E. J. (1995) Interactions between the amino- and carboxyl-terminal regions of G alpha subunits: analysis of mutated G alpha o/G alpha i2 chimeras. *Biochemistry* **34**, 5544-5553

253. Chung, K. Y., Rasmussen, S. G., Liu, T., Li, S., DeVree, B. T., Chae, P. S., Calinski, D., Kobilka, B. K., Woods, V. L., Jr., and Sunahara, R. K. (2011) Conformational changes in the G protein Gs induced by the beta2 adrenergic receptor. *Nature* **477**, 611-615

254. Kimple, R. J., Kimple, M. E., Betts, L., Sondek, J., and Siderovski, D. P. (2002) Structural determinants for GoLoco-induced inhibition of nucleotide release by Galpha subunits. *Nature* **416**, 878-881

255. Bourne, H. R. (1997) G proteins. The arginine finger strikes again. *Nature* **389**, 673-674

256. Maegley, K. A., Admiraal, S. J., and Herschlag, D. (1996) Ras-catalyzed hydrolysis of GTP: a new perspective from model studies. *Proc Natl Acad Sci U S A* **93**, 8160-8166

257. Cozzone, A. J. (1998) Regulation of acetate metabolism by protein phosphorylation in enteric bacteria. *Annu Rev Microbiol* **52**, 127-164

258. Ingram-Smith, C., Martin, S. R., and Smith, K. S. (2006) Acetate kinase: not just a bacterial enzyme. *Trends Microbiol* **14**, 249-253

259. Thauer, R. K., Kaster, A. K., Seedorf, H., Buckel, W., and Hedderich, R. (2008) Methanogenic archaea: ecologically relevant differences in energy conservation. *Nat Rev Microbiol* **6**, 579-591

260. Bragg, P. D., and Reeves, R. E. (1962) Pathways of glucose dissimilation in Laredo strain of Entamoeba histolytica. *Exp Parasitol* **12**, 393-400

261. Reeves, R. E., and Guthrie, J. D. (1975) Acetate kinase (pyrophosphate). A fourth pyrophosphate-dependent kinase from Entamoeba histolytica. *Biochem Biophys Res Commun* **66**, 1389-1395

262. Fowler, M. L., Ingram-Smith, C., and Smith, K. S. (2012) A Novel Pyrophosphate-Forming Acetate Kinase from the Protist Entamoeba histolytica. *Eukaryot Cell* **11**, 1249-1256

263. Buss, K. A., Ingram-Smith, C., Ferry, J. G., Sanders, D. A., and Hasson, M. S. (1997) Crystallization of acetate kinase from Methanosarcina thermophila and prediction of its fold. *Protein Sci* **6**, 2659-2662

264. Hurley, J. H. (1996) The Sugar Kinase/Heat Shock Protein 70/Actin Superfamily: Implications of Conserved Structure for Mechanism. *Annu. Rev. Biophys. Biomol. Struct.* **25**, 137-162

265. Singh-Wissmann, K., Ingram-Smith, C., Miles, R. D., and Ferry, J. G. (1998) Identification of essential glutamates in the acetate kinase from *Methanosarcina thermophila*. *J. Bacteriol.* **180**, 1129-1134

266. Buss, K. A., Cooper, D. R., Ingram-Smith, C., Ferry, J. G., Sanders, D. A., and Hasson, M. S. (2001) Urikinase: Structure of Acetate Kinase, a Member of the ASKHA Superfamily of Phosphotransferases. *Journal of Bacteriology* **183**, 680-686

267. Singh-Wissmann, K., Miles, R. D., Ingram-Smith, C., and Ferry, J. G. (2000) Identification of essential arginines in the acetate kinase from Methanosarcina thermophila. *Biochemistry* **39**, 3671-3677

268. Ingram-Smith, C., Barber, R. D., and Ferry, J. G. (2000) The role of histidines in the acetate kinase from Methanosarcina thermophila. *J Biol Chem* **275**, 33765-33770

269. Miles, R. D., Iyer, P. P., and Ferry, J. G. (2001) Site-directed mutational analysis of active site residues in the acetate kinase from *Methanosarcina thermophila*. *J. Biol. Chem.* **276**, 45059-45064

270. Miles, R. D., Gorrell, A., and Ferry, J. G. (2002) Evidence for a transition state analog, MgADP-aluminum fluoride-acetate, in acetate kinase from *Methanosarcina thermophila*. *J. Biol. Chem.* **277**, 22547-22552

271. Gorrell, A., Lawrence, S. H., and Ferry, J. G. (2005) Structural and Kinetic Analyses of Arginine Residues in the Active Site of the Acetate Kinase from *Methanosarcina thermophila*. *The Journal of Biological Chemistry* **280**, 10731-10742

272. Gorrell, A., and Ferry, J. G. (2007) Investigations of the *Methanosarcina thermophila* Acetate Kinase Mechanism by Fluorescence Quenching. *Biochemistry* **46**, 14170-14176

273. Cowtan, K. (1994) Joint CCP4 and ESF-EACBM Newsletter on Protein Crystallography. **31**, 34-38

274. Brunger, A. T., Adams, P. D., Clore, G. M., DeLano, W. L., Gros, P., Grosse-Kunstleve, R. W., Jiang, J. S., Kuszewski, J., Nilges, M., Pannu, N. S., Read, R. J., Rice, L. M., Simonson, T., and Warren, G. L. (1998) Crystallography & NMR system: A new software suite for macromolecular structure determination. *Acta Crystallogr D Biol Crystallogr* **54**, 905-921

275. Murshudov, G. N., Vagin, A. A., and Dodson, E. J. (1997) Refinement of macromolecular structures by the maximum-likelihood method. *Acta Crystallogr D* **53**, 240-255

276. Schrodinger, LLC. (2010) The PyMOL Molecular Graphics System, Version 1.3r1.

277. Hayward, S., and Lee, R. A. (2002) Improvements in the analysis of domain motions in proteins from conformational change: DynDom version 1.50. *J Mol Graph Model* **21**, 181-183

278. Bork, P., Sander, C., and Valencia, A. (1992) An ATPase domain common to prokaryotic cell cycle proteins, sugar kinases, actin, and hsp70 heat shock proteins. *Proc Natl Acad Sci U S A* **89**, 7290-7294

279. Hayward, S. (2004) Identification of specific interactions that drive ligand-induced closure in five enzymes with classic domain movements. *J Mol Biol* **339**, 1001-102